Diffusion Tensor Imaging of the Central Nervous System Following an Injury to the Spinal Cord and Cell Transplant

Michael Jirjis
Marquette University

DIFFUSION TENSOR IMAGING OF THE CENTRAL NERVOUS SYSTEM FOLLOWING AN INJURY TO THE SPINAL CORD AND CELL TRANSPLANT

by

Michael B. Jirjis, B.S.

A Dissertation submitted to the Faculty of the Graduate School,
Marquette University,
in Partial Fulfillment of the Requirements for
the Degree of Doctor of Philosophy

Milwaukee, Wisconsin

May 2013

ABSTRACT
DIFFUSION TENSOR IMAGING OF THE CENTRAL NERVOUS SYSTEM
FOLLOWING AN INJURY TO THE SPINAL CORD
AND CELL TRANSPLANT

Michael B. Jirjis, B.S.

Marquette University, 2013

The purpose of this dissertation research was to characterize the use of magnetic resonance diffusion tensor imaging (DTI) as a diagnostic and prognostic tool in understanding the changes that occur throughout the spinal cord and brain following a spinal cord injury (SCI) and following stem cell transplant. The diffusion of water inside the nervous system is dramatically altered around the lesion site following a traumatic SCI. However, following damage to the spinal cord, little is known about the diffusion characteristics away from an injury and even less is understood about DTI's sensitivity to structural changes that occur following regenerative transplant therapies. The non-invasive nature of DTI could potentially allow for diagnostic and prognostic indicators of an SCI remote from injury and could provide physicians a method for tracking and monitoring the effectiveness of injected stem cells.

To evaluate the sensitivity of DTI to structural changes in the central nervous system (CNS) following a traumatic SCI, diffusion metrics in the brain and cervical spinal cord were compared for four different injury severities in a thoracic contusion model of a rat SCI. Structural changes in the cervical region of the spinal cord after transplantation of C17.2 neuronal stem cells were also examined with the use of DTI.

The findings from this dissertation suggest that diffusion tensor imaging is sensitive to changes in tissue structure in regions remote from injury and for cellular environments that increased astrocytic sprouting as a result of stem cell transplant. Mean water diffusion in the distal locations of the spinal cord and in the brain decreased following SCI. Neuronal stem cells that are known to elicit astrocytic proliferation produced mean increases in water diffusion. These results further clarify the potential for DTI to provide physicians a method to non-invasively monitor how the CNS changes following SCI and detect structural changes elicited by transplanted regenerative treatments.

ACKNOWLEDGEMENTS

Michael B. Jirjis, B.S.

I am very grateful for the patience, help and counsel of my advisor Dr. Brian Schmit. He has offered many wonderful discussions and provided indispensable guidance as I prepared and worked through my thesis.

I would like to thank the members of my dissertation committee for their continued support and assistance in this research. The members are Brian Schmit, PhD, my advisor and dissertation director, Shekar Kurpad, MD, PhD, Matthew Budde, PhD, Kristina Ropella, PhD, and Taly Schmidt, PhD.

A special thanks goes to the people who devoted their time behind the scenes; I apologize in advance to anyone whose name is not mentioned. Matt Runquist, BS, for his knowledge in running the magnetic resonance scanner. Christy Stadig, BS and the research support team at the Veteran Affairs hospital for their invaluable help with surgical preparation, animal care, and histology. Also, I would like to thank Aditya Vedantam, MD, for his aid with histology and writing.

I sincerely appreciate and thank my colleagues in the Department of Biomedical Engineering who have provided help, instruction, and support throughout my time in graduate school. I would also like to recognize members of Marquette University, the Medical College of Wisconsin, and the VA Hospital.

Finally, I would like to thank my Wife, Jonelle Jirjis, my parents, Bassam and Janet Jirjis, my siblings, Jason and Christina Jirjis, and my friends. I am indebted for their love, encouragement, and support. This research was supported by the Falk Medical Trust Foundation and the U.S. Department of Veterans Affairs grant 5096-08.

TABLE OF CONTENTS

LIST OF TABLES

LIST OF FIGURES

CHAPTER 1
INTRODUCTION AND BACKGROUND

Spinal Cord Injury

Current medical technology is still unable to accurately predict the prognostic and diagnostic outcome after a spinal cord injury (SCI). Following an incomplete SCI, between 50 and 75% of patients will regain some ambulatory function (Papadopoulos et al., 2002; Oleson et al., 2005). While patients with incomplete SCI are able to regain some loss of function, this seemingly random chance of recovery is in part due to the immediate physiological response that masks the true extent of the injury. Motor ability has also been shown to minimally diminish when spinal transections were completed in up to 50% of the spinal cord (Nathan, 1994). Current initial diagnosis of SCI is reliant upon anatomical medical imaging scans and rudimentary functional testing of both the motor and sensory pathways. These limited views of the spinal cord could exhibit complete SCI when in reality the spinal cord damage is minimal after inflammation is reduced and it is also possible that a normal looking spinal cord could be microscopically damaged upon further investigation (Kakulas, 2004a). It is important to fully understand the complexity of a spinal cord injury before being able to provide a way to recovery from the disability. Physicians are able to offer some insight into the initial diagnosis of spinal cord injury, however extent of injury is hard to predict because of the initial inflammatory response (Fleming et al., 2006).

Immediately after trauma to the spinal cord occurs, the area of impact starts to hemorrhage (Tator and Fehlings, 1991). At this time, there is an influx of neutrophils at the lesion site. Minutes to hours after, microglia and macrophage start to arrive in response to the injury at the lesion site. Microglia are activated and transformed into macrophages within minutes after SCI, while blood derived macrophages will arrive a

day or two later (Fleming et al., 2006). Both the neutrophils and macrophages create a phagocytic environment that removes the damaged debris (Carlson et al., 1998). During and following phagocytosis there are more monocytes and macrophages that advance and produce pro-inflammatory cytokines that create an oxidative response to help sterilize the injury site. With the influx of responding cells and the outflow of damaged tissue comes a wide change in the fluidic volume.

This acute inflammatory response caused by mechanical trauma to the blood vessels and cellular structures is characterized by edema and an increase of plasma fluid into extracellular space. This increase results in a pressure induced ischemia where diminished blood flow to the injured region ensues. There is also a cytotoxic response that results in intracellular swelling (Norenberg et al., 2004). In the wake of the acute response resides a cavity that slowly expands as tissue is removed. Astrocytes start to proliferate into the cavity and initiate a fibrous structure that forms the astrocytic scar as early as five days after injury (Kakulas, 2004a) and can continue for as long as a year (Schwab and Bartholdi, 1996). The presence of the oxidative enzymes produced from the acute response damages surrounding tissue and initiates secondary damage outside of the lesion site.

Following the initial traumatic injury and inflammatory response, secondary damage starts to take place in the spinal cord. The injured axons close off and create bulbs that swell and progressively retract (Norenberg et al., 2004). A key mediator in the swelling and axonal degeneration is the entry of calcium into the axoplasm. The calcium influx from the extracellular and intracellular cells activates proteases that contribute to axonal degeneration (Gaudet et al., 2011). Early after SCI, the myelin will start to break down and an influx of macrophages will take away the loose cellular structure. Initial axonal degeneration is thought to partly be caused by proteases that attack the inner myelin wall before macrophages arrive and remove the tissue (Coleman and Perry

2002). One week after injury macrophages can be seen in the cervical segments of the spinal cord following a thoracic injury (Buss 2003). The collapse of cell bodies is not limited to the myelin sheath. The axonal membrane will also start to degenerate away from the injury. Retrograde demyelination will occur more proximal to the lesion site and axons that have lost their major input will start to degrade. Degenerating axons in the cervical cord are found within 3 days after a thoracic injury (Buss 2003). The anterograde degeneration progresses distal to the cell body and can be seen progressing for over a year (Kakulas, 2004a). Until fairly recently, axonal degeneration was debated to actually occur concurrently with Wallerian degeneration (Gaudet et al., 2011). Colemen et al. used wild type mice that exhibited slow Wallerian degeneration (Coleman and Perry, 2002) demonstrating that the axonal degeneration still occurs with delayed Wallerian degeneration. The Wallerian degeneration occurs in the spinal tracts rostral and caudal to the lesion site creating further damage and limiting motor and sensory function; however, the neuronal circuitry is plastic and adapts.

The extensive damage that occurs throughout entire axons following neuronal damage in the spinal cord is not limited to the spinal cord. A number of studies have demonstrated cortical changes as a result of spinal cord injury. Most cortical changes are attributed to reorganization of motor and sensory regions of the brain as the body recovers functionally (Aguilar et al., 2010). This cortical reorganization is not limited to the short term but has also been expressed long-term (Endo et al., 2007).

Immediately after a spinal cord injury, Aguilar et al. noticed increased cortical response when stimulating the forepaw of a rat that was transected in the thoracic region (Aguilar et al., 2010). The findings, identified through electrophysiological testing, include slower and diminished spontaneous activity, which has been correlated with increased cortical response. The cortical regions demonstrating increased activation include somatosensory and motor regions. In these regions, metabolic activity increases,

evidenced through observations of the cerebral blood flow and variations in glucose metabolism (both explored through positron emission tomography (PET) (Roelcke et al., 1997; Bruehlmeier et al., 1998). The activation signal changes not only in regions associated with the primary motor and sensory cortex, but when loss of function occurs in the hind limb, regions of the hand increase and are remapped into regions associated with damage (Bruehlmeier et al., 1998; Curt, Bruehlmeier, et al., 2002). While remapping of surviving functional groups can result in strengthening various pathways, it can also result in neuropathic pain (Wrigley et al., 2009). These changes in functional activation are not limited to the higher cortical areas but have been also observed in the thalamus, cerebellum, internal capsule, and cerebral peduncles (Bruehlmeier et al., 1998; Curt, Bruehlmeier, et al., 2002; Ramu et al., 2006; Wrigley et al., 2009; Gustin et al., 2010; Henderson et al., 2011). Outside of activation patterns and volume, observations of decreased number of neurons in the motor regions of the cortex as well as corticospinal tract regions leading up through the brain have also found (Freund et al., 2011; Oudega and Perez, 2012). The corticospinal tract is not the only pathway appears to be affected. The internal capsule is a bridging structure that relates the sensory motor pathways in the spinal cord with the brain. The bundles of afferent and efferent connections include the corticopontine, corticobulbar, corticospinal and corticoreticular fibers, all of which are related to the sensory and motor changes after an injury.

The pathways of the ascending and descending tracts are not just altered by damage to the spinal cord. Following a traumatic brain injury, diminished motor and sensory function has occurred in associated regions of the body (Fujimoto et al., 2004). Weishaupt et al. studied how the spinal cord is affected from damage to the motor cortex (Weishaupt et al., 2010). In this study, the damage to the motor cortex resulted in Wallerian degeneration that extended down through the spinal cord. The complications that arise from trying to understand the extent of injury and the regions associated with

an injury have resulted in researchers relying on newer medical imaging techniques to better understand the progression of an injury without the need to excise tissue. A common non-invasive imaging technique that has been used in many of the studies previously mentioned is magnetic resonance imaging. Most of the mentioned studies have looked at functional and metabolic changes that occur after a spinal cord injury and few have looked at the structural changes associated with spinal cord injury.

Magnetic Resonance Diffusion Tensor Imaging

Magnetic resonance diffusion tensor imaging (DTI) provides researchers with a non-invasive technique that allows imaging of soft biological tissue such as the spinal cord and the brain. DTI provides significant sensitivity to microstructural changes on a macroscopic scale (Beaulieu, 2002). The underlying principle behind DTI is the ability to image the diffusion of water through biological tissue and this technique is implemented in a magnetic resonance imaging (MRI) scanner.

An MRI measures the electromagnetic signal attenuation from protons in the body relaxing after being given energy through a radiofrequency pulse.

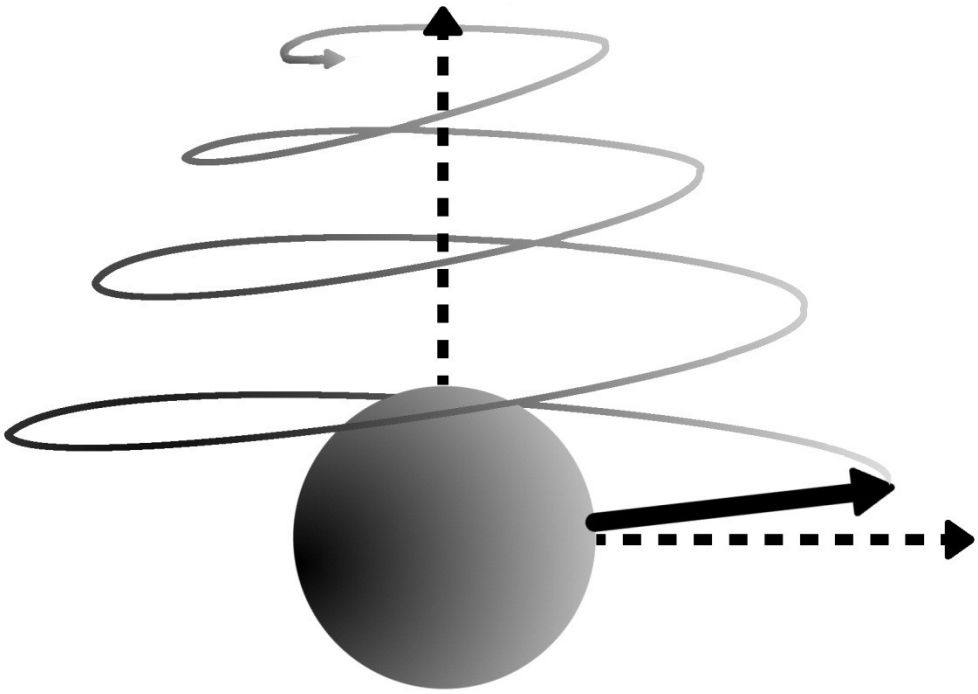

Figure 1-1: Proton relaxation after excitation.

This relaxation of a proton is shown following excitation. In this example the net magnetization is demonstrated. In reality there are multiple protons that fall out of phase limiting the magnitude of the horizontal signal. The dotted arrows represent the longitudinal and transverse directions with respect to the magnet orientation and location of the rf pulse. The solid arrow represents the net orientation of the spins of protons in response to the magnetic field and following excitation from an rf pulse. Shown above would be immediately after excitation where the protons have been excited and are oriented in the same direction. During relaxation, the directions will return to their previous state and will dephase, returning the orientation of the solid arrow to the longitudinal direction.

Different molecular structures will exhibit different relaxation times of this energy signal as it disperses into the surrounding environment (known as spin-lattice or T1 imaging) or as the spins dephase (known as the spin-spin relaxation or T2 imaging). A traditional MRI machine will use the varying relaxation times of different molecular structures in the body to display images that represent soft tissue in the body.

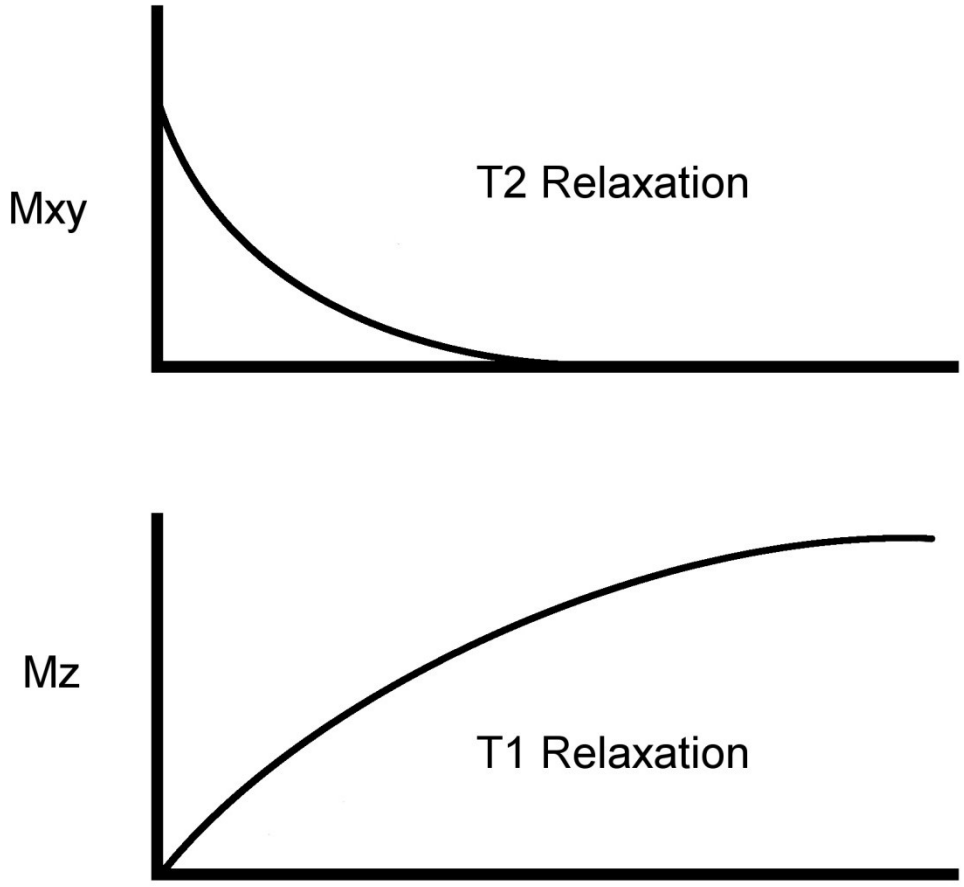

Figure 1-2: Example relaxation times for T1 and T2 weighted images.

Different tissue will result in varying relaxation times. In this example, the x-axis is time. Selection of images is determined by appropriately acquiring the signal during the relaxation phase at a specific time. Depending on what tissue features a physician would want to observe, one could allow the T2 relaxation to fully relax and capture only T1 signal, capture T2 when there is no T1 relaxation, or find a combination of both by acquiring the data when there is a signal in both the Mxy and Mz directions. Mx and Mzy correspond to the transverse and longitudinal directions with respect to the magnetic scanner, respectively.

While an MRI provides good contrast images of different structures in the body like the tissue of the brain and the bone that surrounds it, there are tissue structures that are more complex and not uniform. The brain for example is made up of both gray and

white matter. It is the structural differences in gray matter and white matter tissue that has steered imaging to become more complex. The complexity has prompted researchers to investigate the diffusion of water through the various tissue structures as opposed to looking at just the relaxation times of water molecules as seen in typical T1- and T2-weighted images.

Diffusion imaging is founded on the principle of Brownian motion, that the molecules in an unconstrained medium move about freely in a random motion in random directions due to thermal agitation (Einstein, 1905, 1956). This unconstrained water will slowly diffuse about in all directions fairly evenly in a matter that looks fairly isotropic. If structural barriers are placed around the freely moving molecules, water will diffuse more freely in the direction parallel to the structures than perpendicular to it. Einstein quantified the diffusion of water by looking at the root mean square displacement of the molecules, characterized by:

$$D = \frac{dr^2}{2 * n * t} \qquad \text{[Equation 1.1]}$$

where *D* is the diffusion coefficient, usually mm^2/s, dr^2 is the mean square displacement, *n* is the number of dimensions, and *t* is the diffusion time. To quantify this diffusion of water, an MRI is used in a way that can determine the magnitude and direction of the diffusion of water when it is inside the body.

In a traditional MRI, the electromagnetic gradients are kept as homogenous as possible to ascertain the relaxation times of different molecules under the same circumstances. In diffusion weighted imaging (DWI), the magnetic coils in an MRI are varied in a way to have a linear gradient applied across spatial position. When the

magnetic gradients are reversed, the difference in the radiofrequency energy emitted by molecules is similar for the molecules that were not diffusing.

However, in the case of diffusion, the water is constantly permeating through various structures and the molecules that moved during the different gradient applications will be “tagged” as the molecules that are moving. Since water is constantly moving and the body is primarily made up of water, diffusion images of the tissue shows contrasts in tissue like white and gray matter due to differences in diffusivity. The differences can be accentuated by varying the gradient pulse sequence during the MRI acquisition. The gradient pulse sequence, as eluded to earlier, is made up of two gradient sequences and can be seen in Figure 1-3; these can vary in the amplitude (G), duration of the gradient (δ), and the time between gradients (Δ). The signal response is also dependent on the gyromagnetic ratio (γ) representing the magnetic moment to the angular momentum of the spinning hydrogen atom (42.575 MHz/T).

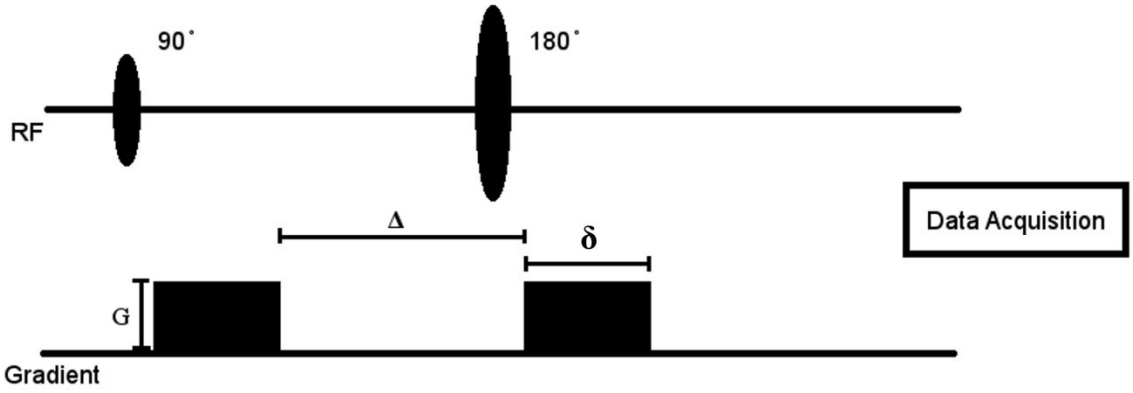

Figure 1-3: Typical gradient setup for spin-echo diffusion weighted sequence.

The general application of gradients is shown for a typical spin-echo diffusion weighted sequence. In this image, the amplitude (G), duration of gradient duration of the gradient (δ), and the time between gradients (Δ) are shown for gradient dephasing and rephasing. For this sequence, RF is the radiofrequency pulses applied over time (x-axis). At first a 90° pulse is applied, rotating the precession in the x-y plane. After a little relaxation, a 180° pulse is applied, allowing the atoms that precess slow and fast to be in

phase again and produce a very strong signal. By applying a magnetic field before and after the 180° pulse, the diffusing water molecules can be tagged. A data acquisition board is used following the rf and gradient pulses to acquire the signal.

The ratio to express the signal when diffusion weighting is applied (S) versus not applied (S0) is:

$$\frac{S}{S_0} = e^{-\gamma^2 G^2 \delta^2 \Delta D} \quad \text{[Equation 1.2]}$$

The gradient characteristics are usually simplified into a b-value:

$$b = \gamma^2 G^2 \delta^2 \Delta \quad \text{[Equation 1.3]}$$

This simplifies the signal equation into:

$$\frac{S}{S_0} = e^{-bD} \quad \text{[Equation 1.4]}$$

Generally, at least one diffusion image with a b = 0 mm^2/s is compared to a b-value > 0 mm^2/s. The measured diffusion, D, is typically referred to the apparent diffusion coefficient (ADC) and represents an average of the water diffusion that is dependent on the diffusion of water in the region, the cellular structure, and the pulse sequence (Schwartz and Hackney, 2003).

The image generated by diffusion weighting only represents the diffusion in one direction in a two-dimensional plane. In order to understand the diffusion inside of a three dimensional structure, the diffusion inside the structure will need to be sampled in various directions. By sampling the diffusion in at least six directions, a mathematical tensor can be created that represents the diffusion of a voxel as a three dimensional ellipsoid, where the eigenvalues and eigenvectors describe the strength of the diffusion

of water and the directions to which those strengths relate. The tensor describing the diffusion weighting is:

$$D = \begin{matrix} D_{xx} & D_{xy} & D_{xz} \\ D_{yx} & D_{yy} & D_{yz} \\ D_{zx} & D_{zy} & D_{zz} \end{matrix} \quad \text{[Equation 1.5]}$$

For a simplistic three-dimensional ellipsoid, the tensor is symmetric and can be simplified into just the six required diffusion directions Dxy, Dxz, Dyz, Dxx, Dyy, and Dzz. While these six directions are able to characterize the diffusion ellipsoid, usually a larger number of diffusion directions are acquired to produce a higher quality image. The diffusion eigenvectors that result from the tensor are usually used to construct a reference frame for the ellipsoid (Basser et al., 1994) and the eigenvalues are usually represented as λ_1, λ_2, λ_3, where λ_1 is associated with the diffusion along the length of the ellipsoid, while λ_2 and λ_3 are the dimensions through the ellipsoid. In current literature, λ_1 is commonly referred to longitudinal apparent diffusion coefficient (lADC) or axial diffusivity, and the average of λ_2 and λ_3 are referred to the transverse apparent diffusion coefficient (tADC) or radial diffusivity (Schwartz, Chin, et al., 2005).

Although lADC and tADC describe the diffusion along the length of the ellipsoid and through the ellipsoid, there are other diffusion metrics that help describe the ellipsoid. Diffusion of the ellipsoid can also be described by how isotropic or anisotropic the ellipsoid is. This diffusion index is represented as the Fractional Anisotropy (FA) index and is characterized by:

$$FA = \sqrt{\frac{1}{2}} \frac{\sqrt{(\lambda_1 - \lambda_2)^2 + (\lambda_2 - \lambda_3)^2 + (\lambda_3 - \lambda_1)^2}}{\sqrt{\lambda_1^2 + \lambda_2^2 + \lambda_3^2}} \quad \text{[Equation 1.6]}$$

The overall diffusion in all three directions is also represented as Mean Diffusivity and is characterized by:

$$MD = \frac{\lambda_1 + \lambda_2 + \lambda_3}{3} \qquad \text{[Equation 1.7]}$$

The diffusion indices of FA, MD, lADC, and tADC are used to help quantitatively understand the diffusion of water as it relates to the microscopic structure through which it diffuses. The resulting quantification of a voxel is a macroscopic view of the underlying microscopic environment.

Prior to being able to characterize the cellular environment, the traditional imaging modalities for understanding the central nervous system utilized an MRI and were used to observe global structural changes due to an injury (Goldberg and Kershah, 2010). T1 and T2 weighted images highlight gross anatomical injury as in the case of traumatic spinal cord injury (Goldberg and Kershah, 2010; Yin et al., 2010; Freund et al., 2012), tumors (Brekke et al., 2007) or abnormalities in the brain (Modo, 2006; Berman et al., 2011). While gross anatomical injury such as edema and hemorrhage appear on an MRI, standard MRI abnormalities in images of injured groups compared to control groups do not always correlate well with injury (Ford et al., 1994). Diffusion imaging offers better insight into injury (Schwartz and Hackney, 2003). Yin et al. reported that diffusion weighted images provide earlier sensitivity to spinal cord injury than a traditional T2-weighted image (Yin et al., 2010).

Raw diffusion images that offer insight into one direction can be used to observe the changes in water diffusion in that direction when membrane structure is altered due to injury or disease. Moseley was able to confirm anisotropic water diffusion in white matter regions of cat brains and spinal cords and that the diffusion in gray matter is

isotropic (Moseley, Cohen, Kucharczyk, et al., 1990). The axial diffusion along the spinal cord is associated with axon diameter. In this case, lADC increases as the axon diameter increases (Schwartz, Cooper, et al., 2005). There is also less restriction of the diffusion of water with larger axons because their cytoskeletal protein density is decreased (Schwartz, Chin, et al., 2005). The same group demonstrated that the diffusion of water is restricted from cell membranes lined with a myelin sheath, and that if that myelin is damaged, the longitudinal apparent diffusion coefficient decreases (Schwartz, Duda, et al., 2005). They mention that this effect is different for cerebral infarcts but the reasoning behind it was not well understood. The diffusion of water in various directions has also been associated with astrocytic proliferation. Vorisek et al. reported that astrocytic proliferation in the extracellular matrix could contribute to decreased water diffusion (Vorísek et al., 2002).

This decrease in axial diffusion has been associated with traumatic injury where axonal and myelin degeneration occurs (Schwartz, Chin, et al., 2005). Kim et al. has reported that lADC decreases after injury (Kim et al., 2007, 2009, 2010). They mention that the mechanism that initiates the decrease in lADC is unknown but can be attributed to the degeneration of myelin. Associated with the change in diffusion after injury is an increase in the radial diffusion in the transverse direction of the spinal cord, though some groups have shown that tADC does change with respect to changes in myelin (Budde et al., 2007; Sundberg et al., 2010). The decreases in lADC and increases in tADC increase following a spinal cord injury at or very close to the injury site. Xu et al. reported that the mean diffusion after traumatic brain injury decreases following injury and fractional anisotropy increases. These changes to diffusion are thought to be associated with cytotoxic edema (Xu et al., 2011). The structural changes that alter the diffusion of water are characterized by changes in tissue architecture. However, changes in the intracellular and extracellular water compartments may also affect water diffusion. The

diffusion of water for intracellular compartments and extracellular compartments can be compared by varying the diffusion b-values to create an exponential curve (Schwartz and Hackney, 2003). Anderson et al. found that the apparent diffusion coefficient in the rat optical nerve related to increased intracellular water volume (Anderson et al., 1996). While diffusion tensor imaging is able to detect the structural changes that occur following a traumatic injury, it may also be useful in monitoring the cellular environment to determine the effectiveness of repair treatments.

Transplant Therapies after Spinal Cord Injury

Following injury to axons, the connections of the axon endings are often severed and the axons degenerate towards the cell bodies. In damaged peripheral nerves the Schwann cells are capable of helping the regeneration after injury. However in the central nervous system there is a lack of a regenerative ability. The nerve fibers in the CNS are unable to find and restore severed connections or initiate new ones. Currently, researchers are trying to find ways to bridge the gap of severed connections (Kakulas, 2004a; Ilies et al., 2011).

After a spinal cord injury, there are numerous factors that inhibit the regrowth of axons through the lesion site. The environment at the lesion site is hostile due to cells that are constantly attacking and removing foreign debris. Astrocytic scaring also contributes to preventing connections being made from either side of the lesion site. The number of axons that are able to regenerate in the CNS is limited and some research suggests that injecting Schwann cells into the injury site creates an environment similar to the peripheral nerves that are able to regenerate (Plant et al., 2001). Attempts at bridging the lesion gap by transplanting entire peripheral nerves into the injury site in hopes that it may allow connections to re-establish between both sides of the lesion have also been made (Aguayo et al., 1990).

While adjustments to the cellular environment to make it less toxic and grafting nerve cells to re-establish connections has had mild success (Li et al., 1995), there is a disconnect in the survival of transplants, the regrowth of axons, and the remyelination of axons. Injecting specific cells into regions lacking these cells has shown some success as well but is only able to make up for specific deficiencies (Yoon et al., 2007). Neuronal stem cells are capable of differentiating into multiple cell types associated with the environment that they are in (Pluchino et al., 2005; Martino and Pluchino, 2006). These neuronal stem cells migrate into damaged regions of the spinal cord and differentiate into cells that promote functional recovery (Wu et al., 2002). This functional recovery is provided by the transplanted cells that have the potential to differentiate into cells that synapse with other cells. Neuronal stem cells can also deliver various neurotrophic factors that aide in structuring the environment to be acceptable to CNS recovery (Okano et al., 2003).

Recovering from a spinal cord injury using neuronal stem cells could re-establish new connections inside the nervous system; however, the establishment of new connections in the spinal cord can also lead to pain and malfunction. Stem cells have also been shown to elicit astrocytic sprouting that produces allodynia (Hofstetter et al., 2005). Macias et al. concluded that specific neuronal stem cells contribute to axonal sprouting but also produce mechanical and thermal allodynia in the forelimbs of rats when the cells were transplanted in a contusion injured rat in the thoracic region of the spinal cord (Macias et al., 2006). There has also been concern for the random differentiation into cells that mutate and create tumors in the central nervous system, although with certain cells there has been little misbehavior in the differentiation process (Illes et al., 2011).

The current neuroimaging techniques to monitor the progression of neuronal stem cells are limited. Within animal models, end point histology is often used as a means for determining progress of transplant injections (Thuret et al., 2006). Removing tissue samples is invasive and is not a feasible option for humans, nevertheless there has been development of non-invasive imaging techniques that track stem cells. However, in these examples the magnetic tracer can produce susceptibility blooming which can degrade the MR image. The contrast agents that are used can also cause harm to renal function (Modo, 2006; Brekke et al., 2007).

Tagging neuronal stem cells with magnetic tracers has allowed physicians to follow the progression of transplants, through the use of MRI, as cells travel through the body to the target site (Magnitsky et al., 2005; Brekke et al., 2007; Moraes et al., 2012; Vande Velde et al., 2012). Magnetic resonance imaging has also been used to verify successful treatments of stroke following the injection of neural progenitor cells (Jiang et al., 2006). In the spinal cord, T2-weighted images have been used to confirm regeneration in the spine following transplantation of stem cells in humans at the location of injury (Kang et al., 2005). While T2-weighted images can successfully track the location of the stem cells, the effects of the stem cells on the microstructural environment are not known. There have been a few studies where changes in water diffusion reflect axonal regeneration following the transplantation of fibroblasts (Schwartz, Chin, et al., 2005) or autoimmune T cells (Nevo et al., 2001). The changes in axonal structure found through variations in water diffusion from these cell types suggest that neuronal stem cells that differentiate into cells specific to the central nervous system will impact the diffusion of water in a similar way.

General Aims

Aim 1: *Utilize diffusion tensor imaging as a biomarker for severity of SCI.*

The purpose of this study was to determine whether differences in severity of a T8 spinal cord injury can be detected using ex vivo diffusion tensor imaging of the cervical spinal cord. To test this, forty Sprague-Dawley rats were given a sham, mild, moderate, or severe contusion injury over the 7 - 9 thoracic vertebral level. Rat spinal cords were extracted and scanned ex vivo in a 9.4 T magnetic resonance magnet to compare the water diffusion changes of the control rats to the injured rats. We hypothesized that the mean diffusion and fractional anisotropy would be correlated with injury severity.

Aim 2: *Non-invasively monitor systematic changes in the brain following a traumatic spinal cord injury through the use of diffusion tensor imaging.*

In this study we investigated the diffusion changes in the brain following a spinal cord injury. Following a similar approach to Aim 1, forty rats were given thoracic spinal cord contusions from various heights. Ten weeks after injury the rat brains were extracted and scanned ex vivo in a 9.4 T MRI. Voxel-based statistical comparisons as well as an ROI analysis were completed to compare structural changes in the rat following a spinal cord injury. We hypothesize that the structural changes in the brain following a spinal cord injury elicit changes in the diffusion of water that are detectable with MRI.

Aim 3: *Demonstrate that diffusion tensor imaging is sensitive to neuronal stem cell treatments.*

For this last experiment we investigated the sensitivity of diffusion tensor imaging to the structural changes that occur from neuronal stem cell transplants following a spinal cord injury. In this experiment, rats were given a moderate thoracic spinal cord injury over the T7-T9 vertebral level. One week following injury, rats were injected with C17.2 neuronal stem cells and compared to control rats that were given no transplant injection, sterile phosphate buffered saline, or sterile PBS with an immunosuppressant drug. In vivo diffusion measurements were used to compare the structural changes associated with the neuronal stem cells at 2, 5, and 10 weeks after a spinal cord injury. Rat brains were also scanned ex vivo following 10 weeks. For this study we hypothesized that the environmental changes due to stem cell treatment were detectable using diffusion imaging.

CHAPTER 2

EX VIVO DIFFUSION TENSOR IMAGING OF VARYING SPINAL CORD INJURY IN RATS

Introduction

Measurements of water diffusion within the spinal cord after an injury may provide valuable insight into the severity of injury, even for data obtained in regions distant from the injury site. Water diffusion within biological tissues can be measured noninvasively using magnetic resonance diffusion tensor imaging (DTI). Since diffusion barriers within the tissue change after injury, DTI has provided researchers with an invaluable tool to monitor histological changes to the spinal cord after a spinal cord injury (SCI), however, most studies have focused on diffusion measurements at or within a few segments of the site of injury (Deo et al., 2006; Sundberg et al., 2010; Kim et al., 2011). Although DTI at the injury site provides information about the histological structure of the injured spinal cord, imaging of the injury site after trauma can be challenging because of tissue disruption and the insertion of metal stabilization devices that cause artifacts in magnetic resonance imaging. The purpose of the current study was to determine whether DTI at sites rostral and caudal to the injury provide measures of injury severity in graded contusion injuries in rats.

DTI parameters of the spinal cord are sensitive to histological changes that occur after a traumatic injury. In addition to the primary injury, there is secondary damage to the spinal cord in regions distant from the injury site that results in histological changes that affect water diffusion, including degeneration of fiber tracts, ischemia, edema, and oxidative damage to the tissue membranes that act as barriers to diffusion (Avellino et al., 1995; Carlson et al., 1998; Kakulas, 2004a). This inflammatory response results in impaired medullary circulation and changes to spinal cord structure, which consequently

develops necrosis that has been documented throughout the entire length of the spinal cord, up to the brainstem (Ito et al., 1996). The resulting demyelination of tracts at significant distances away from the lesion continues for over a year (Totoiu and Keirstead, 2005). These physical changes to the cellular microstructure, including axon number and volume changes, as well as alterations in intracellular and extracellular water balance, correlate with changes in apparent diffusion, including both longitudinal diffusion (along the tracts) and transverse diffusion (across the spinal tracts)(Schwartz and Hackney, 2003). Axon morphometric parameters in various white matter tracts appear to underlie differences in overall diffusion, which could be useful in detecting injury to spinal white matter tracts (Gullapalli et al., 2006). Thus, DTI measurements of diffusion throughout the spinal cord after an injury might be used as a biomarker for injury severity.

There is evidence of decreases in diffusivity of water in the spinal cord in regions rostral to a chronic injury, possibly as a result of secondary injury processes throughout the entire spinal cord. Previously, our group has found changes to the diffusion of water along the entire length of the spinal cord after a moderate SCI to the eighth thoracic vertebrae in rats (Ellingson, Kurpad, et al., 2008a). Mean diffusivity significantly decreases in regions away from the lesion site consistent with secondary injury processes such as cytotoxic edema, chronic atrophy and axonal loss. Changes in mean diffusivity have also been documented in the high cervical spinal cord (rostral to an injury) in humans with chronic spinal cord injury (Ellingson, Kurpad, et al., 2008b; Ellingson, Ulmer, et al., 2008; Cheran et al., 2011; cf. however, Petersen et al., 2012). These observations raise the question of whether changes in diffusivity in regions distant from the injury are related to injury severity. Further, it is expected that severity of injury would change the secondary injury processes, as the extent of demyelination and remyelination depends on the number of axons that are disrupted by the injury (Schwab

and Bartholdi, 1996). The severity of injury also determines the time course of recovery; in cases of remyelination, smaller lesions acquire myelin sheath faster than larger ones (Harrison and McDonald, 1977). Consequently, it might be possible to predict the severity of injury from diffusion measurements of the spinal cord over time. Recently, Kim et al. (Kim et al., 2011) demonstrated that DTI of the injury site in the hyperacute stage (< 3 hrs) can be used to predict functional recovery after a thoracic injury in rats. Although promising, there is limited additional evidence that DTI of the injury site or elsewhere in the spinal cord correlates with functional recovery. In the current study we hypothesized that changes in DTI of the high cervical spinal cord are related to functional recovery in rats with low thoracic spinal contusions.

In order to determine whether mean diffusivity varies with injury severity, we tested DTI in a contusion model of rat SCI using 4 different injury severities. Rats were given one of four severities of injury at the thoracic level (T8) and ex vivo DTI of the entire spinal cord was conducted at 10 weeks post injury. Changes to diffusion characteristics of the cervical spinal cord were then compared to behavioral tests of motor and sensory function. We expected that there would be greater reduction in MD for specimens with more severe injuries.

Methods

Forty female Sprague-Dawley rats (200-250 grams) were used for this experiment. Rats were evenly divided into sham, mild, moderate, and severe groups (i.e. n = 10 for each group) and given a contusion injury with the magnitude of the contusion severity determined by group categorization. Rats were then allowed to survive for 10 weeks, after which ex vivo DTI scans were performed on the spinal cord. All procedures were approved by the Institutional Animal Care and Use Committees (IACUC) at

Marquette University, the Medical College of Wisconsin, and the Zablocki VA Medical Center.

Spinal Cord Injury Procedure

A contusion injury was produced in each rat. Rats were first anesthetized with an intraperitoneal (IP) injection of 40 µL xylazine, 0.1 mL of acepromazine, and 0.75 µL of ketamine hydrochloride diluted 1:1 with deionized water. The initial dose of the anesthetic was 0.890 mL per kilogram of body weight, with additional anesthetic depending on leg flexion-withdrawal and cornea reflexes. The rats were then shaved, sterilized with a povidone-iodine scrub pack and secured to a surgical board. An incision was made over the mid-thoracic region and a laminectomy was performed on the T7-T9 spinal segments. The rats were then placed in a MASCIS impactor (W.M. Keck Center for Collaborative Neuroscience; Piscataway, NJ) and a 10 gram rod was dropped from a height of 0 mm, 10 mm, 25 mm, or 50 mm to induce a sham, mild, moderate, or severe injury, respectively.

After surgery, rats were placed on post-operative care. The bi-daily procedure involved bladder expression, one dose of enrofloxacin (10 mg/kg subcutaneously; Bayer Healthcare LLC; Shawnee Mission, KS), buprenorphine hydrochloride (0.1-0.5 mg/kg subcutaneously; Rickitt Benckiser Health Care Ltd; Hull, UK), and 6 cc of lactated ringers. Animals were kept under post-operative care procedures until bladder function returned and specimens showed no signs of infection or stress.

Behavioral Assessment

Open field walking was evaluated according to the BBB rating scale (Basso et al., 1995) every week after the surgical procedure. Following the standard BBB protocol, rats were placed on a flat, one meter diameter surface and observed for 3 minutes. Hind

limb function was assessed according to the 0-21 BBB scoring where 0 is flaccid paralysis and 21 is normal gait.

Ex Vivo MRI Protocol

Ex vivo images were obtained at 11 weeks after injury. Animals were euthanized with an IP injection of sodium pentobarbital (100 mg/kg body weight) and perfused through the heart with a 300 mL saline buffer followed by 600 mL of 10% formalin. The spinal cords were extracted and post-fixed in a 10% formalin solution. On the day of the ex vivo scanning session, the spinal cords were embedded in an agarose gelatin mixture made up of agarose powder dissolved in distilled H_20 following the protocol of Ellingson et al. (Ellingson, Kurpad, et al., 2008a). Specimens were then placed in a 9.4T Bruker BioSpec 94/30 USR Spectroscopy Imaging System (Bruker BioSpin; Billerica, MA). A quadrature coil was used for transmitting and receiving radio signals (Doty Scientific; Columbia, SC). Diffusion weighted images (DWIs) were acquired using a 6-direction spin echo imaging sequence with a field of view (FOV) size of 5.12 cm, slice thickness of 2 mm, interslice gap of 1 mm, and number of excitations (NEX) of 2. The matrix size was 512 x 512 and the b-values were 0 and 500 s/mm^2.

DTI Analysis

DTI parameters were then calculated for the entire sample. Images were imported into the Analysis of Functional NeuroImages software package (AFNI; available at http://afni.nimh.nih.gov/). The DWIs were then co-registered, using an iterative weighted least squares fit to the T2-weighted images to correct for eddy-current and susceptibility distortions. Following registration, the resulting matrix volume data were used to calculate the diffusion tensor images from the DWIs. The eigenvalues (λ_1, λ_2, λ_3) and vectors were calculated from the 3 x 3 diffusion tensor. The eigenvalues were then

used to calculate diffusion indices. The indices included the longitudinal apparent diffusion coefficient (lADC), represented by λ_1, and the transverse apparent diffusion coefficient (tADC) calculated by the mean of eigenvalues λ_2 and λ_3. The mean diffusivity (MD) was also calculated as the trace of the tensor (i.e. the mean of all three eigenvalues). The fractional anisotropy (FA), which represents the overall anisotropy of diffusion at a certain voxel, was calculated using the formula prescribed by Basser et al. (Basser and Pierpaoli, 1996).

Image analysis was then performed in Matlab (The MathWorks Inc; Natick, MA). Regions of interests (ROIs) were manually defined for each of the diffusion indices in each axial slice. One ROI was defined as the entire transverse cord (i.e. the whole cord ROI). Separate ROIs were also identified for gray matter (GM), as well as dorsal columns (DWM), lateral columns (LWM), and ventral columns (VWM) in the white matter segments, as shown in Figure 1, and were the size of roughly 30 voxels.

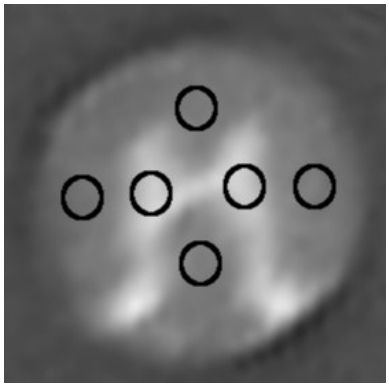

Figure 2-1: Typical Placement of Individual Region of Interest Drawings.

Shown in the image are typical placements of individual region of interest drawings (ROIs) for dorsal, lateral, ventral columns as well as gray matter. ROIs overlaid onto a spin echo image.

The average diffusion indices for the LWM and GM ROIs were found by combining the left and right ROIs. Images were excluded if significant variations in image

quality were found due to image ghosting, low signal to noise ratio (>2 standard deviations (SD) of average group signal to noise ratio (SNR)), or if the specimen produced an outlier during BBB scoring that was not consistent with severity level (i.e. severe injuries were expected to have a BBB score less than 7 on both limbs at 10 weeks following an injury and sham injuries were expected to have a BBB score greater than 18 on both limbs at 10 weeks following an injury). The resulting groups were as follows, Sham (n = 8), Severe (n = 8), Mild (n=10), Moderate (n = 9).

Statistical Analysis

All statistical analyses were performed using the Statistical Package for Social Sciences (SPSS version 13.0; SPSS Inc., Chicago, IL). A Student's t-test determined statistical significance between the DTI indices of the SCI rats and shams on a slice by slice basis as well as an average of the overall DTI index in the cervical or thoracic region. Each ROI was averaged at each slice location across all specimens. A two-way, repeated measures, analysis of variance (ANOVA; fixed factors: injury group and slice location (C1-T10 with roughly 2 slices per segment); random factor: specimen) was also completed to look at variations across groups. $P<0.05$ was considered to be statistically significant. A Tukey post hoc test for multiple comparisons was also performed to compare between spinal levels. The correlation between injury group and BBB score was analyzed using the Spearman correlation.

Results

Images of FA and MD in axial slices of the spinal cord are shown in Figure 2 for representative specimens from each severity group. A distinction between white and gray matter regions was observed in all specimens, especially for FA images. Near the

injury site in moderately and severely injured rats, the gray and white matter tracts were harder to distinguish visually.

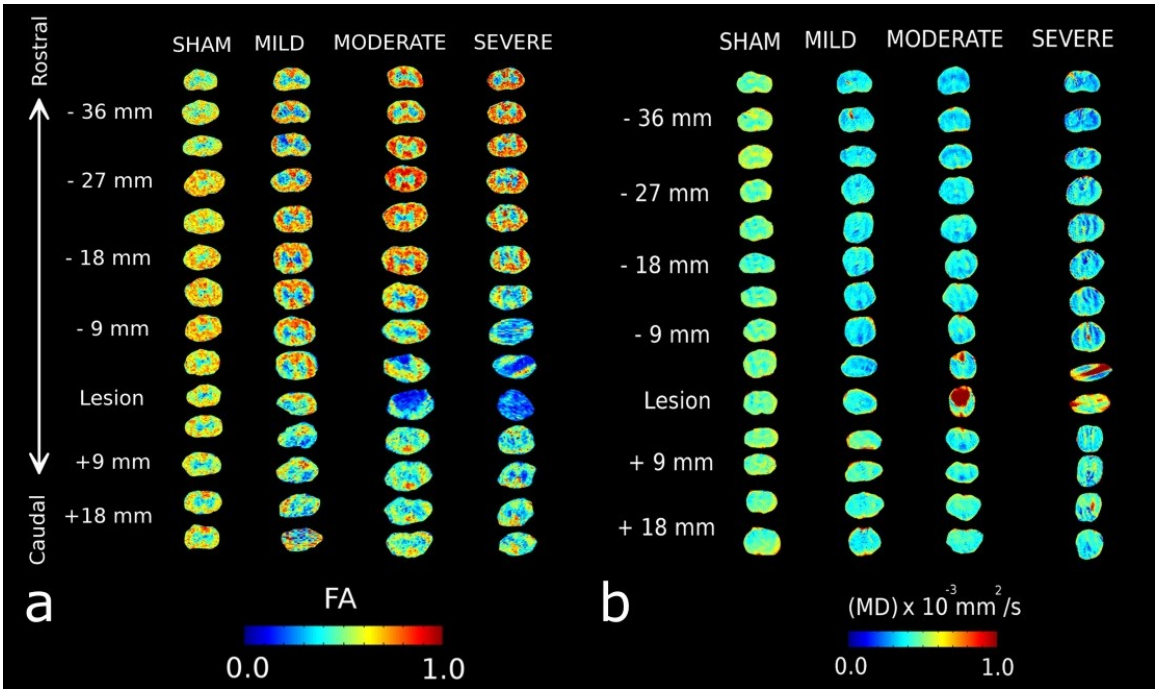

Figure 2-2: Example Region of Interest Selections for Fractional Anisotropy and Mean Diffusivity for Every Slice in Each Severity Group.

ROIs taken for FA (a), MD (b) over the entire length of the cord. One rat was randomly selected from each group and the ROIs were extracted for the entire length of the cord. Separation between white and gray matter is disrupted severely around injury sites for both FA and MD. Color-coded intensity values can be seen to change as severity of injure is increased across spinal segments.

In addition, the MD appeared to be lower in more severely injured specimens, and this lower diffusivity was observed throughout the volume of the spinal cord, except near the lesion. This separation was consistent with the BBB functional motor tests at week 10, which corresponded to the ex vivo scan time points. Interestingly, there was no significance ($p > 0.05$) in the BBB scores at week 10, for mild and moderate injured rats, as seen in Figure 3.

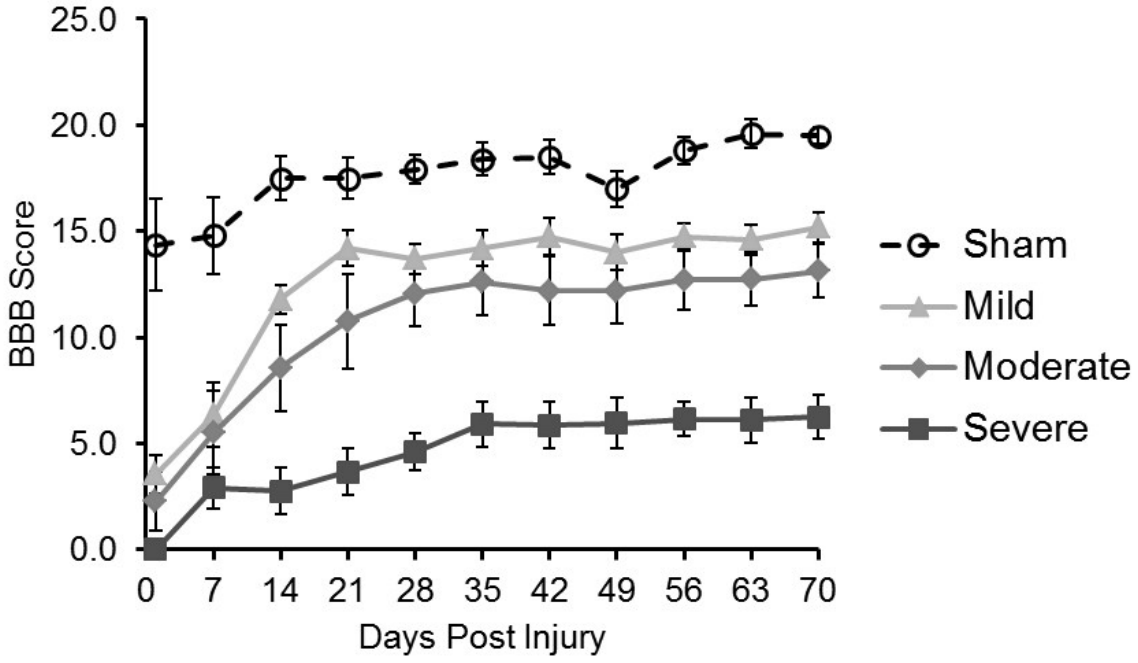

Figure 2-3: Hind Limb Motor Function over a 10 Week Period for Severity Groups.

BBB score depicting rat recovery following spinal cord injury for each severity over 10 weeks. Clear separation between the severe group and the mild and moderate groups occur at 2 weeks after injury and continues until 10 weeks after injury.

DTI Indices in the Sham Group:

DTI indices were consistent over the length of the spinal cord for the sham group. Mean ROIs within the sham group, for FA, MD, lADC, and tADC, had low within-group variations for each DTI index (mean and standard deviation (SD) for the DTI indices are given in Table 1). The variation was smaller for the analysis of the whole cord ROI, with the maximum coefficient of variation (CoV) occurring in tADC (2.32%). The white and gray matter regions were slightly more variable, with the largest COV = 14.65% in the GM lADC. Overall, SD was low for each group, demonstrating consistency within the MRI scanning. As shown in Table 1, the average FA in white matter was greater than the whole cord and gray matter ROIs; conversely, MD, lADC, and tADC for white matter

were considerably lower than the whole cord values but within each WM/GM ROI, these DTI parameters were still consistent over the length of the cord.

Table 2-1: Diffusion Tensor Imaging Metrics for Sham Spinal Cords

	FA	MD ($x10^{-3}$ mm^2/s)	lADC ($x10^{-3}$ mm^2/s)	tADC ($x10^{-3}$ mm^2/s)
Whole Cord	0.51±0.003	0.75±0.004	1.01±0.012	0.56±0.013
White Matter	0.58±0.060	0.71±0.048	0.93±0.003	0.45±0.049
Gray Matter	0.31±0.095	0.78±0.052	0.71±0.104	0.68±0.052

The mean and standard deviation for DTI metrics in different ROIs.

Whole Cord ROI Analysis

There was a strong correlation between mean MD across the spinal cord and BBB score (r^2=0.80), as seen in Figure 4. Mean FA, MD, lADC, and tADC were calculated for each specimen, over the C1-C7 cervical segments for each specimen, and compared to individual BBB scores.

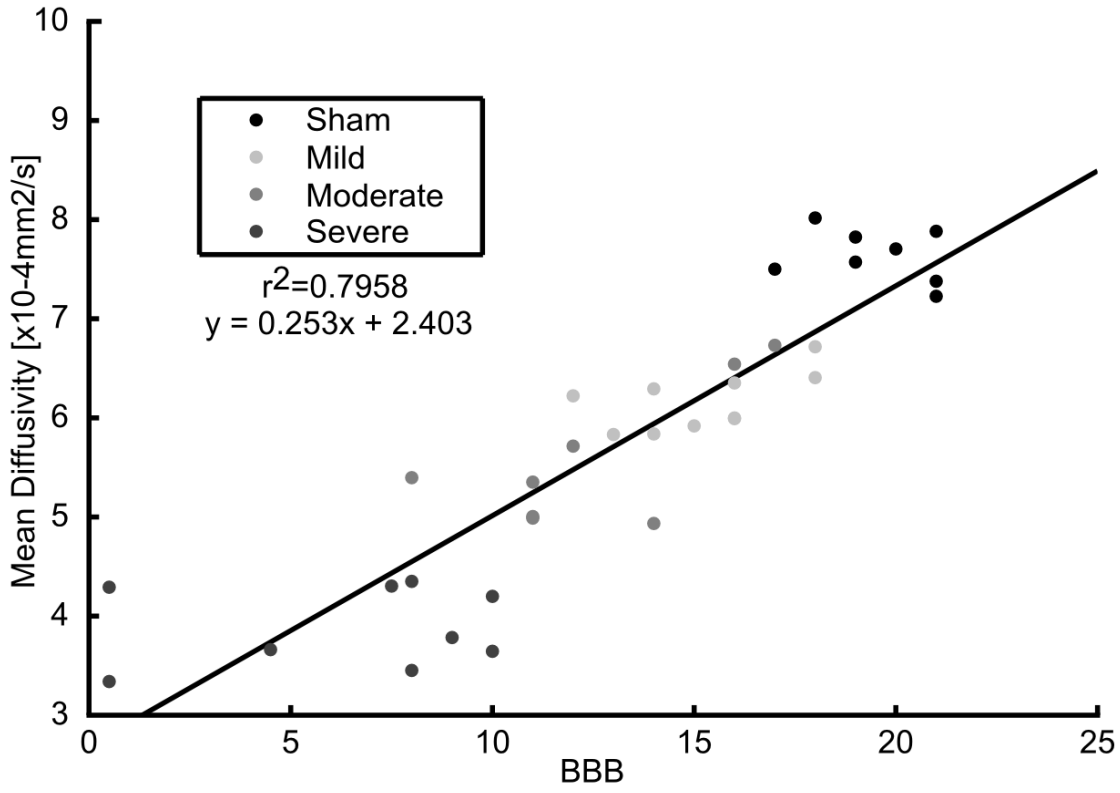

Figure 2-4: Correlation between Mean Diffusivity and Individual BBB Scores.

Whole cord MD, averaged across slices, correlated to individual BBB scores. An r^2 = 0.7958 demonstrates a strong correlation between mean diffusivity of the cervical spinal cord compared to average BBB score of rats at Week 10.

The resulting correlations ranged from r=0.53 to 0.94 in white matter ROIs, and between r= 0.33 and 0.82 in the gray matter ROI, as shown in Table 2. The stronger correlations (r > 0.7) occurred in MD, lADC, and tADC. All groups had a significance of p< 0.001 with the exception of lADC for LWM and FA for GM which were significant at the p<0.01 level.

Table 2-2: BBB Score Correlation with Whole Cord ROI for DTI Metrics

	FA	MD	lADC	tADC
Whole Cord	-0.548 (<0.001)	0.935 (<0.001)	0.785 (<0.001)	0.868 (<0.001)
VWM	0.609 (<0.001)	0.759 (<0.001)	0.700 (<0.001)	0.575 (<0.001)
DWM	0.575 (<0.001)	0.829 (<0.001)	0.681 (<0.001)	0.565 (<0.001)
LWM	0.565 (<0.001)	0.752 (<0.001)	0.527 (0.001)	0.899 (<0.001)
GM	0.329 (0.006)	0.783 (<0.001)	0.531 (<0.001)	0.818 (<0.001)

Spearman correlation coefficients (p values in parentheses) for the correlation between BBB scores for individual rats and their ROIs across the individual DTI metrics (FA, MD, lADC, and tADC).

There was variation in DTI indices along the length of the spinal cord, with notable differences at the injury site. DTI indices for each slice were analyzed from -40 mm rostral to the injury site to 20 mm caudal to the injury site as shown in Figure 5.

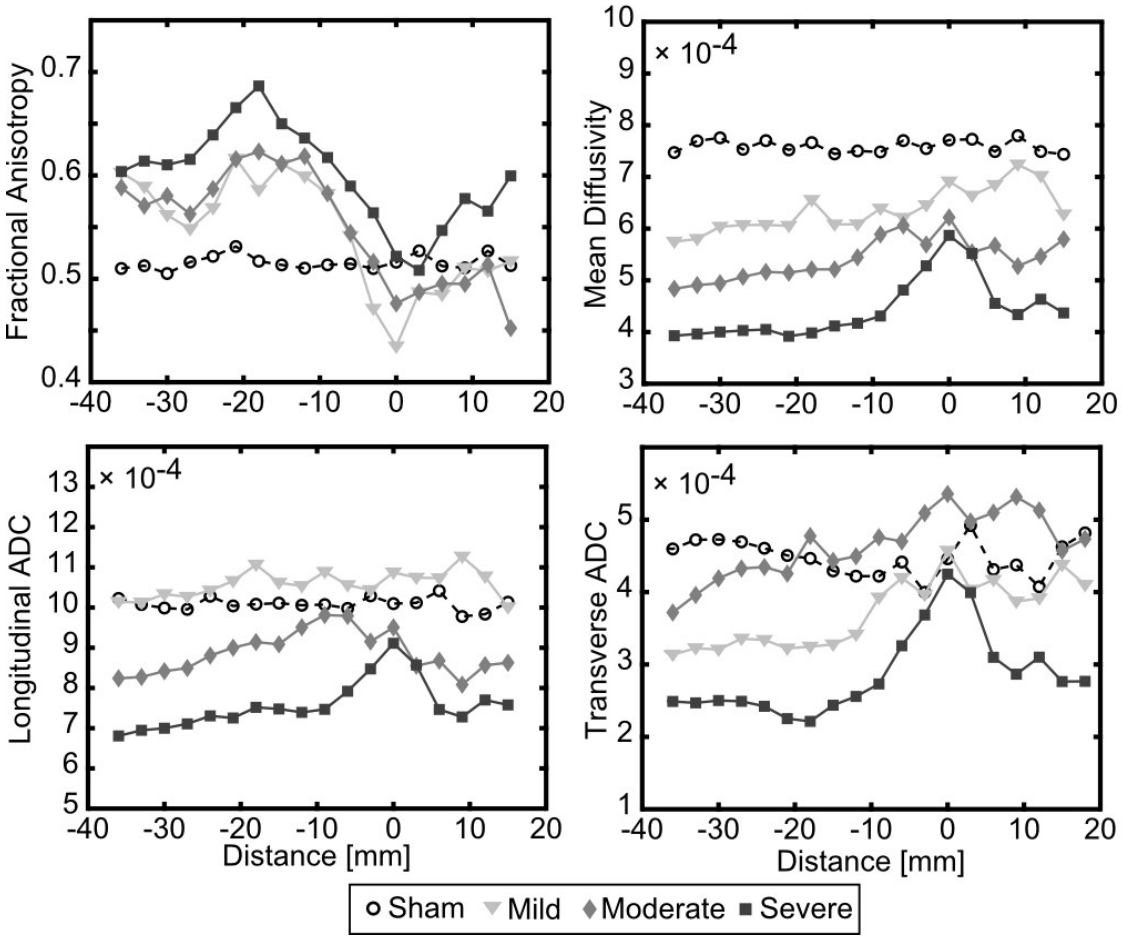

Figure 2-5: A Comparison between Severity Groups Rostral and Caudal to the Injury Site for Fractional Anisotropy, Mean Diffusivity, Longitudinal Apparent Diffusion Coefficient, and Transverse Apparent Diffusion Coefficient.

A comparison between severity groups rostral and caudal to the injury site. Here the injury site is located at 10 mm. FA (a), MD (b), lADC (c), and tADC (d) is shown for a whole cord ROI which includes white and gray matter. Spinal cord regions at and around the lesion site (0 mm) demonstrates drastically altered diffusion values than distal regions of the spinal cord. The clearest separation of diffusion values for each of the severity groups can be observed with the mean diffusivity metric.

Visually, there was a clear separation between severity groups throughout the entire length of the cord, with the greatest difference occurring in mean diffusivity, which showed an 18% reduction for regions cephalad to injury. This separation is also

represented in Figure 6 with Mild, Moderate, and Severe groups being significantly different than the Sham group when comparing average MD across the C1-C7 cervical segments for each specimen.

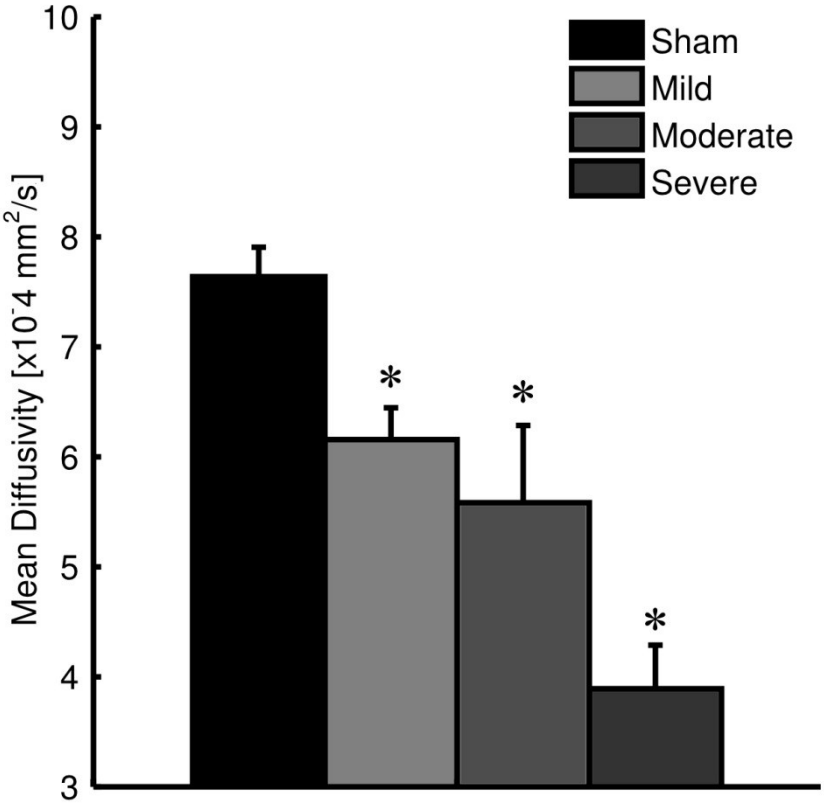

Figure 2-6: Bar Chart for Average Mean Diffusivity in the Cervical Segments of the Spinal Cord.

Average MD over the cervical segments of the spinal cord for each severity group. Mild, Moderate, and Severe injuries were found to be significantly different than the Sham group ($p < 0.05$).

Comparing gray matter and white matter tracts (Figure 7), the separation between groups was consistent over the length of the cord for white matter tracts. The gray matter also showed separation based on severity, which was most visually apparent in MD and tADC.

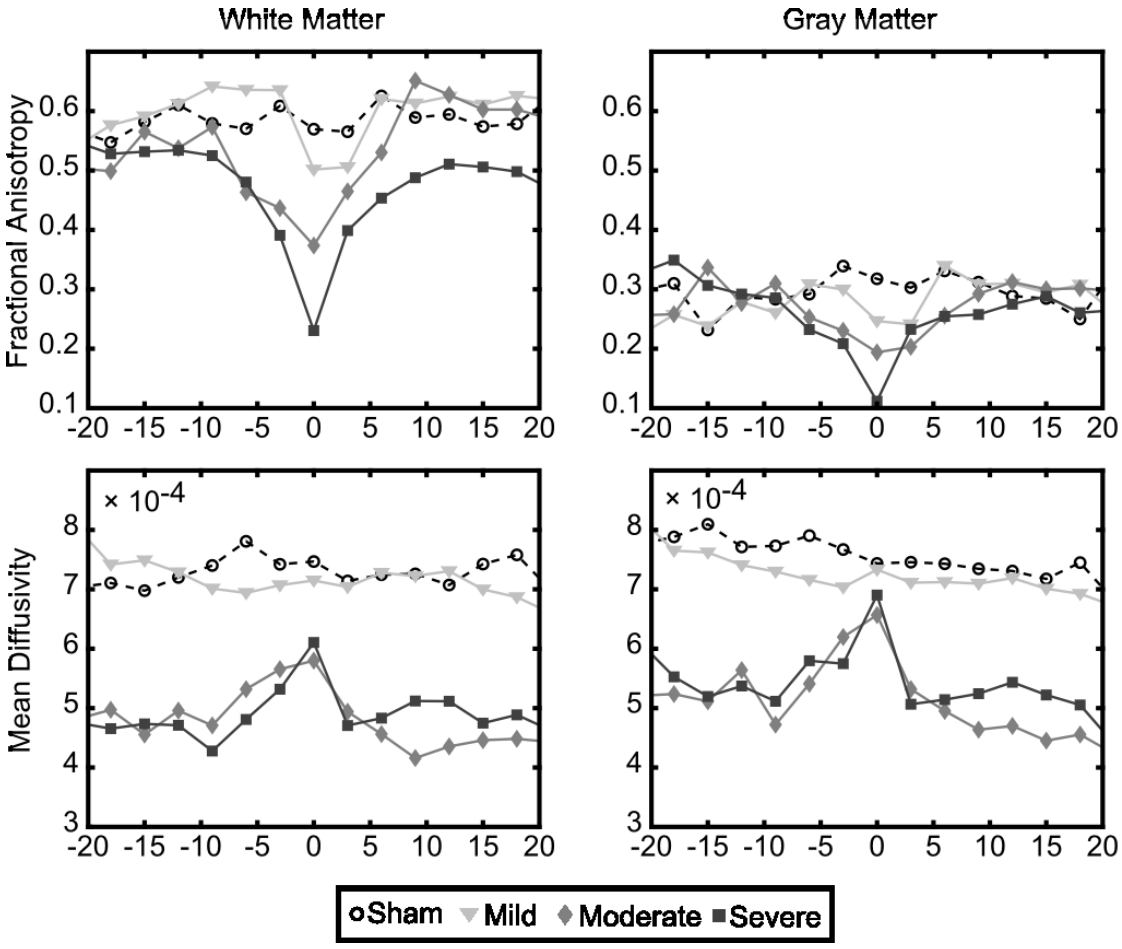

Figure 2-7: White Matter and Gray Matter Differences between Severity Groups.

A comparison between white and gray matter values for FA, MD, lADC, and tADC across severity groups. The comparison extends over 20 mm rostral and caudal to the injury site (0 mm). Drastic difference in white and gray matter values are shown with the most severe changes in diffusion occurring around the lesion site. FA and MD are sensitive to diffusion changes at the lesion site for white matter. FA is less altered in gray matter at the lesion site when comparing groups.

Statistical differences were found between severity groups for the DTI indices and ROIs, with some exceptions. In comparing the different severity groups over the entire length of the cord (Table 3), VWM, DWM, LWM, and GM were statistically different ($p < 0.01$) between the severe injury group and the other groups in all indices except when compared to moderate injuries for FA and MD in VWM, DWM, LWM, and

GM. lADC and tADC showed significant differences ($p < 0.01$) between groups in all of the ROIs except between the mild and sham group in VWM, and mild and moderate groups in VWM and DWM for lADC only. Conversely, the sham and mild injured rats were not significantly different for any of the DTI metrics ($p > 0.05$). There was also no significant difference ($p > 0.05$) between tADC values at, and caudal to the site of injury. In addition, no significant difference ($p > 0.05$) was observed for FA in gray matter between the mild and severe injuries. Other comparisons between groups showed FA was not significantly different between the sham group and the mild group for all ROIs as well as the sham group and the moderate group in VWM, DWM, LWM, and GM.

Table 2-3: Analysis of Differences between Groups

WC

	FA			**MD**		
	MILD	MODERATE	SEVERE	MILD	MODERATE	SEVERE
SHAM	0.274	0.233	<0.001	<0.001	<0.001	<0.001
MILD	-	1.000	0.001	-	<0.001	<0.001
MODERATE		-	0.001		-	<0.001
	lADC			**tADC**		
SHAM	0.004	<0.001	<0.001	<0.001	<0.001	<0.001
MILD	-	<0.001	<0.001	-	0.039	<0.001
MODERATE		-	<0.001		-	<0.001

VWM

	FA			MD		
	MILD	MODERATE	SEVERE	MILD	MODERATE	SEVERE
SHAM	0.977	0.017	<0.001	0.039	<0.001	<0.001
MILD	-	0.050	<0.001	-	<0.001	<0.001
MODERATE		-	0.065		-	0.061
	IADC			**tADC**		
SHAM	0.760	0.001	<0.001	0.914	<0.001	<0.001
MILD	-	0.016	<0.001	-	<0.001	<0.001
MODERATE		-	<0.001		-	<0.001

DWM

	FA			MD		
	MILD	MODERATE	SEVERE	MILD	MODERATE	SEVERE
SHAM	0.516	0.182	<0.001	<0.001	<0.001	<0.001
MILD	-	0.006	<0.001	-	<0.001	<0.001
MODERATE		-	0.014		-	0.707
	IADC			**tADC**		
SHAM	0.728	0.004	<0.001	<0.001	<0.001	<0.001
MILD	-	0.066	<0.001	-	<0.001	<0.001
MODERATE		-	0.001		-	<0.001

LWM

	FA			MD		
	MILD	MODERATE	SEVERE	MILD	MODERATE	SEVERE
SHAM	0.842	0.144	<0.001	0.989	<0.001	<0.001
MILD	-	0.020	<0.001	-	<0.001	<0.001
MODERATE		-	0.074		-	0.052
	IADC			**tADC**		
SHAM	0.647	0.441	<0.001	0.001	<0.001	<0.001
MILD	-	0.046	<0.001	-	<0.001	<0.001
MODERATE		-	<0.001		-	<0.001

GM

	FA			MD		
	MILD	MODERATE	SEVERE	MILD	MODERATE	SEVERE
SHAM	0.325	0.148	0.015	0.136	<0.001	<0.001
MILD	-	0.972	0.515	-	<0.001	<0.001
MODERATE		-	0.781		-	0.064
	lADC			**tADC**		
SHAM	0.308	0.807	<0.001	0.084	<0.001	<0.001
MILD	-	0.829	<0.001	-	<0.001	<0.001
MODERATE		-	<0.001		-	<0.001

Analysis of Variance (ANOVA) results for differences between the severity groups for each DTI metric within each ROI group. ROIs included whole cord, ventral white matter tracts, dorsal white matter tracts, lateral white matter tracts, and gray matter.

Discussion

Results from this study suggest that diffusion tensor imaging is sensitive enough to detect secondary injury rostral to a contusion injury site. These secondary injury effects were manifested as a decrease in mean diffusivity in the cervical spinal cord following a thoracic (T8) contusion that was proportional to the severity of injury. We observed a strong correlation (r^2=0.80) between MD of the cervical spinal cord and functional outcome, measured by the BBB motor score. Changes in diffusivity were also noted at the primary injury site, with relative changes along the length of the spinal cord that were consistent with reported results at or near the injury (Nevo et al., 2001; Deo et al., 2006; Ellingson, Kurpad, et al., 2008a).

Decreased measures of the apparent diffusion coefficient could be a result of axonal degeneration. The changes in diffusion parameters away from the injury site indicate changes in tissue structure of the cervical spinal cord. Buss et al. reported that degenerating changes were seen in the cervical portion of the spinal cord when a thoracic injury occurred (Buss and Schwab, 2003). A decrease in diffusion magnitude has also been found in regions remote from the site of injury when looking at the

degeneration and regeneration of sea lamprey axons (Takahashi et al., 2002). Our results demonstrate that mean diffusivity decreases following spinal cord injury at distal regions of the spinal cord. These results appear to suggest that Wallerian and axonal degeneration would greatly affect the membrane structure and in turn decrease the ADC. A few researchers have associated increases in tADC with Wallerian degeneration (Kim et al., 2007; Sundberg et al., 2010). We observed decreases in tADC (and thus decreases in MD), suggesting that membrane breakdown is not the only contributing factor to diffusion following an injury. Schwartz et al. found a lack of correlation between tADC and myelin sheath thickness (Schwartz, Cooper, et al., 2005) and Kozlowski et al. found that distal regions of the corticospinal tracts got significantly smaller following a spinal cord injury (Kozlowski et al., 2008). With smaller tract sizes in regions remote from injury there is potentially more restrictive membranes that may obstruct the diffusivity in the transverse direction. In distal regions of the spinal cord, the transverse components may also play less of a role in mean diffusion. Konomi et al. noticed that in segments outside the lesion site showed decreases in only lADC suggestive of axonal degeneration and not myelin degeneration (Konomi et al., 2012).

These changes were mostly associated with white matter alterations. Many studies have investigated Wallerian degeneration following various types of injury (DeBoy et al., 2007; Guleria et al., 2008; Zhang et al., 2009; Kim et al., 2010) and, while changes to the white matter surrounding the cord are thought to affect diffusion values, we have seen evidence for changes in gray matter diffusion characteristics as well. A limited number of studies have reported diffusion characteristics from gray matter regions (Ford et al., 1994; Ellingson et al., 2010) and it is thought that some of these changes occur because of an interaction of astrocytes in both the white and gray matter (Buss et al., 2004).

We observed a decrease in MD, lADC, and tADC with respect to the sham across the entire length of the cord. This decrease was correlated with the severity for up to 40 mm rostral to the injury site which is consistent with an increase in fiber density, after trauma to the spinal cord there is a formation of a dense astrocytic scar and glial responses throughout the spinal cord (Avellino et al., 1995; Schwab and Bartholdi, 1996; Buss et al., 2004) which could be the cause of restricted diffusion in both longitudinal and transverse directions. Schwab examined multiple studies where the effect and intensity of the spinal cord injury was amplified by both changes to the axonal structure as well as the inflammatory response that changed the cellular microstructure of the surrounding environment. Specifically, Vorisek et al. contributed a decrease in water diffusion to an increased proliferation of astrocytes and an increase of chondroitin sulfate proteoglycan (Vorísek et al., 2002). Moreover, these diffusion changes have been associated with axonal changes throughout the spinal cord (DeBoy et al., 2007; Sundberg et al., 2010).

The restrictive properties of cell breakdown and influx of inflammatory cells as time progresses could also explain the gradual decline away from the injury site. Changes in tissue structure in regions outside the lesion site were attributed to cytotoxic inflammatory products in this study. Xu et al. found that following cortical impact causing axonal damage there was a decrease in MD and an increase in FA suggestive of cytotoxic edema (Xu et al., 2011). In general, there is strong evidence of changes in the number of inflammatory cells at locations away from the injury site (Koshinaga and Whittemore, 1995; Moisse et al., 2008; Shi et al., 2009; Weishaupt et al., 2010) and even outside of the spinal cord (Gris et al., 2008). The activation of the inflammatory processes helps to explain the changes in water diffusion following SCI in regions remote from the injury site although changes between intracellular and extracellular water compartments cannot be excluded.

Results from this study support the hypothesis that DTI is sensitive to changes in intracellular and extracellular water compartments. Significant decreases in water diffusion have been seen following injury to the CNS (Moseley, Cohen, Kucharczyk, et al., 1990; Ford et al., 1994; Zhong et al., 1995). Duong et al. proposed that the primary reason for this decrease is the relationship between the intra- and extra-cellular water compartments, specifically, the resulting intracellular water diffusion (Duong et al., 2001). Further, Silva et al. also found that the intracellular water compartment is the overall determinate for changes in water diffusion (Silva et al., 2002). These studies demonstrated that ischemic trauma to the spinal cord causes a reduction in ADC leading to the possibility that changes in perfusion away from the injury feasibly decrease the diffusion of water.

In addition, the observed changes in diffusivity that we see might be reflected by a change in water balance due to edema or other inflammatory processes. Up-regulation of the primary water channel, Aquaporin-4, have also been seen in areas away from the lesion site in chronic injury, suggesting altered water transport, edema, and syringomyelia (Nesic et al., 2006). Changes in water balance are thought to greatly affect the diffusion of water within tissue (Lu and Sun, 2003; Ellingson, Kurpad, et al., 2008a; Sundberg et al., 2010). Investigators looking at ion concentrations have noted that calcium fluctuations deriving from the extracellular and intracellular stores are indicative of further injury-inducing secondary degeneration effects. The significant decrease in the diffusion values for MD, lADC, and tADC appear to suggest that the changes to the cellular fluidic environment could be a direct cause of the changes to water diffusion, however, further investigation into the water volume shift between intracellular and extracellular compartments is needed.

Changes in MD were consistently observed in the gray matter and individual tract ROIs, although the statistical tests were less conclusive than the whole cord ROI. The

increased variability due to smaller size of the individual tract ROIs probably accounts for the differences in the statistical tests. There has been a persistent interest in imaging specific tracts of the spinal cord following an injury in order to ascertain whether functional outcomes might be associated with particular tract loss. As such, there has been a desire to obtain improved resolution images with higher SNR (Cercignani et al., 2003; Mogatadakala and Narayana, 2009; Laganà et al., 2010). The current study benefitted in this regard from the use of ex vivo scans; however, additional resolution and improved SNR might be obtained with new coil designs and improved image sequences. Although image quality is important, especially with the use of the lower quality in vivo scans, the current results suggest that the whole cord ROI provides reasonable estimates of useful DTI metrics. Since similar changes occur throughout gray and white matter, a whole cord ROI, for which it is relatively easy to delineate between cord and the surrounding cerebrospinal fluid, might be the best option for identifying a DTI parameter that reflects injury severity.

The primary and secondary damage resulting after a spinal cord injury are complex events occurring throughout the spinal cord. Although past research has pointed to various hypotheses explaining what is happening away from the injury site with regards to changes in diffusion, there needs to be a more accurate assessment through histological and immunohistochemical techniques. Staining for neurofilament density with SMI-31 and SMI-32 for instance, has been associated with changes to water diffusion (DeBoy et al., 2007; Kim et al., 2011). Measurements of astrocyte and macrophage interactions in the cervical segments of the spinal cord might offer better insight into the severity related changes that are picked up by diffusion measurements. Examining the degradation of GFAP to assess the axonal degradation along the cord appears to be a promising avenue of research as well.

Conclusion

In conclusion, we have demonstrated that changes to the spinal cord away from injury site vary with respect to injury severity and that ex vivo diffusion tensor imaging is sensitive enough to detect the variability from those changes. Our results support the hypothesis that injury severity is associated with respective diffusion changes over the entire length of the spinal cord.

CHAPTER 3

VARYING SPINAL CORD INJURY IS DETECTABLE IN THE BRAIN USING DIFFUSION TENSOR IMAGING

Introduction

Understanding how the cortex reorganizes after a spinal cord injury (SCI) could provide useful clinical insight that may improve the prognostic outcome after an injury and aide in the planning of therapeutic regimens. Magnetic resonance diffusion tensor imaging (DTI) may provide a non-invasive, macroscopic, visualization into the microstructural changes that take place in the brain after an SCI. DTI has proven beneficial in monitoring the structural changes that occur in the brain after injuries such as stroke (Moseley, Cohen, Mintorovitch, et al., 1990; Beauchamp et al., 1999; Werring et al., 2000; Sotak, 2002; Jiang et al., 2006), head contusion (Rugg-Gunn et al., 2001; Inglese et al., 2005; Mac Donald et al., 2007; Kumar et al., 2009; Budde et al., 2011), and tumors (Holodny et al., 2005; Kitahara et al., 2005; Lee et al., 2012) and only recently has been shown to be sensitive to the cortical reorganization after an injury to the spinal cord (Ramu et al., 2008; Wrigley et al., 2009; Gustin et al., 2010; Freund et al., 2012). Although brain diffusion metrics are altered following SCI, an extensive look into characterizing DTI in the brain with respect to varying levels of injury in the spinal cord has yet to be established. The purpose of the current study was to determine whether DTI of the brain is sensitive to varying levels of contusion injury in the rats.

Diffusion tensor imaging allows the detection of structural connections in the brain, and diffusion indices such as fractional anisotropy (FA) and mean diffusivity (MD) correlate to cellular degeneration (Basser and Pierpaoli, 1996), changes in axon orientation and symmetry (Schwartz and Hackney, 2003), and are indicative of axonal degeneration, demyelination, and regrowth ((Concha et al., 2006; Voss et al., 2006; Lo

et al., 2009; Jiang et al., 2011). Recently we have found that there are systemic changes that occur along the entire spinal cord following an SCI (Ellingson, Kurpad, et al., 2008a) and that these changes are correlated to severity of injury (manuscript in preparation). The spinal cord is comprised of ascending and descending tracts to and from the brain. We believe that the severity changes are not restricted to the spinal cord but extend throughout the entire central nervous system (CNS).

DTI has revealed structural changes in the brain of spinal cord injured rats and patients, with significant differences occurring in the thalamus, corticospinal tract, primary somatosensory cortex, corona radiate, and internal capsule regions in the brain after a spinal cord is injured (Guleria et al., 2008; Ramu et al., 2008; Wolpaw, 2010; Freund et al., 2012). However, comprehending the microstructural changes that occur after an SCI can be challenging. Both Ramu et al. and Freund et al. reported unilateral changes in the internal capsule region when bilateral differences should be expected in subjects demonstrating diminished functional outcome for left and right limbs (Ramu et al., 2008; Freund et al., 2012). There have been multiple studies that demonstrate cortical reorganization after spinal cord injury. Imaging modalities such as positron emission tomography (PET) have demonstrated a change in the metabolic activity and expansion of cortical areas towards regions associated with damage (Roelcke et al., 1997; Bruehlmeier et al., 1998; Curt, Bruehlmeier, et al., 2002). Functional magnetic resonance imaging has demonstrated changes in volume of activation and differences in the patterns of activation following SCI (Curt, Alkadhi, et al., 2002; Ramu et al., 2006, 2007; Seminowicz et al., 2012). It is also not clear from the literature utilizing DTI, fMRI, or PET whether these changes are related to the level of injury severity and whether the plasticity of the brain is altered through adaptation of missing connections or a die back of existing systems.

In order to determine whether diffusivity in the brain varies with injury severity, we examined a contusion model of a rat at four different injury severities using DTI. In this study a controlled weight-dropped contusion was delivered from varying heights to elicit a sham, mild, moderate, or severe injury. The injury occurred at the thoracic level in thirty-two rats (N=8 per group). Diffusion characteristics were examined ex vivo at 10 weeks post injury and immunohistochemistry confirmed findings. Our results demonstrate that bilateral structural changes to the brain can be detected through monitoring changes in water diffusion and that diffusion tensor imaging of the brain is sensitive to varying spinal cord injury.

Methods

Animals and Spinal cord Injury Procedure

All experimental procedures were approved by the Institutional Animal Care and Use Committees (IACUC) at Marquette University, the Medical College of Wisconsin, and the Zablocki VA Medical Center. Rats were anesthetized with a 0.890 mL per kilogram of body weight intraperitoneal (IP) dose of 40 µL xylazine, 0.1 mL of acepromazine, and 0.75 µL of ketamine hydrochloride diluted 1:1 with deionized water. Additional half doses were given based on leg flexion-withdrawal and cornea reflexes. Laminectomies were performed for thirty-two adult female Sprague-Dawley rats weighing between 200 and 250 grams. A weight-dropped (10 gram rod) contusion injury was delivered from a height of 0 mm, 10 mm, 25 mm, or 50 mm to prompt a sham, mild, moderate, or severe injury respectively using a MASCIS impactor (W.M. Keck Center for Collaborative Neuroscience; Piscataway, NJ).

Following surgery, rats were placed on a bi-daily post-operative care procedure involving bladder expression, one dose of enrofloxacin (10 mg/kg subcutaneously; Bayer

Healthcare LLC; Shawnee Mission, KS), Buprenorphine hydrochloride (0.1-0.5 mg/kg subcutaneously; Rickitt Benckiser Health Care Ltd; Hull, UK), and 6 cc of lactated ringers. Animals were kept under post-operative care procedures until manual bladder expression was no longer needed and signs of stress or infection were no longer present.

Behavioral Assessment

Hind limb function was assessed following the open field walking procedure outlined by the Basso, Beattie, and Bresnahan scale (Basso et al., 1995). Briefly, rats were observed for 3 minutes on a flat, one meter diameter surface. BBB scoring was determined where 0 is flaccid paralysis and 21 is normal gait.

Ex Vivo MRI Protocol

Specimen brains were extracted 11 weeks after injury and prepared for ex vivo imaging. Animals were euthanized with an IP injection of sodium pentobarbital (100 mg/kg body weight) and perfused through the heart with 300 mL saline buffer followed by 600 mL of 10% formalin. The brains were extracted and post-fixed in a 10% formalin solution until the day of scanning. The brains were immersed in a susceptibility-matching fluid (Fomblin; Solvay Solexis, Inc, West Deptford, NJ) and placed in an inductively coupled 20 mm diameter loop gap radiofrequency coil. Specimens were positioned in a 9.4T Bruker BioSpec 94/30 USR Spectroscopy Imaging System (Bruker BioSpin; Billerica, MA). A multi-echo spin-echo sequence was used to acquire 12 diffusion weighted images (DWIs) with a b-value of 2000 s/mm^2 and two images with a b-value of 0 s/mm^2. An echo time (TE) of 25 ms and a repetition time (TR) of 3000 ms was used when acquiring scans that had a field of view (FOV) size of 20 mm by 20 mm,

acquisition matrix of 128x128, and 0.75 mm thick slices that were contiguously arranged for 30 slices.

DTI Analysis

Diffusion MRI data was imported into the Analysis of Functional NeuroImages software package (AFNI; available at http://afni.nimh.nih.gov/) and co-registered using an iterative least squares fit to the T2-weighted images to correct for eddy-current and susceptibility distortions. Following registration, the resulting matrix volume data was imported into an in-house software suite and each specimen's diffusion tensor image was registered to a reference control using Thirion's demons deformable image registration method (Thirion, 1998). Registered tensor volumes were then re-imported into AFNI and the eigenvalues were then used to calculate the mean diffusivity (MD; mean of all three eigenvalues) and fractional anisotropy (FA; calculated using a formula prescribed by Pierpaoli and Basser (Basser and Pierpaoli, 1996). Registration was visually inspected for alignment at each slice and brains that appeared to not line up appropriately were removed. A voxel-wise statistical analysis was completed for both FA and MD diffusion volumes. Region of interest (ROIs) were selected, prior deformable registration, of the internal capsule (IC) as well as corticospinal tract locations in the brainstem to verify that results were not affected by the registration of larger landmarks such as the ventricles.

Immunohistochemistry

Spinal cords and brains from all animals were extracted and fixed in 4% paraformaldehyde. Using an anatomical rat brain atlas, we cut the brain to include two regions of interest for immunohistochemistry: internal capsule and medullary pyramids. Tissue was embedded with paraffin and cut into 20 micron sections using a microtome.

Histological sections that matched regions of interest on DTI maps were deparaffinized and rehydrated. Antigen retrieval was performed by microwave heating the slides for 5 minutes in sodium citrate buffer. Sections were then blocked with blocking buffer (SuperBlock, Thermoscientific, Rockford, IL) for 5 min and incubated overnight with primary antibodies against glial fibrillary acidic protein (1:250, monoclonal GFAP, MAB360, Millipore, Billerica, MA). After washing with 1x PBS, sections were incubated with goat anti-mouse conjugated Texas Red antibodies (1:250, monoclonal, Jackson ImmunoResearch, West Grove, PA) for 30 minutes. The sections were then washed, incubated with nuclear stain, DAPI (1:500, Sigma-Aldrich, St. Louis, MO) for 10 minutes and washed again. Finally, Sudan Black stain was added for 1 minute to reduce auto-fluorescence. The slides were washed and coverslipped with FluorSave (Millipore, MA). Flourescent images of the internal capsule and medullary pyramids were acquired at 20x magnification using a Nikon Eclipse E600 microscope with Nikon NIS-Elements 4.0 software. Percent expression of GFAP was measured by calculating the number of expressed pixels to regions not expressed. ROI measurements were collected in both hemispheres of the internal capsule region and pyramids in the brainstem for randomly selected rats from each severity group.

Luxol Fast Blue

Sections were stained with luxol fast blue using the method described by Kluver and Barrera (Kluver and Barrera, 1953). Cresyl violet counterstaining was not performed. Representative images were acquired using an inverted Nikon TE2000-U microscope equipped with a color digital camera at 20x. Only one rat per group was used to confirm histological changes to verify the more in-depth statistical analysis that has already been completed in previous literature (Krassioukov and Fehlings, 1999; Endo et al., 2007; Ramu et al., 2008).

Statistical Analysis

Statistical analysis was carried out using AFNI and the Statistical Package for Social Sciences (SPSS version 13.0; SPSS Inc., Chicago, IL). A one-way analysis of variance (ANOVA) was performed on a voxel by voxel basis to observe statistical variations across groups (fixed factor: injury group; random factor: specimen). Prior to voxel wise statistical tests AFNI was used to estimate how spatially smooth the data was as a starting estimate for cluster size to determine appropriate p-value. AFNI's implementation of false discovery rate algorithm was used to threshold the voxel wise statistics. Cluster threshold was completed for $F > 4.35$ and $F > 8.45$ with clusters needing to connect more than 100 voxels. A student's t-test was also completed between each severity group and $p < 0.05$ was considered to be statistically significant. The number of pixels that were significant were compared to regions of slice that were not significant as well as the number of significant pixels that fell within the brainstem and internal capsule regions of mild, moderate, and severe injured rats using Image J 1.46r (National Institute of Health, Bethesda, MD). A correlation between injury group and BBB score was also analyzed using the Spearman correlation on a voxel-by-voxel basis and thresholded for $r^2 > 0.55$.

Results

Diffusion Tensor Imaging of Brain

Diffusion tensor imaging analysis was completed for entire rat brain and brainstem. Example slice locations are shown in Figure 1. A typical RGB map of a coronal section for a sham brain at the level consistent with around 3.0 mm posterior to the bregma is shown in Figure 2. In this image, the blue voxels represent rostral to

caudal fiber orientation, green represents fiber orientations in the ventral/dorsal direction, and red fiber orientation is in the medial/lateral direction. A one-way ANOVA revealed significant effect for the MD and FA at regions consistent with the internal capsule and thalamus, denoted by voxels in green ($p < 0.05$). FA displayed a higher number of significant regions in the cortex and midbrain as seen in Figure 2. The significant regions appear to be in line with the corticospinal tract when following the highlighted regions in the three-dimensional view of the brain (Figure 3).

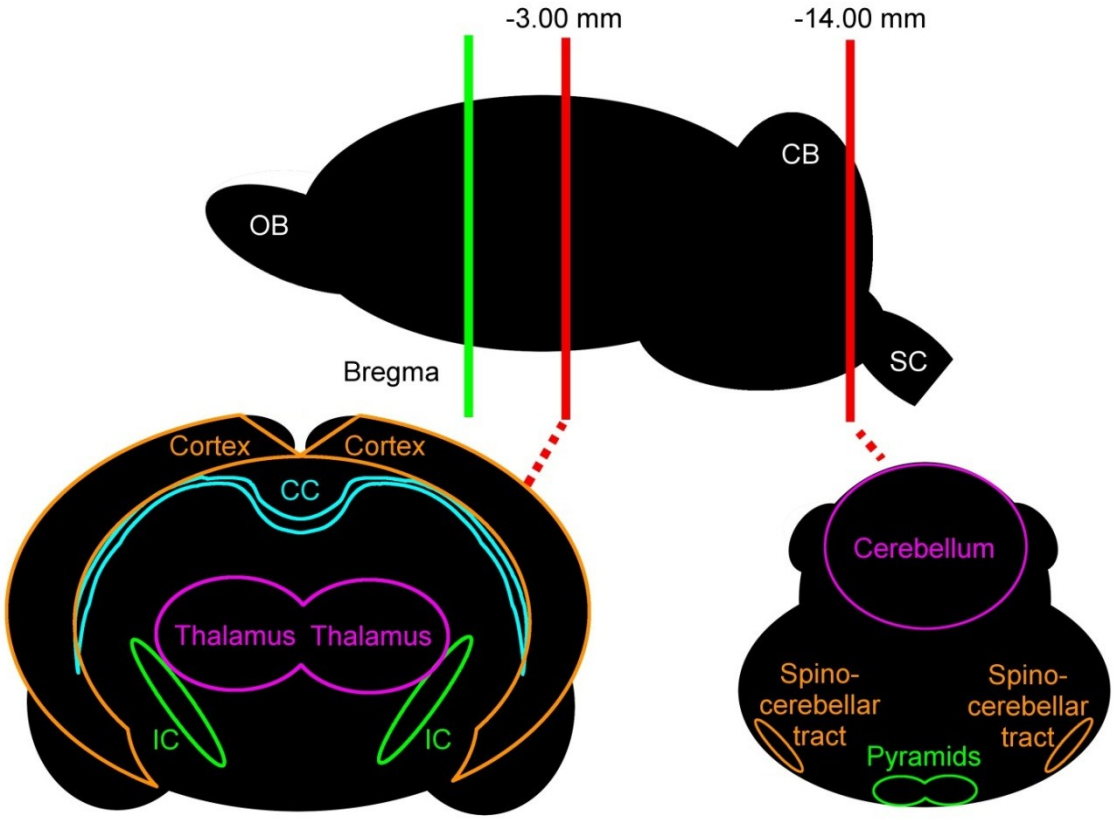

Figure 3-1: Example Slice Locations for Internal Capsule and Brainstem.

Example slice locations of the internal capsule and brainstem. The brain image containing the internal capsule was taken -3.00 mm from bregma and the brainstem slice was taken -14.00 mm from bregma. Abbreviated regions are as follows: olfactory bulbs (OB), cerebellum (CB), spinal cord (SC), corpus collosum (CC), and the internal capsule (IC).

Rat MD indices at each voxel in the brain were correlated with combined right and left hindlimb scores for each rat. Correlation values for each voxel were mapped and a threshold above r^2=0.55 was shown in regions consistent with the internal capsule in the midbrain as well as regions extending out into the cortex. The correlation for FA indices and BBB scoring did not display large enough clusters around the internal capsule region to be considered relevant at that level of threshold.

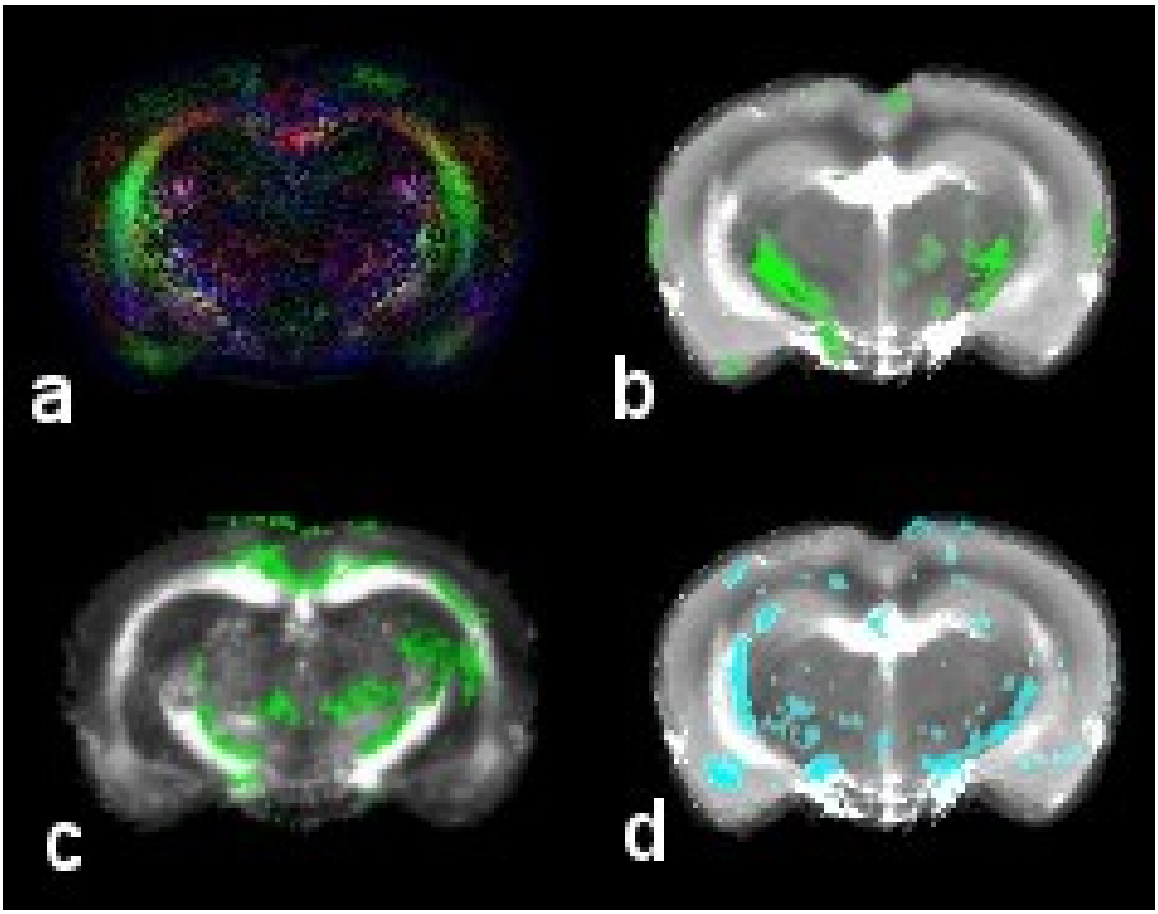

Figure 3-2: Red- Green- Blue map, Mean Diffusivity and Fractional Anisotropy F-maps, and Correlation Map for Mean Diffusivity and Basso, Beattie, and Bresnahan scoring.

Typical (a) RGB map and F-map for (b) mean diffusivity (MD), (c) fractional anisotropy (FA), and voxel wise (d) correlation map between MD and Basso, Beattie, and Bresnahan (BBB) scoring. Significant differences in variance of the severity groups are identified by green labels ($p < 0.05$) for both MD and FA. Correlation on a voxel by voxel basis between rat MD value and average hind limb motor score is presented with

stronger correlated values (r^2>0.55) identified in blue. Sections shown are located roughly 3.0 mm posterior to the bregma.

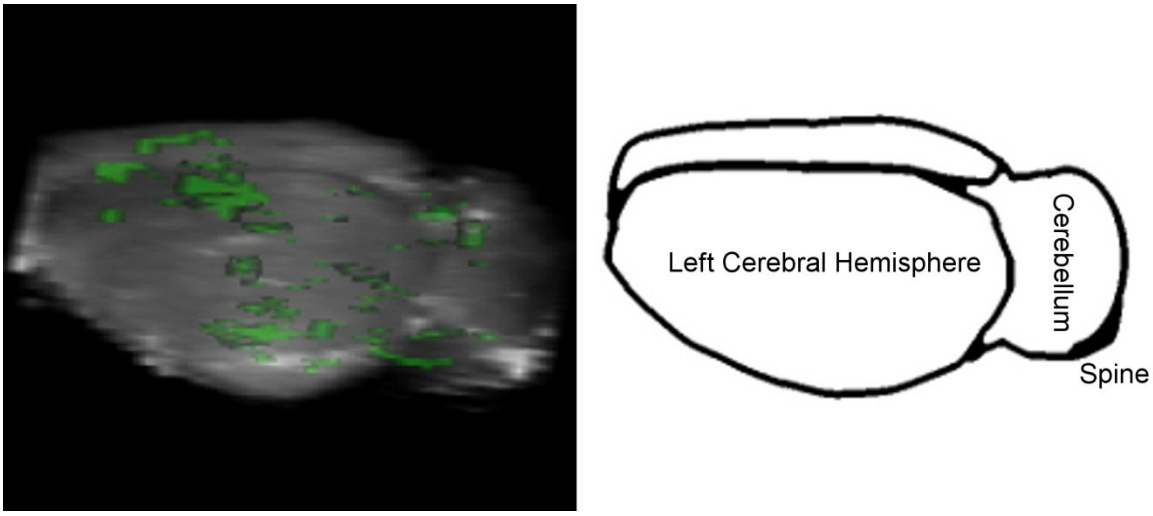

Figure 3-3: Three Dimensional Rat Brain with Significant Differences between Severity Groups

Significant differences in variance between severity groups are highlighted in this three dimensional rat brain representing mean diffusivity. Significant regions ($p < 0.05$) are denoted by the green labels.

Mean diffusion t-test comparisons between the sham brain and the mild, moderate, and severe brains are shown in Figure 4. Voxel indices representing t-values that were clustered with a $p < 0.05$ were significantly different between the sham and all three spinal cord injured groups at locations consistent with the internal capsule regions. The measured FA values in regions corresponding to the internal capsule also showed significant bilateral changes in the internal capsule regions ($p < 0.05$) indicative of a significant increase in the fiber count of the injured groups compared to the sham group.

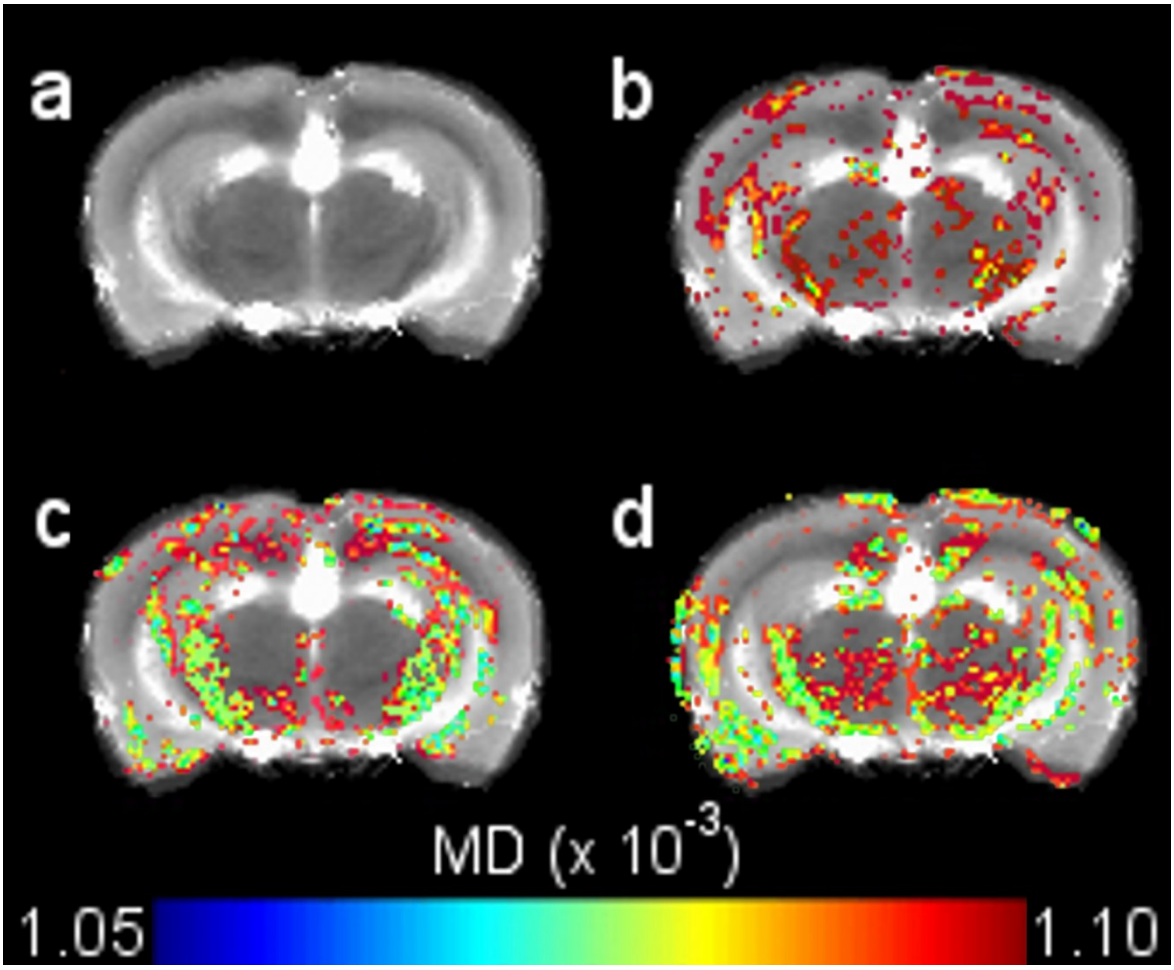

Figure 3-4: Brain Mean Diffusivity T-maps for Mild, Moderate, and Severe comparisons.

Average mean diffusivity (MD) for the (a) sham group and the differences (t-maps) between the sham brain and the brains from the (b) mild, (c) moderate and (d) severely injured rats. Sections were taken roughly 3.0 mm posterior to the bregma. Significant differences between the sham brain and the injured brain are identified by green labels ($p < 0.05$).

Diffusion Tensor Imaging of the Brainstem

In order to verify that the significant results were not just in cortical and subcortical areas, voxel wise differences were examined in the brainstem to see if changes corresponded to the corticospinal tract. The mean diffusivity t-maps highlighted significant differences between the sham group and the injury groups at regions

consistent with regions containing the corticospinal tract as seen by the cluster of green labeled voxels, representing a $p < 0.05$ in Figure 5.

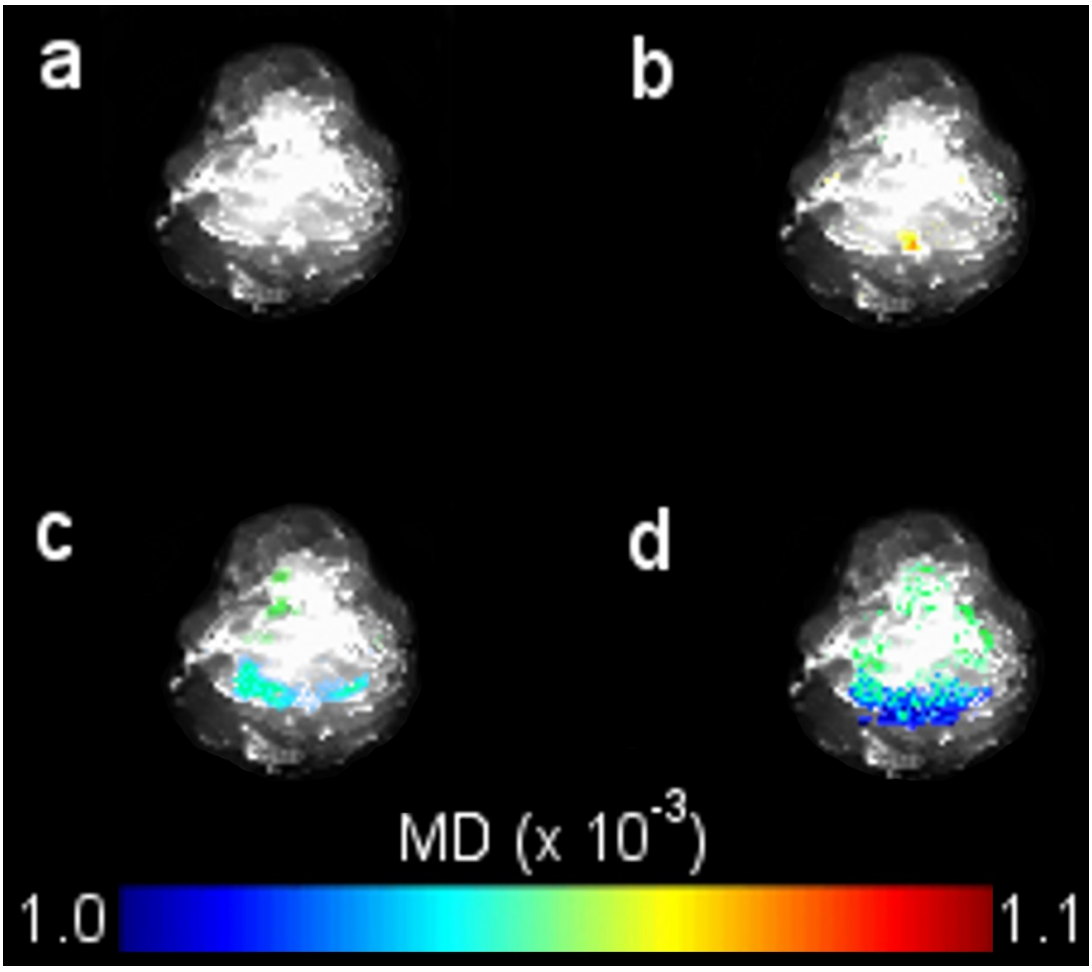

Figure 3-5: Brainstem Mean Diffusivity T-maps for Mild, Moderate, and Severe comparisons.

Average mean diffusivity (MD) for the (a) sham group and the differences (t-maps) between the sham brainstem and the brainstems from the (b) mild, (c) moderate and (d) severely injured rats. Significant differences between the sham brainstem and the injured brainstems are identified by green labels ($p < 0.05$). Sections were taken roughly 14.0 mm posterior to the bregma.

The volume of significant differences with respect to the rest of brain was also calculated for both the brainstem and the internal capsule regions of the brain (Figure

6a). The percent of that volume that was contained within the internal capsule or brainstem region was also found (Figure 6b).

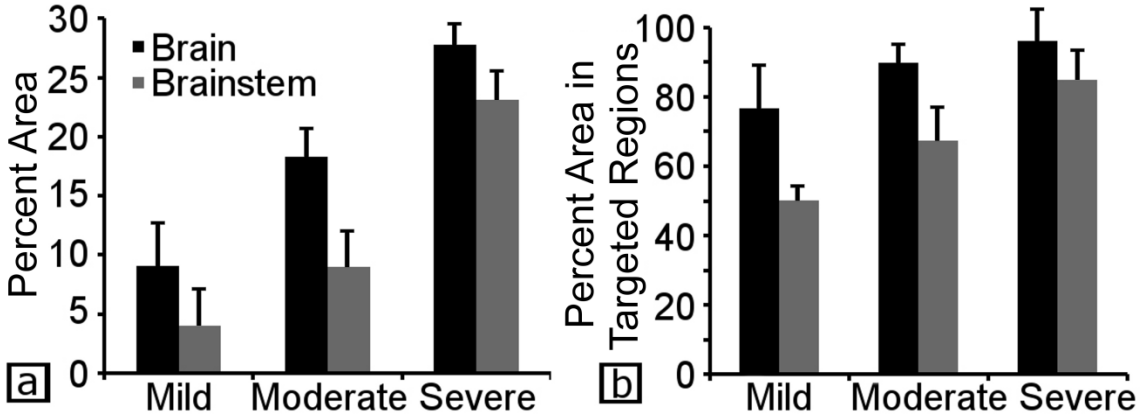

Figure 3-6: Percent Volume of Significant Voxels in Brain and Brainstem regions.

Percent volume of significant differences in both the brainstem and internal capsule was calculated for the mild, moderate, and severe groups, Figure 6 (a). Percent of volume that is attributed to either the internal capsule or the pyramidal tracts was also determined Figure 6 (b). Percent volume of significance is shown for the internal capsule and the pyramids.

Manual Region of Interest Verification

Manual ROIs of the internal capsule and the corticospinal tract in the brainstem were defined prior to group registration. Average diffusion indices for each severity group are found in Table 1. Consistent with the voxel-wise statistical results, the internal capsule regions mean diffusion of the sham group was 1.131×10^{-3} mm^2/s. The mean diffusivity for the internal capsule regions of the injured groups were 1.090×10^{-3} mm^2/s, 1.074×10^{-3} mm^2/s, and 1.076×10^{-3} mm^2/s for mild, moderate and severe injured spinal cords. There was also an increasing trend in FA, as severity increased, that matched the voxel-wise statistical analysis. The sham group's average FA was 0.304 while the mild, moderate, and severe groups were 0.348, 0.352, and 0.395, respectively. MD and FA

ROI's of the whole sham brain were not significantly different than the other severity groups ($P > 0.05$).

Table 3-1: Average Manual Region of Interest Selections of Internal Capsule and Brainstem

	Sham	Mild	Moderate	Severe
FA(IC)	0.304(±0.05)	0.348 (±0.06)	0.352 (±0.11)*	0.395 (±0.07)***
MD (IC)	1.131 (±0.03)	1.099 (±0.02)*	1.074 (±0.06)*	1.076 (±0.01)**
FA (CS)	0.424 (±0.03)	0.529 (±0.11)	0.550 (±0.08)	0.574 (±0.09)
MD (CS)	1.260 (±0.01)	1.058 (±0.01)*	1.045 (±0.00)**	0.950 (±0.00)**

Average (and standard deviation) of MD and FA for the internal capsule (IC) and corticospinal tract (CS) regions found in the sham, mild, moderate, and severe injured rats. Mean diffusivity measurements represented as x 10^{-3} mm^2/s. Significant differences found between the sham group and the mild, moderate, and severe group are denoted * for $p < 0.05$, ** for $p < 0.01$, *** for $p < 0.001$.

Immunohistochemical Characteriziation

Immunohistochemical staining for two brains for each severity group was completed following ex vivo imaging. A coronal section of tissue, 3.0 mm posterior to the bregma, was selected to compare the locations of significant difference between the sham brain and the injury brains (Figure 8). Severely injured animals expressed less GFAP compared to the sham brain in the internal capsule region. Mild and moderate GFAP expression was not as drastic as the severe rats for the brainstem (Figure 9) and internal capsule (Figure 9).

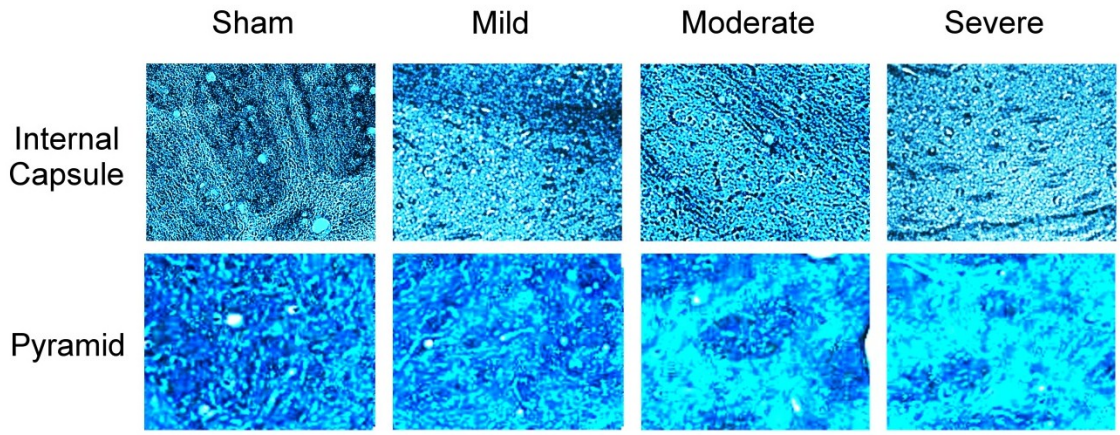

Figure 3-7: Histological Staining of Sham, Mild, Moderate, and Severe White Matter regions using Luxol Fast Blue.

Histological examples of un-injured vs injured (left to right) luxol fast blue stain for myelin in the internal capsule (top row) and the pyramids (bottom row). There is less staining in the white matter as the severity of injury increased which is more evident in the pyramid location in the brainstem.

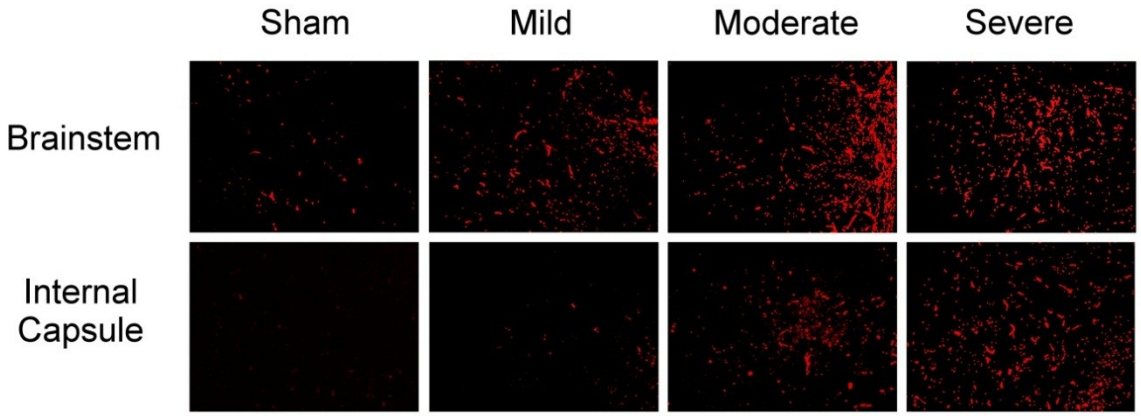

Figure 3-8: Representative Glial Fibrillary Acidic Protein Stain of Brain and Brainstem for Sham, Mild, Moderate, and Severe Groups.

Representative glial fibrillary acidic protein (GFAP) immunohistochemical stain for sham, mild, moderate, and severe animal brains in the brainstem and internal capsule regions. Sections sliced approximately 3.0 mm posterior to the bregma. As the severity increases, there is an increase in expression of GFAP.

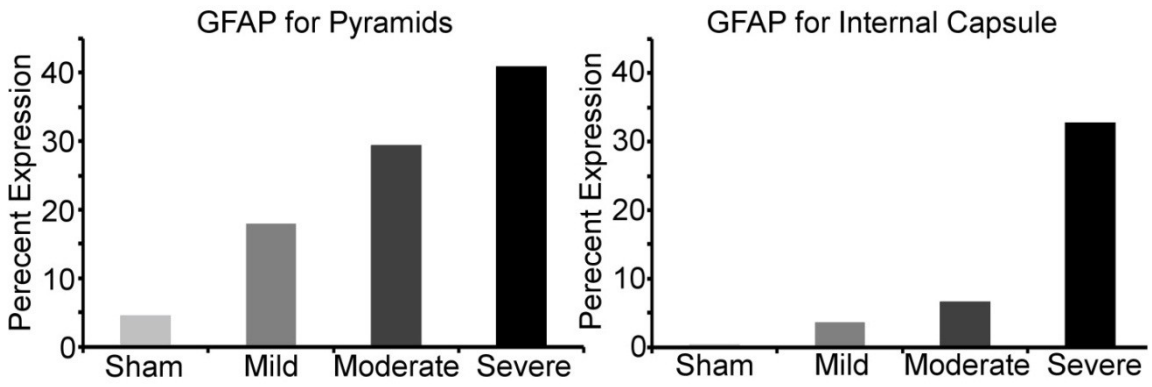

Figure 3-9: Percent Expression of Glial Fibrillary Acidic Protein immunohistochemical Stain in Brain and Brainstem.

Percent expression of the immunolabeled GFAP in the Pyramids. There is an increasing trend in the density for the GFAP in the injured rats when compared to the sham group (left). Also shown is percent expression of the immunolabeled GFAP in the Internal Capsule (right). There is an increase in the density for the GFAP in the severe group when compared to the sham group.

Discussion

The results from this study indicate that diffusion tensor imaging is capable of detecting the subtle structural changes that occur in brain following a spinal cord injury. Rat brains with a sham, mild, moderate, or severe contusion spinal injury were scanned ex vivo ten weeks after injury in order to characterize how internal structures of the brain vary with injury severity. Automatic voxel based statistical analysis was completed and verified through manual selection of ROIs. Following DTI, histological analysis verified structural locations associated with imaging results. Diffusion indices indicated structural changes to the corticospinal tract and internal capsule regions in the brain and brainstem that correlated ($r^2 > 0.55$) with a decrease in motor function associated with injury severity.

Interpreting findings in the brain

We observed a strong separation between group variances ($p < 0.05$) for both MD and FA. Results demonstrate significant bilateral findings in the internal capsule region of the brain. Ramu et al. and Freund et al. have both shown unilateral diffusion findings in the internal capsule (Ramu et al., 2008; Freund et al., 2012). We believe that both studies were limited by the sample size examined. The corticospinal tract descends through both left and right hemispheres into the spine and an injury to the spine that results in sensorimotor dysfunction for all body parts below the lesion would impact both the left and right internal capsule regions. Our study confirmed these results by demonstrating structural changes in left and right internal capsule regions.

A decrease in mean diffusion in the internal capsule region was associated with damaged hind limb motor function. Previously our lab has found MD to decrease in the spinal cord around the site of injury and extending rostral and caudal to the injury (Ellingson 2008). We have also found that the decrease in mean diffusivity correlates to injury severity (Manuscript in preparation). Diffusivity measurements are sensitive to microstructural changes that occur following damage to neurons (Beaulieu 2002, Schwartz and Hackney 2003) and damage to the spinal cord axons have resulted in functional reorganization of the motor regions in the brain(Crawley et al., 2004; Ghosh et al., 2009; Sydekum et al., 2009). These studies demonstrated changes in functional activation size in the higher cortex regions such as the somatosensory and motor cortex regions after a spinal cord injury occurs. It is believed that the regions of the brain associated with motor planning and movement experience higher glucose metabolism in patients with SCI (Roelcke et al., 1997) as well as decreases in myelin and neurofilaments that are detectable with DTI (Ramu et al., 2008). The molecular change in the brain is thought to be attributed to either the reorganization of the structures in the

brain based on synaptic plasticity in existing circuits and the organization of new circuits from axonal sprouting (Raineteau and Schwab, 2001). These mechanistic changes are seen to occur in cortical, subcortical and spinal systems.

Diffusion characteristics in the brainstem

Our study demonstrated a decrease in the diffusion of water in regions of the brainstem associated with the corticospinal tract and an increase in the fractional anisotropic index in corresponding regions. Mean diffusion for sham rats were significantly different than the moderate and severe groups in the corticospinal tract regions of the brainstem ($P < 0.05$). Weishaupt et al. found that cytotoxic inflammation as a result of damage to the motor cortex occurred in regions of Wallerian degeneration extending down through the spinal cord in connected axons (Weishaupt et al., 2010). Also following a thoracic lesion in the rat, additional sprouting of descending fibers from the midbrain rostral to a thoracic lesion occurs (Raineteau and Schwab, 2001). These results suggest that damage to both ascending and descending tracts anywhere in the CNS will impact both the brain and spinal cord.

Manual region of interest selections verified the findings found through the voxel-based statistical analysis. Few research groups have focused on the internal capsule region for changes induced by the spinal cord (Ramu et al., 2008; Freund et al., 2012). The proximity to the lateral ventricles provide a potential problem for registering multiple brains, and although the registration techniques we used provided excellent alignment upon visual inspection for most slices of the brain, we chose to perform additional manual ROIs for each rat brain to eliminate the possibility of registration interference with the voxel based statistical approach. Mean diffusion in the sham brain was significantly different than the mild ($p < 0.05$), moderate ($p < 0.05$), and severe ($p < 0.01$) internal capsule regions in the brain and corticospinal tract region ($p < 0.05$, $p < 0.01$,

respectively) in the brainstem. Fractional Anisotropy of the sham brain was significantly different than the moderate and severe brains ($p < 0.05$ and $p < 0.001$, respectively) but not of the corticospinal tract in the brainstem regions. FA of the corticospinal group in the injured spinal cord groups did trend towards increasing with severity, though the results were not significant in the manual ROIs. In order to determine that the changes in water diffusion were specific to certain locations and not an overall brain change, whole brain ROIs were completed. MD and FA of the whole sham brain were not significantly different than the other severity groups ($p > 0.05$). Similar findings in the manual ROIs demonstrated findings similar to those found in the registration technique, verifying that the voxel based alignment found provides a sufficient method for statistical analysis.

Immunohistochemical Comparison

The findings of this study were confirmed though immunohistochemistry. Histological staining confirmed differences in expression of injured rats compared to control group. These findings confirm previous quantitative findings by other groups (Krassioukov and Fehlings, 1999; Endo et al., 2007; Ramu et al., 2008). Changes in MD and FA were associated with a decrease in myelin and an increase in astrocytes for the internal capsule region in the brain and the corticospinal tract regions of the brainstem. Ramu et al. also demonstrated an increase in GFAP and reported a lower percentage of MBP in the internal capsule (Ramu 2008). Our results indicated that there was a progressive reduction in myelin in the internal capsule as severity of injury increased for luxol fast blue staining. GFAP showed a similar trend with increases in the GFAP expression as injury severity increased.

Study Limitations

While animal models allowed for a more detailed examination of biological tissue through immunohistochemistry and ex vivo DTI, a detailed quantitative analysis was not completed for histological staining. However, histological comparisons between myelin degradation and astrocytic expression of spinal cord injured rats have already been shown in the brain. The end goal of this research would be to translate these results into a clinical benefit. One potential limitation to this study relates to the longer scan time used to acquire images. Although the diffusion metrics resulted in significant changes with respect to injury severity, a thorough investigation with short tolerable scan times in human patients with SCI would better characterize the capabilities of DTI. Our study used a multi-echo spin-echo sequence and the results of this study would benefit from utilizing a multi-shot echo planar imaging technique that would allow for faster acquisition. Furthermore, the use of faster imaging techniques allow for the acquisition of more directions, averages, or larger acquisition sizes, which in turn provide significantly higher image quality.

Finally, although our results showed significant changes in MD and FA of the internal capsule and corticospinal tract, a more detailed look into the longitudinal and transverse apparent diffusion coefficients would provide a deeper understanding of intracellular and extracellular water volume changes, axon count, and neurofilament densities (Song 2003, Schwartz 2003).

Conclusion

We have demonstrated that a traumatic SCI results in structural modifications in the brain that are dependent on the level of severity. Through voxel based statistical analysis and manual ROI selections, our results indicated that DTI of the brain is

sensitive to varying injury severity following SCI. Diffusion of water in regions associated with tracts that descend into or ascend from the spinal cord are associated with severity of injury. Our results from immunohistochemistry demonstrate that the structural changes in the internal capsule and regions of the corticospinal tract had an increase in the astrocytic response and myelin degradation around the axons that were affected from the SCI. Results from this study support the hypothesis that DTI of the rat brain is a non-invasive medical imaging technique that is sensitive to injury severity occurring in remote regions of the spinal cord.

CHAPTER 4

DIFFUSION TENSOR IMAGING IS SENSITIVE TO NEURONAL STEM CELL TREATMENTS

Introduction

Imaging provides a possible means to noninvasively monitor changes in spinal cord tissue after cellular transplant interventions to treat spinal cord injury (SCI). In particular, diffusion tensor magnetic resonance imaging (DTI) characterizes the changes to tissue structure based on the anisotropy of water diffusion in spinal tissue. DTI is sensitive to changes in water diffusion associated with injury in both the acute (Loy et al., 2007; Kim et al., 2010, 2011; Yin et al., 2010) and chronic stages of SCI (Schwartz, Duda, et al., 2005; Ellingson, Ulmer, et al., 2008; Guleria et al., 2008; Sundberg et al., 2010). For example, directional diffusivities correlate to changes in axon count, myelin volume, intracellular and extracellular water volume (Schwartz and Hackney, 2003) as well as microfilament and neurofilament densities (Song et al., 2002). Sensitivity to changes in the cellular microstructure makes DTI an appealing tool for non-invasively monitoring the effect of cellular transplants in the spinal cord, which themselves are designed to produce structural changes that improve spinal cord function (Keirstead et al., 2005; Lu et al., 2007).

In order to help ameliorate the insufficient recovery process of the central nervous system (CNS) and improve the cellular microstructure environment, current research has focused on the delivery of therapeutic interventions such as the transplantation of stem cells into the spinal cord or the elicitation of endogenous stem cells (Sieber-Blum, 2010). The differentiation of NSCs into neurons, astrocytes, and oligodendrocytes provides an environment filled with cells that mediate repair, help remyelinate axons, increase axon regeneration, and provide neuroprotection and trophic

support during recovery (Gage, 2000; Lindvall and Kokaia, 2006; Martino and Pluchino, 2006; Thuret et al., 2006) but have also been shown to increase forelimb allodynia following transplantation. In addition to cell differentiation the immortalized cell line, C17.2, has demonstrated that the differentiated neurons were able to form synapses with other cells (Snyder et al., 1992) and that the line showed production for up to a year after injection (Snyder et al., 1995) . However, rats given C17.2 cells were hypersensitive in regions outside the injury site, with astrocytic sprouting occurring in the dorsal horns of the rat cervical cord. Although there have been groups that have tried to diminish the astrocytic sprouting through the use of transduced NSCs with neurogenin-2 (Hofstetter et al., 2005) or transfecting NSCs with glial derived neurotrophic factor (GDNF) (Macias et al., 2006), the basic structural changes that occur from the stem cells provides an excellent platform for trying to non-invasively examine the changes that occur after cell transplantation with DTI.

Following cell injection current research relies on basic neuroimaging techniques to track the stem cells and monitor the success of the transplantation. Monitoring the progression of the stem cells after injection as they travel to target regions is done by tagging the transplant cells with magnetic isotopes and using magnetic resonance imaging (Magnitsky et al., 2005; Brekke et al., 2007; Moraes et al., 2012; Vande Velde et al., 2012). However, the stem cells may arrive in the correct region but it can be difficult to tell if cellular reactions are taking place. Kang et al. was able to confirm expansion in a crushed spine following transplantation of stem cells using T2-weighted images (Kang et al., 2005). The diffusion of water has been shown to be associated with white matter regeneration following the injection of neural progenitor cells in stroke (Jiang et al., 2006) as well as decreased diffusion in axonal tracts associated with axonal regrowth following the injection of fibroblast transplants (Schwartz, Chin, et al., 2005) and autoimmune T cells (Nevo et al., 2001). The changes axonal structure found through changes in water

diffusion from these cell types suggest that neuronal stem cells that derive into cells specific to the central nervous system will impact the diffusion of water in a similar way.

In this study, we sought to determine whether DTI was sensitive to spinal cord tissue changes that accompany stem implants. We hypothesized that non-invasive measures of DTI detect structural changes in the cervical region of the spinal cord that occur after the transplantation of C17.2 NSCs at a lower thoracic (T8) contusion injury site. Our rationale for choosing the cervical imaging site was based on previous studies that have documented allodynia of the forepaws and evidence of tissue structural changes in the cervical spinal cord. Specimens were imaged at multiple time points up to 10 weeks in vivo and then imaged ex vivo to capture the temporal effects of stem cells on the anatomical structure. Rats were tested for motor and sensory function, and end of life histology was examined. Image data were compared to a sham injury control and injury with injections of control substances.

Methods

This study consisted of a spinal contusion injury, injection of stem cells or controls, and survival for 10 weeks in a rat animal model. Sensory and motor tests were conducted over the course of the study and DTI was performed both in vivo and ex vivo. Structural changes were documented with immunochemical staining for CGRP and GAP43. The study protocol was approved under the guidelines of the Institutional Animal Care and Use Committees (IACUC) at Marquette University, the Medical College of Wisconsin, and the Zablocki VA Medical Center.

Spinal Cord Injury

A spinal contusion injury was produced in forty female Sprague-Dawley rats (200-250 grams) for this study. Rats were anesthetized prior to surgery using a 2-3% isoflurane and oxygen mixture. Animals were then placed in the prone position and an incision was made over the mid thoracic region. Following incision, laminectomies were performed over the T7-9 vertebral levels and a moderate contusion injury was delivered using the MASCIS impactor (W.M. Keck Center for Collaborative Neuroscience; Piscataway, NJ) with a 10 gram rod dropped from a height of 25 mm directly onto the dura. The sham group (n=10) only received laminectomies without SCI. Post-operative regimen consisted of one dose of enrofloxacn (10 mg/kg subcutaneously; Bayer Healthcare LLC; Shawnee Mission, KS), Buprenorphine hydrochloride (0.1-0.5 mg/kg subcutaneously; Reckitt Benckiser Health Care Ltd; Hull, UK) as needed, 6 cc of lactated Ringers solution subcutaneously, and manual bladder expression twice a day.

Cell Transplantation

Spinal cord injections were made one week after injury. Rats were re-anesthetized using the same procedure used when producing the spinal injury and the contusion site was re-exposed for stereotactic injection. Rats were randomized into 4 groups to receive no transplant injection (n=10, sham group), sterile phosphate buffered saline (PBS, n=10), sterile PBS with 50 mg/kg of the immunosuppressant drug Tacrolimus (Prograf; n=10; Mylan Pharmaceuticals Inc; Canonsburg, PA), or C17.2 neural stem cells (NSCs) with Prograf (n=10).

Neural Stem Cell Line

The NSC line C17.2 was used for the transplant group. Our laboratory previously established and cryopreserved this cell line for transplantation studies (Macias et al., 2006). Prior to surgery, cells were counted using the Trypan Blue exclusion method and plated at 1 x 10^6. Cell harvesting was done with Trypsin and washed with Dulbecco's Modified Eagle's Medium (Life Technologies; Grand Island, NY containing fetal bovine serum and high glucose. Cells were then washed with sterile phosphate-buffered saline (PBS) (pH 7.4), counted using trypan blue, centrifuged, and resuspended at 1 x 10^5 cells/20 µl in sterile PBS. The cell suspension was placed on ice and gently titrated before each injection. Transplant injections were delivered stereotactically into the spinal cord under microscopic visualization at four injection sites: 1 mm rostral and 1 mm caudal to the injury site, as well as on either side of the midline. The surgical site was closed in layers and animals received post-operative care as described above.

Behavioral Testing

Animals were tested on a weekly basis for locomotor function, thermal stimulation response, and mechanical stimulation response. The Basso, Beattie, and Bresnahan (BBB) scoring was used to evaluate locomotor function by placing the rats on a flat surface, one meter in diameter, and evaluating the hind limb function of the rat for 3 minutes (Basso et al., 1995). Rats were then scored between 0, being flaccid paralysis, and 21, representing normal gait. Thermal response was measured by placing the rats on a hot plate of 55˚C and measuring the latency of forelimb and hindlimb paw withdrawal to heat. Animals that did not respond after 60 seconds were removed from the hot plate. Mechanical stimulation was recorded by measuring the number of withdrawal responses to forelimb and hindlimb paw to Von Frey testing. Ten

applications, randomly applied among the four paws for 3.92 mN, 9.8 mN, and 254.9 mN filaments, were delivered at 3 second intervals.

In Vivo Diffusion Tensor Imaging

In vivo imaging was performed at 2, 5, and 10 weeks following SCI. Magnetic resonance images were collected using a 9.4 T Bruker BioSpec 94/30 USR Spectroscopy Imaging System (Bruker BioSpin; Billerica, MA). Radio frequency signals were transmitted and received using a quadrature coil (Doty Scientific; Columbia, SC). Animals were anesthetized with an isoflurane (1-1.5%) and oxygen mixture and placed in the supine position inside the scanner. Core body temperature was maintained with a circulating warm water (37˚C) pad and MR images were respiratory-gated to avoid breathing artifacts.

Twelve equally spaced diffusion weighted directions were collected using a spin echo sequence with a TE of 25.11 ms and a TR $\geq$ 600 ms (reliant on respiratory rate). The images were acquired with a b = 500 s/mm^2, number of excitations (NEX) = 2, field of view (FOV) = 40 mm^2, and an acquisition matrix of 128 x 128. Two diffusion sensitizing images with a b-value of 0 s/mm^2 were acquired. Three images with a 2 mm slice thickness and a 1 mm interslice gap was acquired over the cervical segments C6 through T1. This region of the spinal cord was selected because changes in histology, along with behavioral changes in the forepaws have been associated with these spinal segments after cell transplant (Macias et al., 2006).

Ex vivo DTI

Following the 10 week *in vivo* scan, animals were euthanized with sodium pentobarbital (100 mg/kg body weight) and perfused with 300 mL of saline buffer followed by 600 mL of 10% formalin. Spinal cords were dissected and post-fixed in 10%

formalin. Ex vivo DTI images of the extracted cords were obtained on the same scanner that was used for in vivo imaging. On the day of scanning, the spinal cords were embedded in agarose gelatin following the protocol of Ellingson et al. (Ellingson, Kurpad, et al., 2008a). Six diffusion weighted images were collected using a spin echo imaging sequence with a TE of 27.3 ms and a TR of 6250 milliseconds. The images were collected with a FOV of 70 mm^2, NEX of 2, and a matrix size of 512 x 512. Diffusion images were acquired with a b of 500 s/mm^2 and two T2-weighted images (b = 0 s/mm^2). A total of 25 slices were obtained with a 2 mm slice thickness and a 1 mm interslice gap over the entire spinal cord.

Diffusion Tensor Data Analysis

Calculation of the diffusion tensor was conducted using AFNI (http://afni.nimh.nih.gov/afni). Raw image files were imported into AFNI and the diffusion weighted images were co-registered to the T2-weighted images using an interative weighted least squares fit method. Following registration, the tensor estimate was found using AFNI and the resulting eigenvalues were used to calculate fractional anisotropy (FA, defined by Basser et al. (Basser and Pierpaoli, 1996)), mean diffusivity (MD, average of all three eigenvalues), longitudinal apparent diffusion coefficient (lADC, primary eigenvalue) and transverse apparent diffusion coefficient (tADC, average of the second and third eigenvalues).

Regions of interest (ROIs) were manually selected from each axial slice for both in vivo and ex vivo images. Using MATLAB (Mathwords, Natick, MA), ROIs of the entire cord encompassing both white and gray matter regions, were traced for each axial slice.

Immunohistochemistry

Following ex vivo imaging, two spinal cords per group were randomly selected for immunohistochemistry. The C6-T1 region of the spinal cord was identified and resected for fluorescent staining. C6-T1 regions were selected because allodynia of the forepaws and cytoarchitectural changes in these regions are observed in specimens with spinal implants of C17.2 cells (Oku et al., 1987; Snyder et al., 1992). Immunohistochemistry was performed using a previously described protocol (Macias et al., 2006). Tissue samples were post-fixed in 4% paraformaldehyde/PBS at 4˚C for an hour, frozen in OCT compound (Sakura Finetek U.S.A., Inc.; Torrance, CA) and stored in -80C until sectioning. Tissue was sectioned into 20 μm slices using a Leica CM3050 S cryostat (Leica Microsystems Inc.; Buffalo Grove, IL) and placed on vectabond coated slides.

Tissue sections were allowed to thaw for one hour before incubating in primary antibodies. The sections were double labeled with a 1:1000 polyclonal CGRP (Chemicon International Inc.; Temecula, CA) and 1:1000 monoclonal GAP43 (Chemicon) followed by a wash and then incubated with a 1:500 diluted goat anti-mouse conjugated fluorescein isothiocyanate (FITC) (Jackson ImmunoResearch Inc.; West Grove, PA) and a 1:500 diluted Alexa Fluor 594 goat anti-rabbit (Invitrogen Corporation; Carlsbad, CA). All sections were counterstained with a 1:500 dilution of the non-specific nuclear staining with DAPI (Sigma-Aldrich Co; St. Louis, MO) and then imaged on a Nikon Eclipse E600 microscope equipped with a Nikon Digital Sight D5-U3 color camera at 40x magnification. Cell counts were completed using ImageJ (National Institute of Health, Bethesda, MD).

Dorsal horn densitometry was measured by the optical density (OD) of the dorsal horn region subtracted by the OD of the background. Images of immunolabeled sections

were converted to gray scale (0 – 255) representing black to white intensity values and ImageJ was used to determine the resulting OD for each rat around laminae II-IV for slices in the C6-T1 vertebral segments.

Statistical Analysis

Statistical analysis was performed using the Statistical Package for Social Sciences (SPSS version 13.0; SPSS Inc., Chicago, IL). Statistical significance was determined using a repeated measure one-way analysis of variance (ANOVA; fixed factor: transplant group; random factor: specimen) followed by Fisher's post hoc test for hot plate and Von Frey sensory data as well as the dorsal horn cell count measurements. BBB scoring used a one-way ANOVA followed by non-parametric Kruskal-Wallis and Friedman's rank tests with a level of significance $\alpha = 0.05$. Diffusion metric values were averaged at each slice for each specimen and then averaged across specimens. A two-way, repeated measure, ANOVA (fixed factors: transplant group and slice location (C6-T1; random factor: specimen) was also completed.

Results

Behavioral and sensory tests

The hind limb motor function (BBB score) of the rats that received PBS, PBS and Prograf, or the C17.2 NSC transplants was significantly reduced compared to the sham group for weeks 2 through 10 post surgery ($p < 0.01$). As shown in Figure 1, the rats that received an injection were not significantly different than each other ($p > 0.05$). The sham group resulted in no loss of motor function for the recorded weeks.

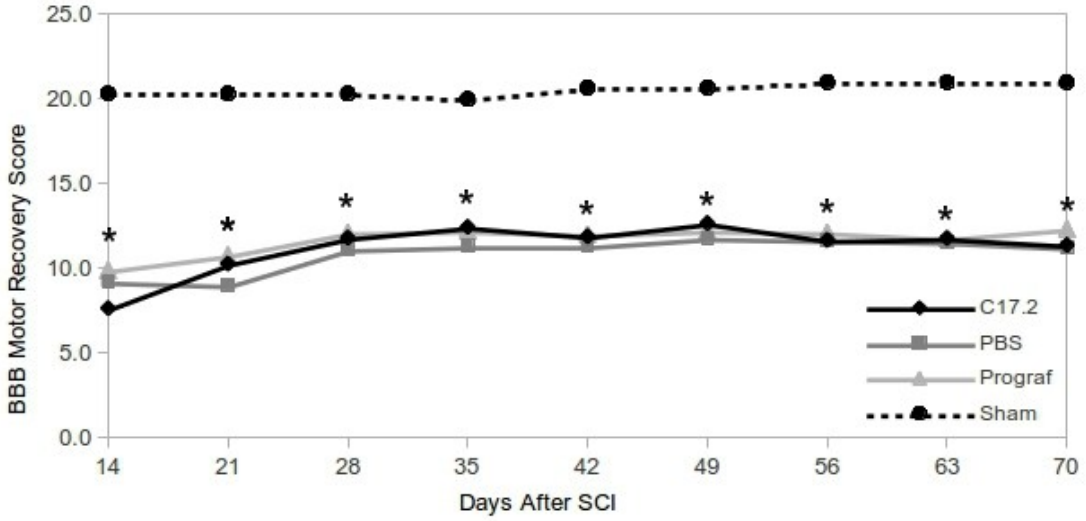

Figure 4-1: Basso, Beattie, and Bresnahan Scoring for Ten Weeks after a Moderate Spinal Cord Injury.

Basso, Beattie, and Bresnahan (BBB) scoring from 2 weeks after a moderate spinal cord injury. Treatment groups start at 1 week post-injection with no transplant solution, normal saline, normal saline with the immunosuppressant Prograf, and C17.2 NSC treatment with Prograf. Sham injury shows showed no motor deficits throughout the course of the 10 weeks. Data are presented as combined hindlimb means. All treatment groups had a significant reduction in hind limb motor capabilities compared to sham (* = $p < 0.01$), but not to each other ($p > 0.05$).

Rats that received the transplanted cells demonstrated a decrease in the withdrawal latency following thermal stimulation to the forelimbs. Following injections, the PBS and Prograf groups had significantly longer withdrawal times than the sham group ($p < 0.05$) but not significantly different than each other. As shown in Figure 2, the PBS and Prograf groups were not significantly different from each other ($p > 0.05$) but were significantly different than to the rats that received the NSC C17.2 transplants ($p < 0.05$) at weeks 3 through 6, as well as at weeks 9 and 10. Withdrawal latency decreased post injection from 8 seconds to 4 seconds, in the rats that received the stem cells over the 8 weeks of sensory recording.

There were no significant differences in response to mechanical stimulation in the 4 groups of rats and thus are not shown.

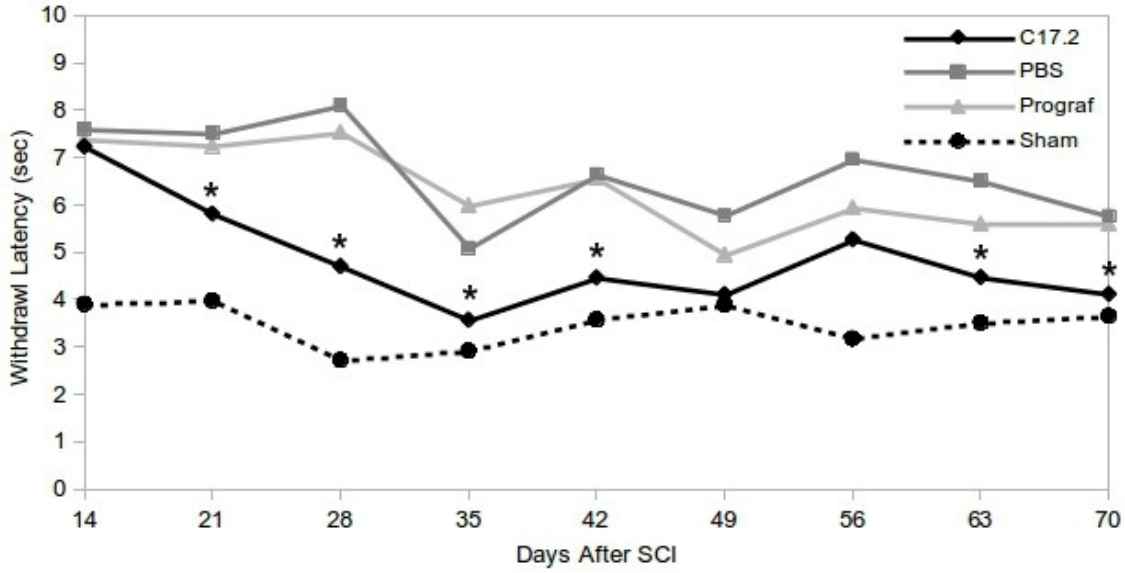

Figure 4-2: Behavioral Response to Thermal Stimulation over Ten Weeks.

Mean rat forelimb behavioral responses to a thermal stimulation of 55˚C. C17.2 NSC transplant group showed a significantly reduced heat tolerance at 3-6, 9, and 10 weeks ($p < 0.05$) in comparison to PBS and Prograf injection groups.

Diffusion tensor imaging of the cervicothoracic region

Diffusivity was quantified by selecting ROIs that encompassed transverse slices through the spinal cord (Figure 3). Rats that received the NSC C17.2 transplant showed significantly different diffusion values compared to the control groups ($p < 0.05$) in multiple time points for MD, lADC, and tADC (Figure 4). Fractional anisotropy for all time points did not indicate that the cell line was significantly different than the control groups ($p > 0.05$). Mean diffusivity showed that at weeks 5 and 10, and in the ex vivo scans that there was a significant increase in the diffusion of water when compared to the control groups ($p < 0.05$). The diffusion in the longitudinal direction (lADC) was also significantly

greater in weeks 5, 10, and ex vivo time points ($p < 0.05$). The diffusion of water through the cord became significantly greater for the rats that received the C17.2 line than the control rats at week 10 and held a significant result for the ex vivo scans ($p < 0.05$).

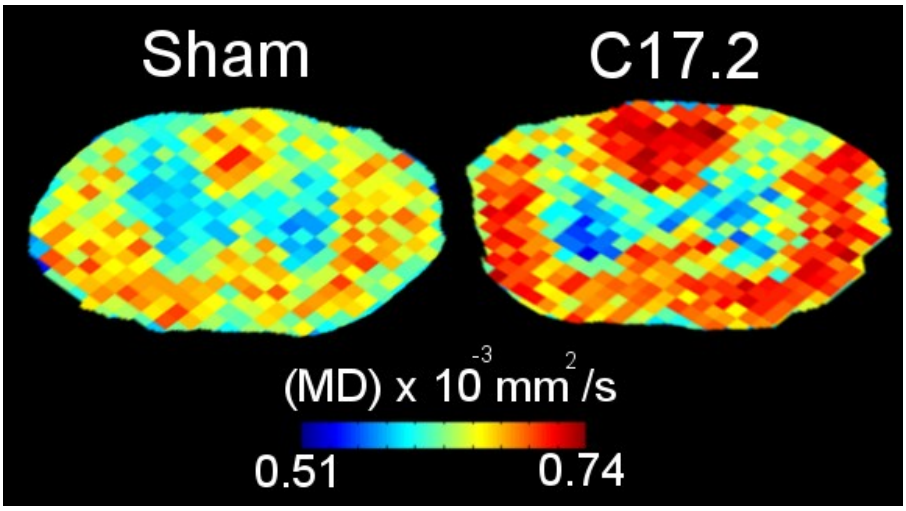

Figure 4-3: Representative Region of Interest Selection for Mean Diffusivity in Sham and Transplant Cell Group.

Representative images of mean diffusivity (MD) from a rat that received no cell transplant (left) and a rat that received the C17.2 cell transplant line (right). Segments were taken at the C7 vertebral segment for both rats and were taken ex vivo, 10 weeks after injury.

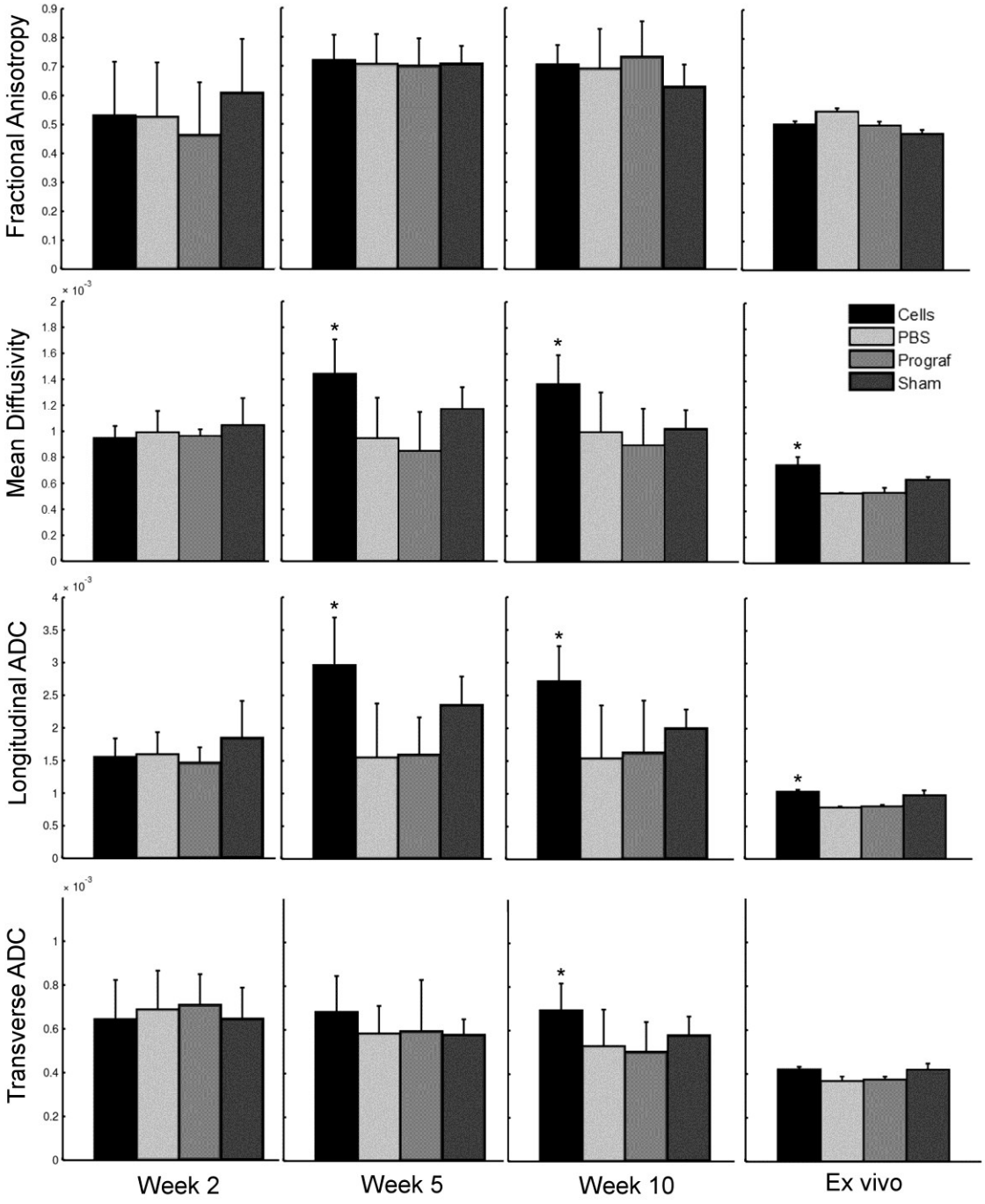

Figure 4-4: Fractional Anisotropy, Mean Diffusivity, Transverse Apparent Diffusion Coefficient, and Longitudinal Apparent Diffusion Coefficient for Two, Five, and Ten Weeks *In Vivo* and Ten Weeks *Ex Vivo*.

In vivo diffusion tensor imaging (DTI) values for weeks 2, 5, 10 as well as ex vivo imaging. Fractional anisotropy (FA), mean diffusivity (MD), longitudinal apparent diffusion coefficient (lADC), and transverse apparent diffusion coefficient (tADC) are shown for each time point. The C17.2 NSC transplant group had a significantly higher

MD at weeks 5, 10, and ex vivo scans compared to controls ($p < 0.05$). lADC showed a significantly higher rate of diffusion at week 5 ($p < 0.05$), and both lADC and tADC showed a significantly higher rate of diffusion at weeks 5 and 10 as well as the ex vivo scans.

Immunohistochemical Characterization

The C17.2 NSC group showed axonal sprouting in the dorsal horn (laminae I-III) in the cervicothoracic (C7-T1) region (Figure 5). On the same image, this region also showed an increase in CGRP and GAP43 immunoreactivity. The C17.2 NSC group showed greater co-localization of CGRP with GAP43 in laminae I-III, as compared to the other groups.

Densitometry results from the immunolabeling of CGRP, GAP43 and the nuclear DAPI stain resulted in a significantly greater density ($p < 0.001$) in laminae II – IV when compared to the other groups (Figure 6).

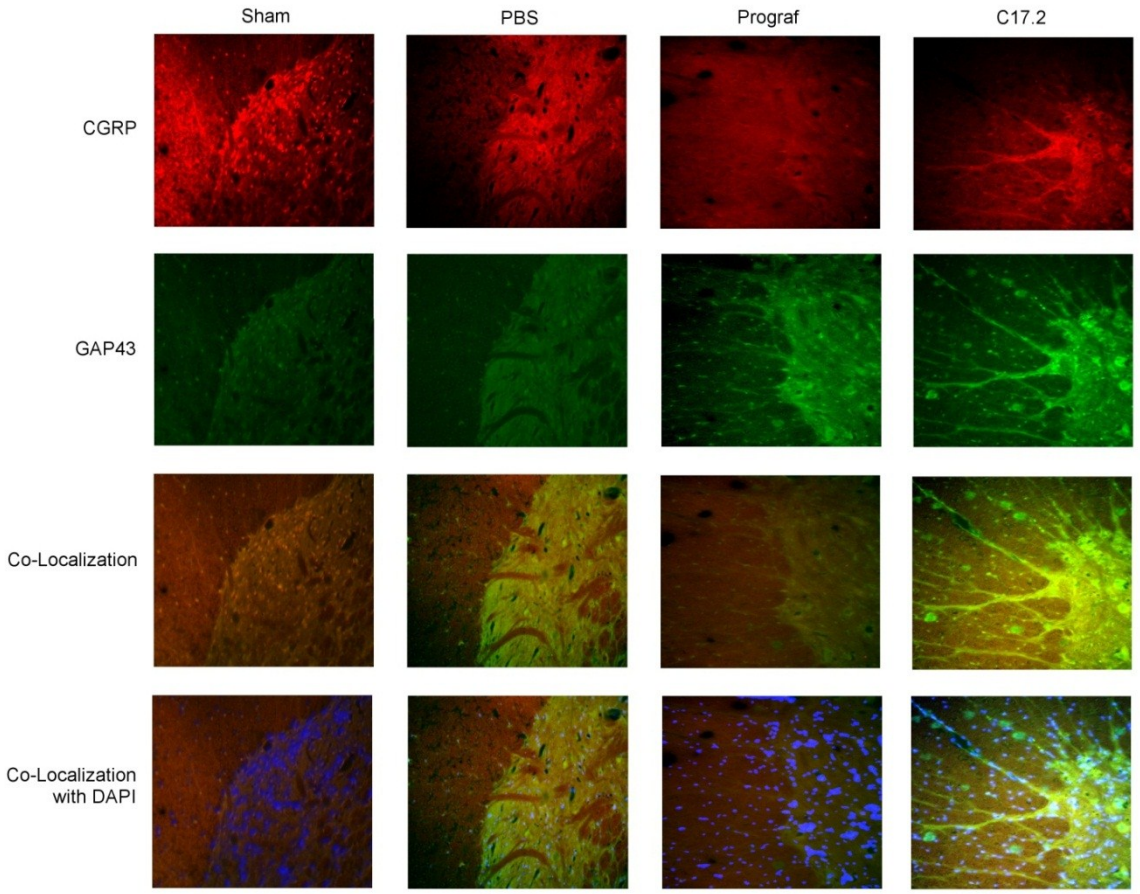

Figure 4-5: Immunohistochemical Labeling in Dorsal Horn of Cervical Segments.

Immunohistochemical labeling in the dorsal horns of the C7 – T1 vertebral segments. Immunofluorescence is shown for CGRP (red), GAP43 (green), co-localization of CGRP and GAP43 (yellow) and co-localization of CGRP and GAP43 with the non-specific labeling for cell nuclei with DAPI (blue). Axon sprouting is demonstrated in the C17.2 NSC transplant group that is not seen in the Sham, PBS, and Prograf groups. Magnification was set at 40x.

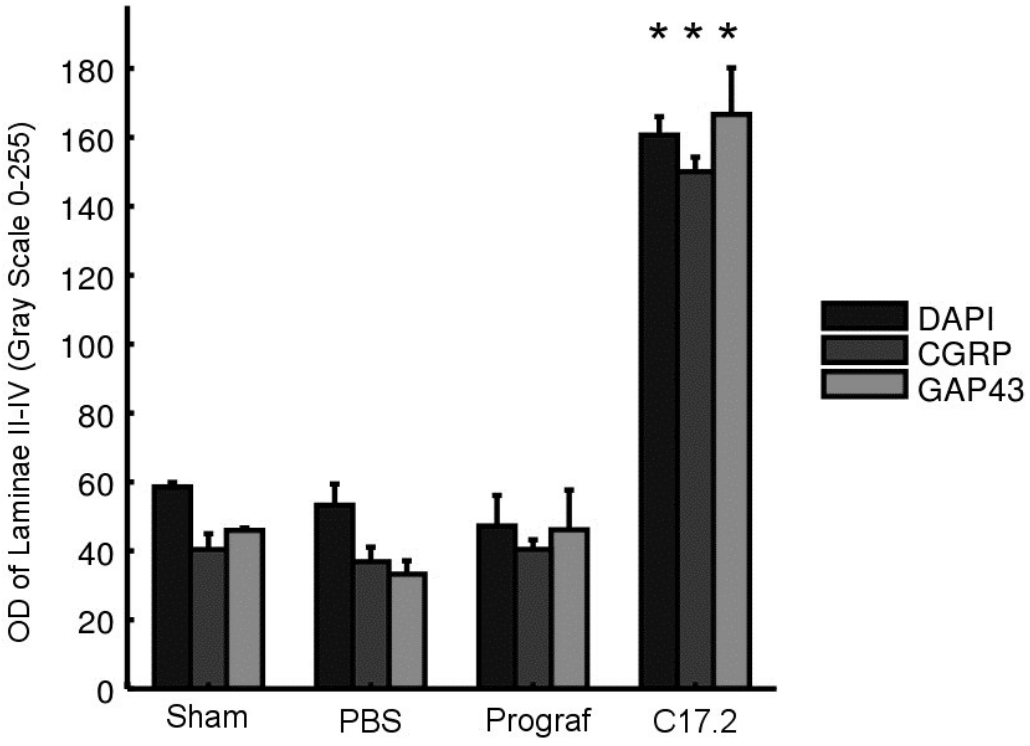

Figure 4-6: Densitometry of Immunolabeled Anti-Body Stains.

Densitometry of the immunolabeled CGRP and GAP43 stains based off of optical density. There is a statistically significant increase ($p < 0.05$) in the density for the CGRP and GAP43 as well as the nuclei stain for DAPI ($p < 0.05$) when compared to the control groups.

Discussion

The results from this study suggest that DTI is an ideal tool for non-invasively observing the effects of cellular transplants in the spinal cord. To the best of our knowledge this is the first study to non-invasively measure the effect of stem cells using diffusion tensor imaging. Spinal cord injuries were treated with stem cells and were then evaluated over a 10-week time period. Spinal cords were imaged in vivo at weeks 2, 5, and 10, then imaged ex vivo and compared against motor and sensory tests as well as end point histology to understand the temporal effects of stem cells on the anatomical

structure. Results demonstrated changes to MD, lADC, and tADC were associated with thermal allodynia and astrocytic growth.

Stem cell transplantation after a SCI manipulates the environment in a way that changes the rate of the diffusion of water through tissue. Following a moderate injury the motor function of the injury groups was significantly reduced for the remaining 10 weeks. However, as seen previously for the C17.2 transplants, the engrafted C17.2 stem cells have been shown to differentiate into astrocytes, eliciting forelimb allodynia (Oku et al., 1987; Macias et al., 2006). This increase in thermal sensitivity was significant at 3-6, 9 and 10 weeks following injury. While weeks 7 and 8 were not significant there was still a separation between the transplant group and the other injection schemes suggesting that an increased N could improve this statistic.

The in vivo diffusion measurements in the cervical cord demonstrated significant differences from control groups at 5 weeks after injury and continued to be significant for the rest of the experiment. Diffusion measurements in both the longitudinal and transverse direction of the cord as well as the mean diffusivity showed significant difference at weeks 5 and 10, as well as ex vivo suggesting DTI could provide insight into the structural changes that occur in both directions. The C17.2 stem cell line has been histologically shown to create astrocytic growth in the cervical segments as early as 10 days after injection (Macias et al., 2006). There was no significant difference in the in vivo diffusion measurements one week after injection suggesting that DTI does not provide further insight into the structural changes occurring immediately after the stem cell transplants.

Histological comparison of the spinal cord was associated with allodynia (Oku et al., 1987; Snyder et al., 1992; Macias et al., 2006). Macias et al. showed that the C17.2 NSCs were characterized by an increase in CGRP and GAP43 sprouting from the dorsal horn. The sprouting has been shown in distal segments following SCI and cell transplant

(Ondarza et al., 2003; Hofstetter et al., 2005; Macias et al., 2006). MD increased with densitometry measurements, which was counter-intuitive at first. However, after secondary degeneration the liquid formation of necrotic tissue has been shown to increase MD (Pierpaoli et al., 2001) and it is also possible that the degenerated debris created by an SCI was removed more efficiently with the increase of differentiated NSCs into cells such as macrophages.

Previous studies have used diffusion measurements to characterize the environmental changes that occur after a spinal cord injury (Schwartz, Chin, et al., 2005; Guleria et al., 2008; Ellingson et al., 2010; Sundberg et al., 2010) but there has been only a few investigations that have looked at the effect of the transplants after an SCI has occurred using non-invasive measurements. Investigators have shown that tagging superparamagnetic particles to neuronal cells can provide a means for tracking the migration (Bulte and Kraitchman, 2004; Modo, 2006). However, in small regions of the body such as the spinal cord, cell labeling can result in susceptibility blooming. Other techniques in stem cell labeling involve the use of contrast agents, such as gadolinium (Modo et al., 2002, 2004; Brekke et al., 2007), that provide better spatial resolution but can cause risks to a subject with anaphylaxis or poor renal function.

One potential limitation to this study was the lack of variation in severity of injury. It is possible that the effect of the C17.2 NSCs could show varying diffusion changes based on if the damaged axons were completely severed or partly recoverable before injection. This study would benefit from mild and severe injuries to the spinal cord to create a better spatio-temporal understanding of the microstructural changes that effect the diffusion of water.

Another possible limitation to this study was the lack of time points after the stem cell injection to accurately portray the diffusion effects. There is an initial inflammatory response after a SCI but the continued axonal and Wallerian degeneration can extend to

more than a year (Kakulas, 2004b). Future studies would benefit from increased time points to better understand how the stem cells affect water diffusion throughout the spinal cord.

Lack of resolution could be inhibiting the in vivo results at week 2. It is possible that an increase in the number of directions or varying b-values would allow for the heightened resolution that would be required to see the acute changes that take place after the injection of the transplant cells. Kim et al. showed that DTI is able to detect changes to the spinal cord that occur within 3 hours after an injury (Kim et al., 2011) suggesting that DTI has the potential to be sensitive the immediate changes that occur after the injection of stem cells.

Conclusion

These results demonstrate that diffusion tensor imaging has the ability to detect changes to the underlying structure of the spinal cord after the transplantation of cells. In this study, there was a significant increase in the overall diffusion of water in regions away from the injury site after 5 weeks post injury. Using a non-invasive technique that can monitor migration of the stem cells and suggest what structural effects could be occurring from the stem cells provides significant clinical implications in the treatment of SCI.

CHAPTER 5

SUMMARY AND FUTURE DIRECTIONS

Summary of the Results

The results of this study contribute to our understanding of spinal cord injury (SCI) by using magnetic resonance diffusion tensor imaging (DTI) as a biomarker for diagnostic and prognostic outcome. In Chapters 2 and 3, the results showed there were structural changes along the entire central nervous system following a thoracic SCI in rats and that these changes were detectable with DTI. In addition, the diffusion metrics were shown to be sensitive to varying severity along the length of the spinal cord and through regions encompassing the corticospinal tract. Furthermore, the diffusion metrics in the internal capsule, corticospinal tracts, and the cervical regions of the spinal cord correlated with hind limb motor function after a spinal cord injury. Mean diffusivity was found to decrease in all rats along the length of the spinal cord with respect to injury, this suggests that following a thoracic contusion the axons proceed with Wallerian and axonal degeneration (leading to diffusivity drops along the spinal cord) but are not limited to just membrane disruption as restrictive astrocytic scaring and glial cells restrict diffusion transversely through the cord.

When neuronal stem cell (NSC) transplants are injected into the spine to aid in regenerating and repairing the spinal cord after trauma, there is a reverse effect in diffusion. When C17.2 NSCs were injected, there was an increase in astrocytic branching in the dorsal horn regions of the spinal cord, which has been shown previously with this stem cell line. Mean diffusivity was shown to increase with the rats that showed astrocytic sprouting and these results were confirmed through immunohistochemistry.

Taken together these findings demonstrate, on a macroscopic scale, the sensitivity of DTI to microstructural changes that occur in the spinal cord and brain following trauma and following the transplant of neuronal stem cells. The results further clarify diffusion tensor imaging as a prognostic and diagnostic biomarker following SCI.

Implications

The results from this study suggest that diffusion tensor imaging may be used as a biomarker for prognostic and diagnostic indication following SCI. Spinal stabilization devices are usually implemented following an SCI in order to prevent further damage from occurring to the spinal cord. The resulting hardware limits the physicians understanding of how the injury may be progressing because the hardware often interferes with neuroimaging techniques such as MRI. The results in our study demonstrate that DTI may be used in regions remote from the injury site and associated hardware to gain an understanding of the injury severity. Furthermore, the results from this study demonstrate that these severity-based changes to the diffusion of water may be found in all parts of the central nervous system.

The diffusion changes associated with injury severity are useful for characterizing the structural changes resulting from the progression of secondary injury; these changes may not be limited to degeneration but could include cortically driven reorganization. New rehabilitation techniques may be developed because of an improved understanding how the brain adapts following a spinal cord injury. The diffusion metrics of non-normal tissue could be used as an indication of the cellular changes that would need to be reverted back to normal to regain function. One possible therapy for re-establishing these connections is through therapeutic techniques such as stem cells. Our results show that DTI can be used as a biomarker to understand the success of stem cell

transplantation. Furthermore, the diffusion metrics of the stem cell transplantation were found to be significantly different than the sham group in scans as early as 5 weeks, while functional results were not seen until week 6, suggesting that DTI may be used as an earlier indicator of structural changes than conventional functional tests.

Future Directions

The findings of our studies have led to an improved understanding of diffusion tensor imaging in spinal cord injury. However, these results were completed in an animal model and future research is needed to understand the implications of our findings when translated into humans. Conducting research in the animal model affords the liberty of being able to run a very controlled experiment. In the case of the animal model presented in the three aims for this dissertation, the injuries were created in a lab using precise tools that limited the variability in the injury groups. It is also easier to obtain appropriate numbers for experimental procedures, and being able to conduct a detailed histological examination provides enticing arguments for the use of animal models. When translating the animal research findings into humans, differences in the human motor and sensory pathways should be considered, where the pathways may be affected differently compared to animals. Studies aimed at characterizing the sensitivity of DTI to the changes that occur following traumatic injury in humans are needed. Moving forward, it would be beneficial to run the experiments presented here in the clinical setting. The American Spinal Injury Association (ASIA) classifies motor impairment into 5 different categories (A-E). By recruiting human subjects with injuries in each ASIA group, and scanning regions remote from the injury site, the research findings in Aim 1 and 2 of this dissertation could be compared and quantitatively translated into the clinical setting for a more accurate representation of how diffusion in

the CNS changes following a spinal cord injury. The potential findings could provide physicians with a more direct clinical measure of SCI outside the injury site, providing physicians information about the injury while avoiding the stabilization devices that have been implanted.

Our findings suggest that DTI is sensitive to structural changes that occur following an SCI. However, the cellular changes provide only part of the picture for how neural pathways adapt after injury. Combining diffusion tensor imaging with other neuroimaging techniques such as functional magnetic resonance imaging (fMRI) or electroencephalography (EEG) may provide an understanding of how the brain adapts following the structural changes associated with a spinal cord injury. As presented in Aim 2, some literature has focused on understanding the plasticity of the brain following a spinal cord injury. However, it is really unknown whether ongoing plasticity is affected by severity of injury to the spinal cord. It would be interesting to run an experiment with varying levels of injury, similar to Aim 1 and Aim 2 of this research, but to use EEG or fMRI to observe the hemodynamic changes in the resting state for injured animals or, if possible during some stimulus driven task. Ideally it would be appealling to look at lower limb movement of the rat in a controlled task and compare cortical contribution and cortical impairment following spinal cord injury. There are complex challenges associated with getting a rat to perform a movement task inside of an MRI, however there have been passive movement studies where the limbs are moved for the subject, and using an appropriate anesthetic level for the rat, movement of the lower rat limbs could potentially be measured in a more controlled SCI model setting.

A current limitation to our study was the lack of understanding of the cellular alterations underlying structural changes that occur in remote regions of the central nervous system following SCI. Our results suggested that there was cellular expression, indicating the introduction of cells like astrocytes into the environment. However, utilizing

molecular imaging techniques such as a two-photon microscope might reveal some of the complex changes that occur following SCI. Future studies could utilize molecular imaging techniques, like the two photon microscope, to try and understand the complex temporal and spatial changes to the molecular structure that occur after a spinal cord injury. In vivo imaging of the spinal cord using a two—photon microscope could allow for a detailed high-resolution scan of the microglia and vasculature. Combining this technique with DTI could potentially provide a detailed comparison of the changes that occur to the microstructure of the spinal cord following an injury, with non-invasive imaging techniques such as DTI, to provide clinicians with better diagnostic tools to identify the structural changes that occur in the central nervous system. This live tissue imaging would provide insight into underlying tissue changes after SCI by identifying changes in perfusion and water cellularity, and could potentially provide longitudinal studies on the cellular environment changes that occur following an SCI.

These studies could benefit from improved scan quality. The imaging sequences chosen in this study were designed to accommodate scan times and hardware provided by the institution. However, designing a custom coil that could be implanted into the spinal cord in order to produce higher transmission and improve receive signals by being closer to the spinal cord could potentially provide higher quality images. Although limited, longer scan times could also provide this research with a higher quality image set to analyze. However, longer scan times do pose a potential problem for translating into the clinical setting. The longer scan times in MRI sequences could be problematic for patients that need to be as still as possible to avoid motion artifacts from occurring in the diffusion images. Nevertheless, it may be possible to improve scan quality by imaging many more directions than what was acquired in our scans. Another possibility is to use different scan sequences such as a multi-shot echo planar imaging (EPI) sequence to improve scan quality for the amount of time by being able to acquire multiple lines of k

space in the same or less time that it took for the spin echo sequence that was applied in the three aims. Imaging sequences such as high angular resolution diffusion imaging (HARDI) provide a higher probabilistic distribution of the water diffusion as opposed to forcing the model of water diffusion to be represented in a tensor model. This imaging sequence could provide a more realistic and potentially higher quality scan sequence that could provide further insight into individual tracts of the central nervous system. Further research would benefit by improving scan sequences such as through the use of custom coils, longer scan times, and more advanced scan sequences such as q-space imaging in order to further delineate the anatomical structures and the connectivity between the regions associated with spinal cord injury.

Conclusion

This research set out to characterize the sensitivity of diffusion tensor imaging to severity of spinal cord injury and following neuronal stem cell transplant. The results from this study indicate that the diffusion metrics of diffusion tensor magnetic resonance imaging are sensitive to changes in neuronal structure and thus support our hypothesis that DTI measurements of the central nervous system can be used as a biomarker for injury severity and transplant therapies.

BIBLIOGRAPHY

Aguayo, a J., Bray, G.M., Carter, D. a, Villegas-Perez, M.P., Vidal-Sanz, M., Rasminsky, M., 1990. Regrowth and connectivity of injured central nervous system axons in adult rodents. Acta neurobiologiae experimentalis 50, 381–9.

Aguilar, J., Humanes-Valera, D., Alonso-Calviño, E., Yague, J.G., Moxon, K. a, Oliviero, A., Foffani, G., 2010. Spinal cord injury immediately changes the state of the brain. The Journal of neuroscience : the official journal of the Society for Neuroscience 30, 7528–37.

Anderson, a W., Zhong, J., Petroff, O. a, Szafer, a, Ransom, B.R., Prichard, J.W., Gore, J.C., 1996. Effects of osmotically driven cell volume changes on diffusion-weighted imaging of the rat optic nerve. Magnetic resonance in medicine : official journal of the Society of Magnetic Resonance in Medicine / Society of Magnetic Resonance in Medicine 35, 162–7.

Avellino, A.M., Hart, D., Dailey, A.T., MacKinnon, M., Ellegala, D., Kliot, M., 1995. Differential macrophage responses in the peripheral and central nervous system during wallerian degeneration of axons. Experimental neurology 136, 183–98.

Basser, P.J., Mattiello, J., LeBihan, D., 1994. MR diffusion tensor spectroscopy and imaging. Biophysical journal 66, 259–67.

Basser, P.J., Pierpaoli, C., 1996. Microstructural and physiological features of tissues elucidated by quantitative-diffusion-tensor MRI. Journal of magnetic resonance. Series B 111, 209–19.

Basso, D.M., Beattie, M.S., Bresnahan, J.C., 1995. A sensitive and reliable locomotor rating scale for open field testing in rats. Journal Of Neurotrauma 12, 1–21.

Beauchamp, N.J., Barker, P.B., Wang, P.Y., VanZijl, P.C., 1999. Imaging of acute cerebral ischemia. Radiology 212, 307–24.

Beaulieu, C., 2002. The basis of anisotropic water diffusion in the nervous system - a technical review. NMR in biomedicine 15, 435–55.

Berman, S.M.C., Walczak, P., Bulte, J.W.M., 2011. Magnetic Resonance Neuroimaging. Humana Press, Totowa, NJ.

Brekke, C., Williams, S.C., Price, J., Thorsen, F., Modo, M., 2007. Cellular multiparametric MRI of neural stem cell therapy in a rat glioma model. NeuroImage 37, 769–82.

Bruehlmeier, M., Dietz, V., Leenders, K.L., Roelcke, U., Missimer, J., Curt, A., 1998. How does the human brain deal with a spinal cord injury? The European journal of neuroscience 10, 3918–22.

Budde, M.D., Janes, L., Gold, E., Turtzo, L.C., Frank, J. a, 2011. The contribution of gliosis to diffusion tensor anisotropy and tractography following traumatic brain injury: validation in the rat using Fourier analysis of stained tissue sections. Brain : a journal of neurology 134, 2248–60.

Budde, M.D., Kim, J.H., Liang, H.-F., Schmidt, R.E., Russell, J.H., Cross, A.H., Song, S.-K., 2007. Toward accurate diagnosis of white matter pathology using diffusion tensor imaging. Magnetic resonance in medicine : official journal of the Society of Magnetic Resonance in Medicine / Society of Magnetic Resonance in Medicine 57, 688–95.

Bulte, J.W.M., Kraitchman, D.L., 2004. Iron oxide MR contrast agents for molecular and cellular imaging. NMR in biomedicine 17, 484–99.

Buss, a, Brook, G. a, Kakulas, B., Martin, D., Franzen, R., Schoenen, J., Noth, J., Schmitt, a B., 2004. Gradual loss of myelin and formation of an astrocytic scar during Wallerian degeneration in the human spinal cord. Brain : a journal of neurology 127, 34–44.

Buss, A., Schwab, M.E., 2003. Sequential loss of myelin proteins during Wallerian degeneration in the rat spinal cord. Glia 42, 424–32.

Carlson, S.L., Parrish, M.E., Springer, J.E., Doty, K., Dossett, L., 1998. Acute inflammatory response in spinal cord following impact injury. Experimental neurology 151, 77–88.

Cercignani, M., Horsfield, M. a, Agosta, F., Filippi, M., 2003. Sensitivity-encoded diffusion tensor MR imaging of the cervical cord. AJNR. American journal of neuroradiology 24, 1254–6.

Cheran, S., Shanmuganathan, K., Zhuo, J., Mirvis, S.E., Aarabi, B., Alexander, M.T., Gullapalli, R.P., 2011. Correlation of MR diffusion tensor imaging parameters with ASIA motor scores in hemorrhagic and nonhemorrhagic acute spinal cord injury. Journal of neurotrauma 28, 1881–92.

Coleman, M.P., Perry, V.H., 2002. Axon pathology in neurological disease: a neglected therapeutic target. Trends in neurosciences 25, 532–7.

Concha, L., Gross, D.W., Wheatley, B.M., Beaulieu, C., 2006. Diffusion tensor imaging of time-dependent axonal and myelin degradation after corpus callosotomy in epilepsy patients. NeuroImage 32, 1090–9.

Crawley, A.P., Jurkiewicz, M.T., Yim, A., Heyn, S., Verrier, M.C., Fehlings, M.G., Mikulis, D.J., 2004. Absence of localized grey matter volume changes in the motor cortex following spinal cord injury. Brain research 1028, 19–25.

Curt, a, Bruehlmeier, M., Leenders, K.L., Roelcke, U., Dietz, V., 2002. Differential effect of spinal cord injury and functional impairment on human brain activation. Journal of neurotrauma 19, 43–51.

Curt, A., Alkadhi, H., Crelier, G.R., Boendermaker, S.H., Hepp-Reymond, M.-C., Kollias, S.S., 2002. Changes of non-affected upper limb cortical representation in paraplegic patients as assessed by fMRI. Brain : a journal of neurology 125, 2567–78.

DeBoy, C. a, Zhang, J., Dike, S., Shats, I., Jones, M., Reich, D.S., Mori, S., Nguyen, T., Rothstein, B., Miller, R.H., Griffin, J.T., Kerr, D. a, Calabresi, P. a, 2007. High resolution diffusion tensor imaging of axonal damage in focal inflammatory and demyelinating lesions in rat spinal cord. Brain : a journal of neurology 130, 2199–210.

Deo, A.A., Grill, R.J., Hasan, K.M., Narayana, P.A., 2006. In vivo serial diffusion tensor imaging of experimental spinal cord injury. Journal of neuroscience research 83, 801–10.

Duong, T.Q., Sehy, J. V, Yablonskiy, D. a, Snider, B.J., Ackerman, J.J., Neil, J.J., 2001. Extracellular apparent diffusion in rat brain. Magnetic resonance in medicine : official journal of the Society of Magnetic Resonance in Medicine / Society of Magnetic Resonance in Medicine 45, 801–10.

Einstein, A., 1905. On the movement of small particles suspended in stationary liquids required by the molecular-kinetic theory of heat. Ann. Phys., Lpz 17, 549.

Einstein, A., 1956. Investigations on the Theory of Brownian Movement., Dover publications. Dover Publications.

Ellingson, B.M., Kurpad, S.N., Schmit, B.D., 2008a. Ex vivo diffusion tensor imaging and quantitative tractography of the rat spinal cord during long-term recovery from moderate spinal contusion. Journal of magnetic resonance imaging : JMRI 28, 1068–79.

Ellingson, B.M., Kurpad, S.N., Schmit, B.D., 2008b. Functional correlates of diffusion tensor imaging in spinal cord injury. Biomedical sciences instrumentation 44, 28–33.

Ellingson, B.M., Schmit, B.D., Kurpad, S.N., 2010. Lesion growth and degeneration patterns measured using diffusion tensor 9.4-T magnetic resonance imaging in rat spinal cord injury. Journal of neurosurgery. Spine 13, 181–92.

Ellingson, B.M., Ulmer, J.L., Kurpad, S.N., Schmit, B.D., 2008. Diffusion tensor MR imaging in chronic spinal cord injury. AJNR. American journal of neuroradiology 29, 1976–82.

Endo, T., Spenger, C., Tominaga, T., Brené, S., Olson, L., 2007. Cortical sensory map rearrangement after spinal cord injury: fMRI responses linked to Nogo signalling. Brain : a journal of neurology 130, 2951–61.

Fleming, J.C., Norenberg, M.D., Ramsay, D. a, Dekaban, G. a, Marcillo, A.E., Saenz, A.D., Pasquale-Styles, M., Dietrich, W.D., Weaver, L.C., 2006. The cellular

inflammatory response in human spinal cords after injury. Brain : a journal of neurology 129, 3249–69.

Ford, J.C., Hackney, D.B., Alsop, D.C., Jara, H., Joseph, P.M., Hand, C.M., Black, P., 1994. MRI characterization of diffusion coefficients in a rat spinal cord injury model. Magnetic Resonance in Medicine 31, 488–494.

Freund, P., Schneider, T., Nagy, Z., Hutton, C., Weiskopf, N., Friston, K., Wheeler-Kingshott, C. a, Thompson, A.J., 2012. Degeneration of the injured cervical cord is associated with remote changes in corticospinal tract integrity and upper limb impairment. PloS one 7, e51729.

Freund, P., Weiskopf, N., Ward, N.S., Hutton, C., Gall, A., Ciccarelli, O., Craggs, M., Friston, K., Thompson, A.J., 2011. Disability, atrophy and cortical reorganization following spinal cord injury. Brain : a journal of neurology 134, 1610–22.

Fujimoto, S.T., Longhi, L., Saatman, K.E., Conte, V., Stocchetti, N., McIntosh, T.K., 2004. Motor and cognitive function evaluation following experimental traumatic brain injury. Neuroscience and biobehavioral reviews 28, 365–78.

Gage, F.H., 2000. Mammalian Neural Stem Cells. Science 287, 1433–1438.

Gaudet, A.D., Popovich, P.G., Ramer, M.S., 2011. Wallerian degeneration: gaining perspective on inflammatory events after peripheral nerve injury. Journal of neuroinflammation 8, 110.

Ghosh, A., Sydekum, E., Haiss, F., Peduzzi, S., Zörner, B., Schneider, R., Baltes, C., Rudin, M., Weber, B., Schwab, M.E., 2009. Functional and anatomical reorganization of the sensory-motor cortex after incomplete spinal cord injury in adult rats. The Journal of neuroscience : the official journal of the Society for Neuroscience 29, 12210–9.

Goldberg, A.L., Kershah, S.M., 2010. Advances in imaging of vertebral and spinal cord injury. The journal of spinal cord medicine 33, 105–16.

Gris, D., Hamilton, E.F., Weaver, L.C., 2008. The systemic inflammatory response after spinal cord injury damages lungs and kidneys. Experimental neurology 211, 259–70.

Guleria, S., Gupta, R.K., Saksena, S., Chandra, A., Srivastava, R.N., Husain, M., Rathore, R., Narayana, P. a, 2008. Retrograde Wallerian degeneration of cranial corticospinal tracts in cervical spinal cord injury patients using diffusion tensor imaging. Journal of neuroscience research 86, 2271–80.

Gullapalli, J., Krejza, J., Schwartz, E.D., 2006. In vivo DTI evaluation of white matter tracts in rat spinal cord. Journal of magnetic resonance imaging : JMRI 24, 231–4.

Gustin, S.M., Wrigley, P.J., Siddall, P.J., Henderson, L. a, 2010. Brain anatomy changes associated with persistent neuropathic pain following spinal cord injury. Cerebral cortex (New York, N.Y. : 1991) 20, 1409–19.

Harrison, B.M., McDonald, W.I., 1977. Remyelination after transient experimental compression of the spinal cord. Annals of neurology 1, 542–51.

Henderson, L. a, Gustin, S.M., Macey, P.M., Wrigley, P.J., Siddall, P.J., 2011. Functional reorganization of the brain in humans following spinal cord injury: evidence for underlying changes in cortical anatomy. The Journal of neuroscience : the official journal of the Society for Neuroscience 31, 2630–7.

Hofstetter, C.P., Holmström, N. a V, Lilja, J. a, Schweinhardt, P., Hao, J., Spenger, C., Wiesenfeld-Hallin, Z., Kurpad, S.N., Frisén, J., Olson, L., 2005. Allodynia limits the usefulness of intraspinal neural stem cell grafts; directed differentiation improves outcome. Nature neuroscience 8, 346–53.

Holodny, A.I., Gor, D.M., Watts, R., Gutin, P.H., Ulug, A.M., 2005. Diffusion-tensor MR tractography of somatotopic organization of corticospinal tracts in the internal capsule: initial anatomic results in contradistinction to prior reports. Radiology 234, 649–53.

Illes, J., Reimer, J.C., Kwon, B.K., 2011. Stem cell clinical trials for spinal cord injury: readiness, reluctance, redefinition. Stem cell reviews 7, 997–1005.

Inglese, M., Makani, S., Johnson, G., Cohen, B. a, Silver, J. a, Gonen, O., Grossman, R.I., 2005. Diffuse axonal injury in mild traumatic brain injury: a diffusion tensor imaging study. Journal of neurosurgery 103, 298–303.

Ito, T., Oyanagi, K., Wakabayashi, K., Ikuta, F., 1996. Traumatic spinal cord injury: a neuropathological study on the longitudinal spreading of the lesions. Acta Neuropathologica 93, 13.

Jiang, Q., Qu, C., Chopp, M., Ding, G.L., Davarani, S.P.N.-, Helpern, J.A., Jensen, J.H., Zhang, Z.G., Li, L., Lu, M., Kaplan, D., Hu, J., Shen, Y., Kou, Z., Li, Q., Wang, S., Mahmood, A., 2011. MRI evaluation of axonal reorganization after bone marrow stromal cell treatment of traumatic brain injury. NMR in biomedicine 24, 1119–28.

Jiang, Q., Zhang, Z.G., Ding, G.L., Silver, B., Zhang, L., Meng, H., Lu, M., Pourabdillah-Nejed-D, S., Wang, L., Savant-Bhonsale, S., Li, L., Bagher-Ebadian, H., Hu, J., Arbab, A.S., Vanguri, P., Ewing, J.R., Ledbetter, K.A., Chopp, M., 2006. MRI detects white matter reorganization after neural progenitor cell treatment of stroke. NeuroImage 32, 1080–9.

Kakulas, B. a, 2004a. Neuropathology: the foundation for new treatments in spinal cord injury. Spinal cord 42, 549–63.

Kakulas, B. a, 2004b. Neuropathology: the foundation for new treatments in spinal cord injury. Spinal cord 42, 549–63.

Kang, K.-S., Kim, S.W., Oh, Y.H., Yu, J.W., Kim, K.-Y., Park, H.K., Song, C.-H., Han, H., 2005. A 37-year-old spinal cord-injured female patient, transplanted of multipotent stem cells from human UC blood, with improved sensory perception and mobility, both functionally and morphologically: a case study. Cytotherapy 7, 368–73.

Keirstead, H.S., Nistor, G., Bernal, G., Totoiu, M., Cloutier, F., Sharp, K., Steward, O., 2005. Human embryonic stem cell-derived oligodendrocyte progenitor cell transplants remyelinate and restore locomotion after spinal cord injury. The Journal of neuroscience : the official journal of the Society for Neuroscience 25, 4694–705.

Kim, J., Song, S.-K., Burke, D. a, Magnuson, D.S.K., 2011. Comprehensive locomotor outcomes correlate to hyperacute diffusion tensor measures after spinal cord injury in the adult rat. Experimental neurology.

Kim, J.H., Loy, D.N., Liang, H.-F., Trinkaus, K., Schmidt, R.E., Song, S.-K., 2007. Noninvasive diffusion tensor imaging of evolving white matter pathology in a mouse model of acute spinal cord injury. Magnetic resonance in medicine : official journal of the Society of Magnetic Resonance in Medicine / Society of Magnetic Resonance in Medicine 58, 253–60.

Kim, J.H., Loy, D.N., Wang, Q., Budde, M.D., Schmidt, R.E., Trinkaus, K., Song, S.-K., 2010. Diffusion tensor imaging at 3 hours after traumatic spinal cord injury predicts long-term locomotor recovery. Journal of neurotrauma 27, 587–98.

Kim, T.H., Zollinger, L., Shi, X.F., Rose, J., Jeong, E.-K., 2009. Diffusion tensor imaging of ex vivo cervical spinal cord specimens: the immediate and long-term effects of fixation on diffusivity. Anatomical record (Hoboken, N.J. : 2007) 292, 234–41.

Kitahara, S., Nakasu, S., Murata, K., Sho, K., Ito, R., 2005. Evaluation of treatment-induced cerebral white matter injury by using diffusion-tensor MR imaging: initial experience. AJNR. American journal of neuroradiology 26, 2200–6.

Kluver, H., Barrera, E., 1953. A method for the combined staining of cells and fibers in the nervous system. Journal of neuropathology and experimental neurology 12, 400–3.

Konomi, T., Fujiyoshi, K., Hikishima, K., Komaki, Y., Tsuji, O., Okano, H.J., Toyama, Y., Okano, H., Nakamura, M., 2012. Conditions for quantitative evaluation of injured spinal cord by in vivo diffusion tensor imaging and tractography: Preclinical longitudinal study in common marmosets. NeuroImage 63, 1841–53.

Koshinaga, M., Whittemore, S.R., 1995. The temporal and spatial activation of microglia in fiber tracts undergoing anterograde and retrograde degeneration following spinal cord lesion. Journal of neurotrauma 12, 209–22.

Kozlowski, P., Raj, D., Liu, J., Lam, C., Yung, A.C., Tetzlaff, W., 2008. Characterizing white matter damage in rat spinal cord with quantitative MRI and histology. Journal of neurotrauma 25, 653–76.

Krassioukov, a V, Fehlings, M.G., 1999. Effect of graded spinal cord compression on cardiovascular neurons in the rostro-ventro-lateral medulla. Neuroscience 88, 959–73.

Kumar, R., Husain, M., Gupta, R.K., Hasan, K.M., Haris, M., Agarwal, A.K., Pandey, C.M., Narayana, P. a, 2009. Serial changes in the white matter diffusion tensor imaging metrics in moderate traumatic brain injury and correlation with neuro-cognitive function. Journal of neurotrauma 26, 481–95.

Laganà, M., Rovaris, M., Ceccarelli, a, Venturelli, C., Marini, S., Baselli, G., 2010. DTI parameter optimisation for acquisition at 1.5T: SNR analysis and clinical application. Computational intelligence and neuroscience 2010, 254032.

Lee, R.H., Heckman, C.J., Johnson, M.D., Hyngstrom, A.S., Manuel, M., 2012. Bistability in Spinal Motoneurons In Vivo : Systematic Variations in Persistent Inward Currents Bistability in Spinal Motoneurons In Vivo : Systematic Variations in Persistent Inward Currents 583–593.

Li, L., Wu, W., Lin, L.F., Lei, M., Oppenheim, R.W., Houenou, L.J., 1995. Rescue of adult mouse motoneurons from injury-induced cell death by glial cell line-derived neurotrophic factor. Proceedings of the National Academy of Sciences of the United States of America 92, 9771–5.

Lindvall, O., Kokaia, Z., 2006. Stem cells for the treatment of neurological disorders. Nature 441, 1094–6.

Lo, C., Shifteh, K., Gold, T., Bello, J. a, Lipton, M.L., 2009. Diffusion tensor imaging abnormalities in patients with mild traumatic brain injury and neurocognitive impairment. Journal of computer assisted tomography 33, 293–7.

Loy, D.N., Kim, J.H., Xie, M., Schmidt, R.E., Trinkaus, K., Song, S.-K., 2007. Diffusion tensor imaging predicts hyperacute spinal cord injury severity. Journal of neurotrauma 24, 979–90.

Lu, H., Sun, S.-Q., 2003. A correlative study between AQP4 expression and the manifestation of DWI after the acute ischemic brain edema in rats. Chinese medical journal 116, 1063–9.

Lu, P., Jones, L.L., Tuszynski, M.H., 2007. Axon regeneration through scars and into sites of chronic spinal cord injury. Experimental neurology 203, 8–21.

Mac Donald, C.L., Dikranian, K., Bayly, P., Holtzman, D., Brody, D., 2007. Diffusion tensor imaging reliably detects experimental traumatic axonal injury and indicates approximate time of injury. The Journal of neuroscience : the official journal of the Society for Neuroscience 27, 11869–76.

Macias, M.Y., Syring, M.B., Pizzi, M. a, Crowe, M.J., Alexanian, A.R., Kurpad, S.N., 2006. Pain with no gain: allodynia following neural stem cell transplantation in spinal cord injury. Experimental neurology 201, 335–48.

Magnitsky, S., Watson, D.J., Walton, R.M., Pickup, S., Bulte, J.W.M., Wolfe, J.H., Poptani, H., 2005. In vivo and ex vivo MRI detection of localized and disseminated neural stem cell grafts in the mouse brain. NeuroImage 26, 744–54.

Martino, G., Pluchino, S., 2006. The therapeutic potential of neural stem cells. Nature reviews. Neuroscience 7, 395–406.

Modo, M., 2006. Understanding stem cell-mediated brain repair through neuroimaging. Current stem cell research & therapy 1, 55–63.

Modo, M., Cash, D., Mellodew, K., Williams, S.C.R., Fraser, S.E., Meade, T.J., Price, J., Hodges, H., 2002. Tracking transplanted stem cell migration using bifunctional, contrast agent-enhanced, magnetic resonance imaging. NeuroImage 17, 803–11.

Modo, M., Mellodew, K., Cash, D., Fraser, S.E., Meade, T.J., Price, J., Williams, S.C.R., 2004. Mapping transplanted stem cell migration after a stroke: a serial, in vivo magnetic resonance imaging study. NeuroImage 21, 311–7.

Mogatadakala, K. V, Narayana, P.A., 2009. In vivo diffusion tensor imaging of thoracic and cervical rat spinal cord at 7 T. Magnetic resonance imaging 27, 1236–41.

Moisse, K., Welch, I., Hill, T., Volkening, K., Strong, M.J., 2008. Transient middle cerebral artery occlusion induces microglial priming in the lumbar spinal cord: a novel model of neuroinflammation. Journal of neuroinflammation 5, 29.

Moraes, L., Vasconcelos-dos-Santos, A., Santana, F.C., Godoy, M.A., Rosado-de-Castro, P.H., Jasmin, Azevedo-Pereira, R.L., Cintra, W.M., Gasparetto, E.L., Santiago, M.F., Mendez-Otero, R., 2012. Neuroprotective effects and magnetic resonance imaging of mesenchymal stem cells labeled with SPION in a rat model of Huntington's disease. Stem cell research 9, 143–55.

Moseley, M.E., Cohen, Y., Kucharczyk, J., Mintorovitch, J., Asgari, H.S., Wendland, M.F., Tsuruda, J., Norman, D., 1990. Diffusion-weighted MR imaging of anisotropic water diffusion in cat central nervous system. Radiology 176, 439–45.

Moseley, M.E., Cohen, Y., Mintorovitch, J., Chileuitt, L., Shimizu, H., Kucharczyk, J., Wendland, M.F., Weinstein, P.R., 1990. Early detection of regional cerebral ischemia in cats: comparison of diffusion- and T2-weighted MRI and spectroscopy. Magnetic resonance in medicine : official journal of the Society of Magnetic Resonance in Medicine / Society of Magnetic Resonance in Medicine 14, 330–46.

Nathan, P.W., 1994. Effects on movement of surgical incisions into the human spinal cord. Brain : a journal of neurology 117 (Pt 2, 337–46.

Nesic, O., Lee, J., Ye, Z., Unabia, G.C., Rafati, D., Hulsebosch, C.E., Perez-Polo, J.R., 2006. Acute and chronic changes in aquaporin 4 expression after spinal cord injury. Neuroscience 143, 779–92.

Nevo, U., Hauben, E., Yoles, E., Agranov, E., Akselrod, S., Schwartz, M., Neeman, M., 2001. Diffusion anisotropy MRI for quantitative assessment of recovery in injured rat spinal cord. Magnetic resonance in medicine : official journal of the Society of Magnetic Resonance in Medicine / Society of Magnetic Resonance in Medicine 45, 1–9.

Norenberg, M.D., Smith, J., Marcillo, A., 2004. The pathology of human spinal cord injury: defining the problems. Journal of neurotrauma 21, 429–40.

Okano, H., Ogawa, Y., Nakamura, M., Kaneko, S., Iwanami, A., Toyama, Y., 2003. Transplantation of neural stem cells into the spinal cord after injury. Seminars in Cell & Developmental Biology 14, 191–198.

Oku, R., Satoh, M., Fujii, N., Otaka, A., Yajima, H., Takagi, H., 1987. Calcitonin gene-related peptide promotes mechanical nociception by potentiating release of substance P from the spinal dorsal horn in rats. Brain research 403, 350–4.

Oleson, C. V, Burns, A.S., Ditunno, J.F., Geisler, F.H., Coleman, W.P., 2005. Prognostic value of pinprick preservation in motor complete, sensory incomplete spinal cord injury. Archives of physical medicine and rehabilitation 86, 988–92.

Ondarza, A.B., Ye, Z., Hulsebosch, C.E., 2003. Direct evidence of primary afferent sprouting in distant segments following spinal cord injury in the rat: colocalization of GAP-43 and CGRP. Experimental neurology 184, 373–80.

Oudega, M., Perez, M. a, 2012. Corticospinal reorganization after spinal cord injury. The Journal of physiology 590, 3647–63.

Papadopoulos, S.M., Selden, N.R., Quint, D.J., Patel, N., Gillespie, B., Grube, S., 2002. Immediate spinal cord decompression for cervical spinal cord injury: feasibility and outcome. The Journal of trauma 52, 323–32.

Petersen, J. a, Wilm, B.J., Von Meyenburg, J., Schubert, M., Seifert, B., Najafi, Y., Dietz, V., Kollias, S., 2012. Chronic cervical spinal cord injury: DTI correlates with clinical and electrophysiological measures. Journal of neurotrauma 29, 1556–66.

Pierpaoli, C., Barnett, a, Pajevic, S., Chen, R., Penix, L.R., Virta, a, Basser, P., 2001. Water diffusion changes in Wallerian degeneration and their dependence on white matter architecture. NeuroImage 13, 1174–85.

Plant, G.W., Bates, M.L., Bunge, M.B., 2001. Inhibitory proteoglycan immunoreactivity is higher at the caudal than the rostral Schwann cell graft-transected spinal cord interface. Molecular and cellular neurosciences 17, 471–87.

Pluchino, S., Zanotti, L., Deleidi, M., Martino, G., 2005. Neural stem cells and their use as therapeutic tool in neurological disorders. Brain research. Brain research reviews 48, 211–9.

Raineteau, O., Schwab, M.E., 2001. Plasticity of motor systems after incomplete spinal cord injury. Nature reviews. Neuroscience 2, 263–73.

Ramu, J., Bockhorst, K.H., Grill, R.J., Mogatadakala, K. V, Narayana, P. a, 2007. Cortical reorganization in NT3-treated experimental spinal cord injury: Functional magnetic resonance imaging. Experimental neurology 204, 58–65.

Ramu, J., Bockhorst, K.H., Mogatadakala, K. V, Narayana, P.A., 2006. Functional magnetic resonance imaging in rodents: Methodology and application to spinal cord injury. Journal of neuroscience research 84, 1235–44.

Ramu, J., Herrera, J., Grill, R., Bockhorst, T., Narayana, P., 2008. Brain fiber tract plasticity in experimental spinal cord injury: diffusion tensor imaging. Experimental neurology 212, 100–7.

Roelcke, U., Curt, A., Otte, A., Missimer, J., Maguire, R.P., Dietz, V., Leenders, K.L., 1997. Influence of spinal cord injury on cerebral sensorimotor systems: a PET study. Journal of Neurology, Neurosurgery & Psychiatry 62, 61–65.

Rugg-Gunn, F.J., Symms, M.R., Barker, G.J., Greenwood, R., Duncan, J.S., 2001. Diffusion imaging shows abnormalities after blunt head trauma when conventional magnetic resonance imaging is normal. Journal of neurology, neurosurgery, and psychiatry 70, 530–3.

Schwab, M.E., Bartholdi, D., 1996. Degeneration and regeneration of axons in the lesioned spinal cord. Physiological reviews 76, 319–70.

Schwartz, E.D., Chin, C.-L., Shumsky, J.S., Jawad, A.F., Brown, B.K., Wehrli, S., Tessler, A., Murray, M., Hackney, D.B., 2005. Apparent diffusion coefficients in spinal cord transplants and surrounding white matter correlate with degree of axonal dieback after injury in rats. AJNR. American journal of neuroradiology 26, 7–18.

Schwartz, E.D., Cooper, E.T., Fan, Y., Jawad, A.F., Chin, C., Nissanov, J., Hackney, D.B., 2005. MRI diffusion coefficients in spinal cord correlate with axon morphometry. Neuroreport 16, 73–6.

Schwartz, E.D., Duda, J., Shumsky, J.S., Cooper, E.T., Gee, J., 2005. Spinal cord diffusion tensor imaging and fiber tracking can identify white matter tract disruption and glial scar orientation following lateral funiculotomy. Journal of neurotrauma 22, 1388–98.

Schwartz, E.D., Hackney, D.B., 2003. Diffusion-weighted MRI and the evaluation of spinal cord axonal integrity following injury and treatment. Experimental neurology 184, 570–89.

Seminowicz, D. a, Jiang, L., Ji, Y., Xu, S., Gullapalli, R.P., Masri, R., 2012. Thalamocortical asynchrony in conditions of spinal cord injury pain in rats. The Journal of neuroscience : the official journal of the Society for Neuroscience 32, 15843–8.

Shi, F., Zhu, H., Yang, S., Liu, Y., Feng, Y., Shi, J., Xu, D., Wu, W., You, S., Ma, Z., Zou, J., Lu, P., Xu, X.-M., 2009. Glial response and myelin clearance in areas of wallerian degeneration after spinal cord hemisection in the monkey Macaca fascicularis. Journal of neurotrauma 26, 2083–96.

Sieber-Blum, M., 2010. Epidermal neural crest stem cells and their use in mouse models of spinal cord injury. Brain research bulletin 83, 189–93.

Silva, M.D., Omae, T., Helmer, K.G., Li, F., Fisher, M., Sotak, C.H., 2002. Separating changes in the intra- and extracellular water apparent diffusion coefficient following focal cerebral ischemia in the rat brain. Magnetic resonance in medicine : official journal of the Society of Magnetic Resonance in Medicine / Society of Magnetic Resonance in Medicine 48, 826–37.

Snyder, E.Y., Deitcher, D.L., Walsh, C., Arnold-Aldea, S., Hartwieg, E. a, Cepko, C.L., 1992. Multipotent neural cell lines can engraft and participate in development of mouse cerebellum. Cell 68, 33–51.

Snyder, E.Y., Taylor, R.M., Wolfe, J.H., 1995. Neural progenitor cell engraftment corrects lysosomal storage throughout the MPS VII mouse brain. Nature 374, 367–70.

Song, S.-K., Sun, S.-W., Ramsbottom, M.J., Chang, C., Russell, J., Cross, A.H., 2002. Dysmyelination Revealed through MRI as Increased Radial (but Unchanged Axial) Diffusion of Water. NeuroImage 17, 1429–1436.

Sotak, C.H., 2002. The role of diffusion tensor imaging in the evaluation of ischemic brain injury - a review. NMR in biomedicine 15, 561–9.

Sundberg, L.M., Herrera, J.J., Narayana, P. a, 2010. In vivo longitudinal MRI and behavioral studies in experimental spinal cord injury. Journal of neurotrauma 27, 1753–67.

Sydekum, E., Baltes, C., Ghosh, A., Mueggler, T., Schwab, M.E., Rudin, M., 2009. Functional reorganization in rat somatosensory cortex assessed by fMRI: elastic image registration based on structural landmarks in fMRI images and application to spinal cord injured rats. NeuroImage 44, 1345–54.

Takahashi, M., Hackney, D.B., Zhang, G., Wehrli, S.L., Wright, A.C., O'Brien, W.T., Uematsu, H., Wehrli, F.W., Selzer, M.E., 2002. Magnetic resonance microimaging of intraaxonal water diffusion in live excised lamprey spinal cord. Proceedings of the National Academy of Sciences of the United States of America 99, 16192–6.

Tator, C.H., Fehlings, M.G., 1991. Review of the secondary injury theory of acute spinal cord trauma with emphasis on vascular mechanisms. Journal of neurosurgery 75, 15–26.

Thirion, J.-P., 1998. Image matching as a diffusion process: an analogy with Maxwell's demons. Medical Image Analysis 2, 243–260.

Thuret, S., Moon, L.D.F., Gage, F.H., 2006. Therapeutic interventions after spinal cord injury. Nature reviews. Neuroscience 7, 628–43.

Totoiu, M.O., Keirstead, H.S., 2005. Spinal cord injury is accompanied by chronic progressive demyelination. The Journal of comparative neurology 486, 373–83.

Vande Velde, G., Raman Rangarajan, J., Vreys, R., Guglielmetti, C., Dresselaers, T., Verhoye, M., Van der Linden, A., Debyser, Z., Baekelandt, V., Maes, F., Himmelreich, U., 2012. Quantitative evaluation of MRI-based tracking of ferritin-labeled endogenous neural stem cell progeny in rodent brain. NeuroImage 62, 367–80.

Vorísek, I., Hájek, M., Tintera, J., Nicolay, K., Syková, E., 2002. Water ADC, extracellular space volume, and tortuosity in the rat cortex after traumatic injury. Magnetic resonance in medicine : official journal of the Society of Magnetic Resonance in Medicine / Society of Magnetic Resonance in Medicine 48, 994–1003.

Voss, H.U., Ulu, A.M., Dyke, J.P., Watts, R., Kobylarz, E.J., Mccandliss, B.D., Heier, L.A., Beattie, B.J., Hamacher, K.A., Vallabhajosula, S., Goldsmith, S.J., Ballon, D., Giacino, J.T., Schiff, N.D., 2006. Possible axonal regrowth in late recovery from the minimally conscious state 116, 2005–2011.

Weishaupt, N., Silasi, G., Colbourne, F., Fouad, K., 2010. Secondary damage in the spinal cord after motor cortex injury in rats. Journal of neurotrauma 27, 1387–97.

Werring, D.J., Toosy, a T., Clark, C. a, Parker, G.J., Barker, G.J., Miller, D.H., Thompson, a J., 2000. Diffusion tensor imaging can detect and quantify corticospinal tract degeneration after stroke. Journal of neurology, neurosurgery, and psychiatry 69, 269–72.

Wolpaw, J.R., 2010. What can the spinal cord teach us about learning and memory? The Neuroscientist : a review journal bringing neurobiology, neurology and psychiatry 16, 532–49.

Wrigley, P.J., Gustin, S.M., Macey, P.M., Nash, P.G., Gandevia, S.C., Macefield, V.G., Siddall, P.J., Henderson, L. a, 2009. Anatomical changes in human motor cortex and motor pathways following complete thoracic spinal cord injury. Cerebral cortex (New York, N.Y. : 1991) 19, 224–32.

Wu, S., Suzuki, Y., Noda, T., Bai, H., Kitada, M., Kataoka, K., Nishimura, Y., Ide, C., 2002. Immunohistochemical and electron microscopic study of invasion and differentiation in spinal cord lesion of neural stem cells grafted through cerebrospinal fluid in rat. Journal of neuroscience research 69, 940–5.

Xu, S., Zhuo, J., Racz, J., Shi, D., Roys, S., Fiskum, G., Gullapalli, R., 2011. Early microstructural and metabolic changes following controlled cortical impact injury in rat: a magnetic resonance imaging and spectroscopy study. Journal of neurotrauma 28, 2091–102.

Yin, B., Tang, Y., Ye, J., Wu, Y., Wang, P., Huang, L., Yang, R., Shen, H., 2010. Sensitivity and specificity of in vivo diffusion-weighted MRI in acute spinal cord injury. Journal of clinical neuroscience : official journal of the Neurosurgical Society of Australasia 17, 1173–9.

Yoon, S.H., Shim, Y.S., Park, Y.H., Chung, J.K., Nam, J.H., Kim, M.O., Park, H.C., Park, S.R., Min, B.-H., Kim, E.Y., Choi, B.H., Park, H., Ha, Y., 2007. Complete spinal cord injury treatment using autologous bone marrow cell transplantation and bone marrow stimulation with granulocyte macrophage-colony stimulating factor: Phase I/II clinical trial. Stem cells (Dayton, Ohio) 25, 2066–73.

Zhang, J., Jones, M., DeBoy, C. a, Reich, D.S., Farrell, J. a D., Hoffman, P.N., Griffin, J.W., Sheikh, K. a, Miller, M.I., Mori, S., Calabresi, P. a, 2009. Diffusion tensor magnetic resonance imaging of Wallerian degeneration in rat spinal cord after dorsal root axotomy. The Journal of neuroscience : the official journal of the Society for Neuroscience 29, 3160–71.

Zhong, J., Petroff, O.A., Prichard, J.W., Gore, J.C., 1995. Barbiturate-reversible reduction of water diffusion coefficient in flurothyl-induced status epilepticus in rats. Magnetic resonance in medicine : official journal of the Society of Magnetic Resonance in Medicine / Society of Magnetic Resonance in Medicine 33, 253–6.

APPENDIX A

ADDITIONAL RESULTS FROM CHAPTER 2

Individual tracts:

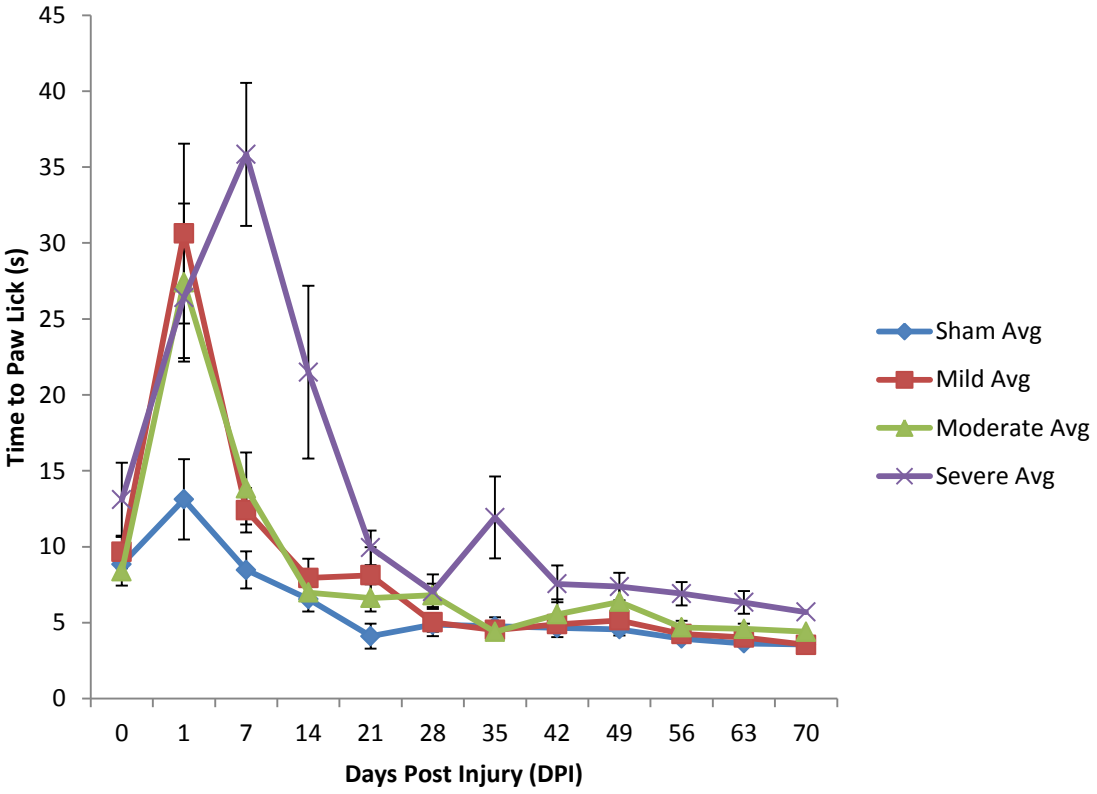

Figure 7-1: Front limb hot plate testing for rats with spinal cord injury.

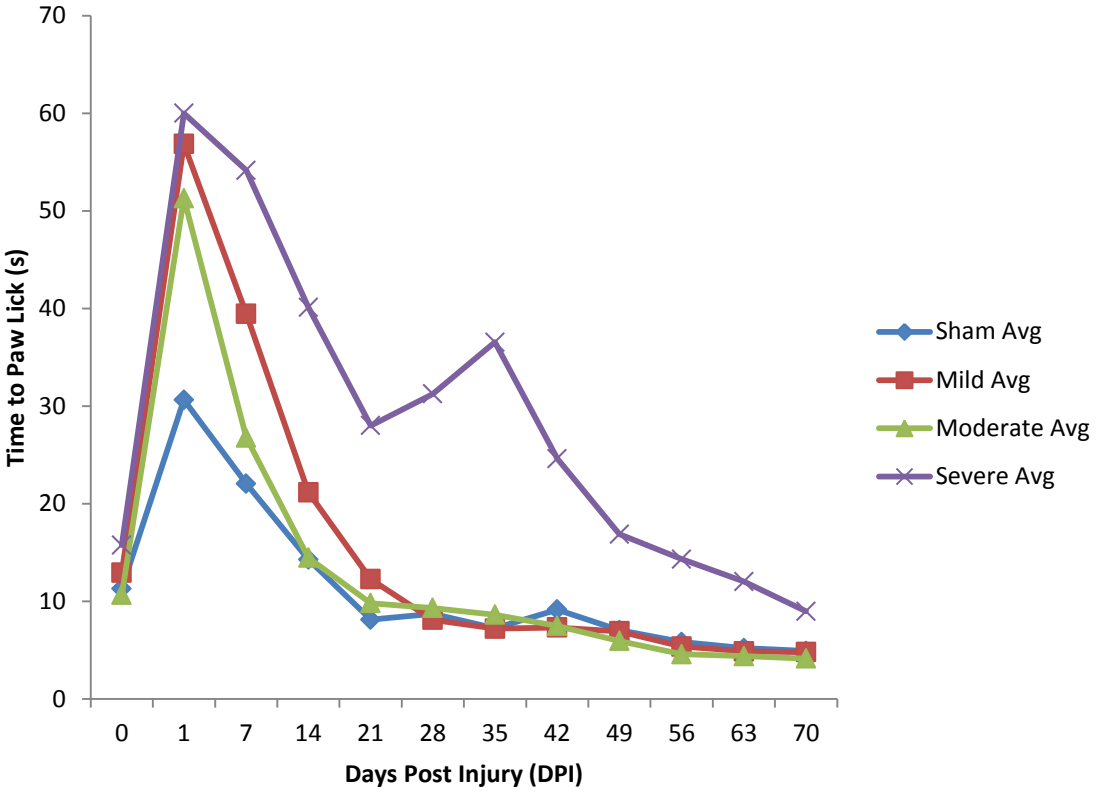

Figure 7-2: Hind limb hot plate testing for rats with spinal cord injury.

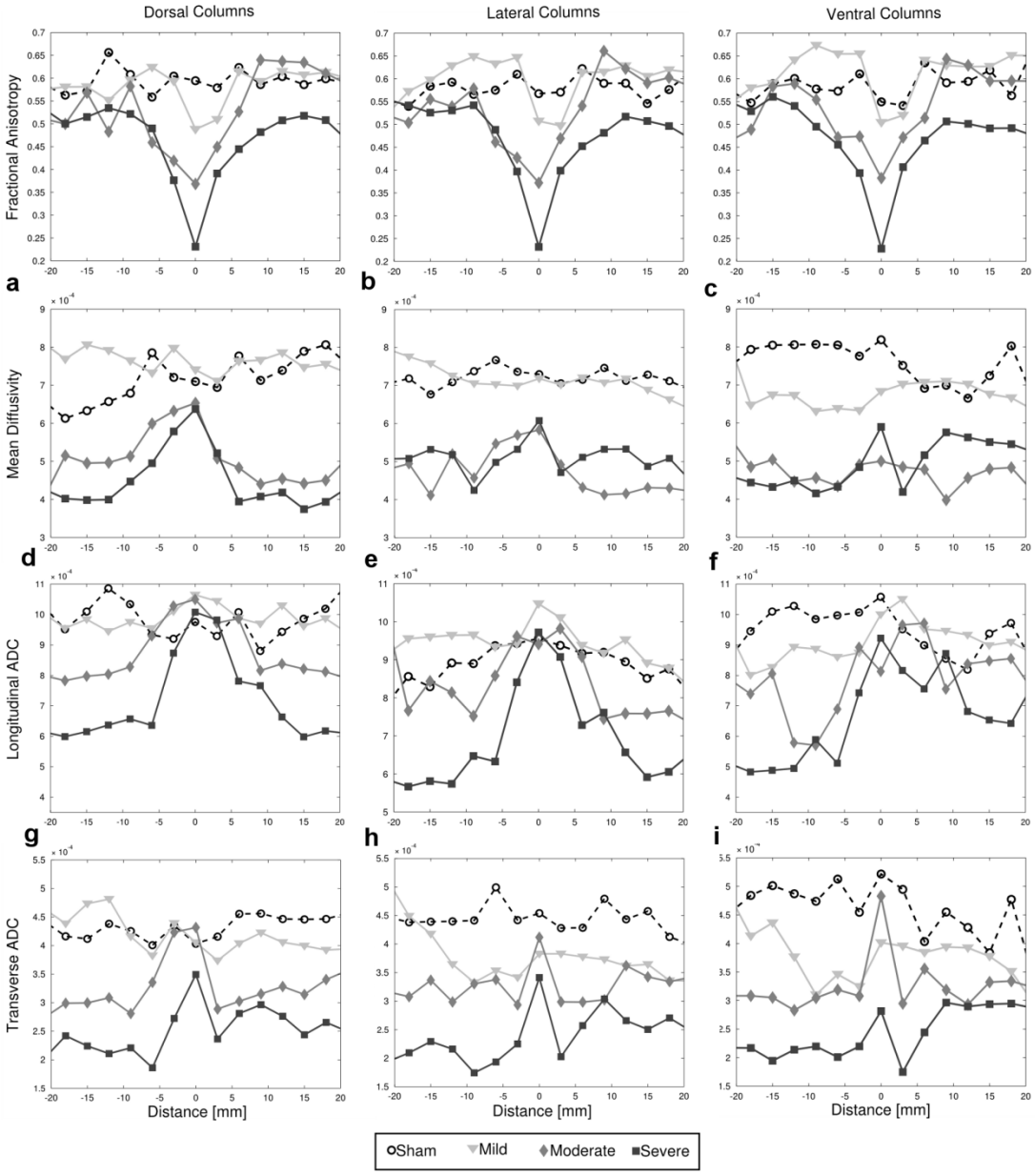

Figure 7-3: Diffusivity measurements for dorsal, ventral, and lateral columns.

Appendix B

EXAMPLE WORKFLOW DIAGRAMS FOR PROCESSING IMAGES

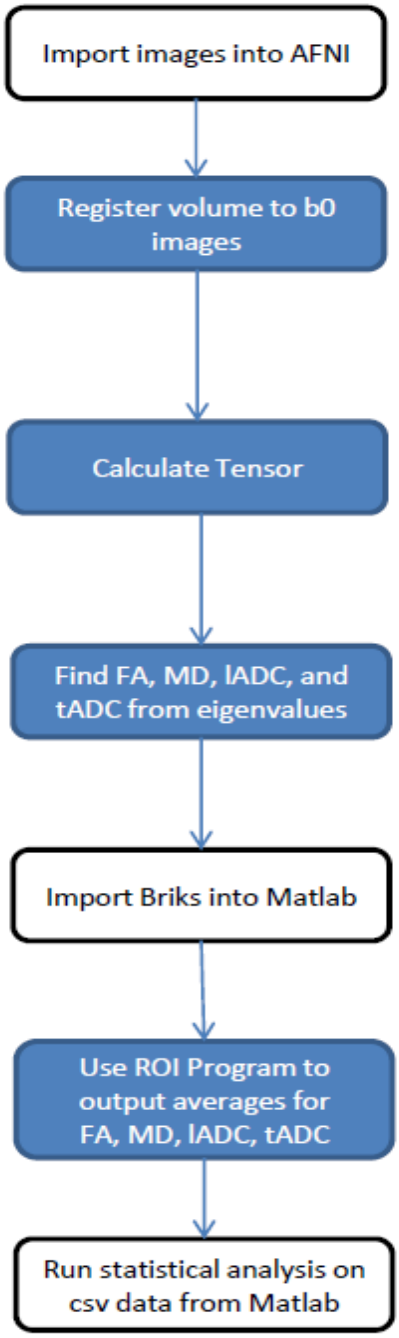

Figure 8-1: Typical workflow for processing images of the spine.

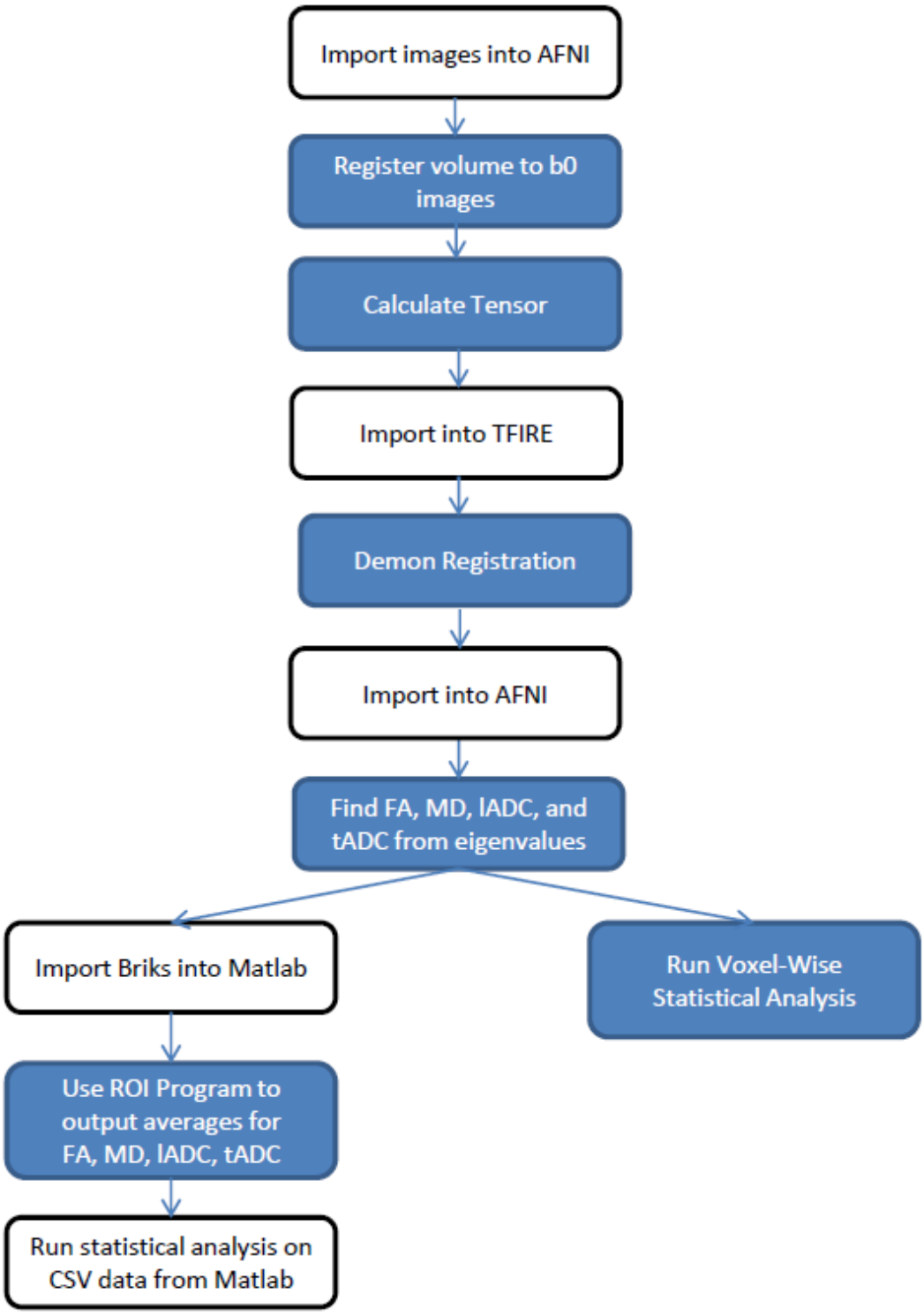

Figure 8-2: Typical workflow for processing images of the brain